

**Experimental and Theoretical Investigations in Solid Phase
Reaction Kinetics and Noncovalent Interactions in Water**

by

Brijesh Bhayana

B.E, Panjab University, 1997

M.S, Carnegie Mellon University, 2002

Submitted to the Graduate Faculty of
School of Arts and Sciences in partial fulfillment
of the requirements for the degree of
Doctor of Philosophy

University of Pittsburgh

2007

UNIVERSITY OF PITTSBURGH

School of Arts and Sciences

This dissertation was presented

by

Brijesh Bhayana

It was defended on February 19, 2007 and approved by

Dr. Stephen Weber, Professor, Chemistry

Dr. Toby Chapman, Professor, Chemistry

Dr. Karl Johnson, Professor, Chemical Engineering

Thesis Director: Dr. Craig S. Wilcox, Professor, Chemistry

**Experimental and Theoretical Investigations in Solid Phase Reaction Kinetics and
Noncovalent Interactions in Water**

Brijesh Bhayana, Ph. D.

University of Pittsburgh, 2007

Factors affecting reaction rates in polystyrene beads used in solid phase organic synthesis have been studied. The role of diffusion and reagent partitioning has been examined theoretically and experimentally. Both of these factors have been found to influence the reaction kinetics of common solid phase organic synthesis reactions. A mathematical model to analyze a simple bimolecular reaction inside a bead has been developed and successfully applied to the experimental data to obtain quantitative information on the influence of diffusion and reagent partitioning on the reaction rates. The effects of diffusion generally increase with the size and decreased swelling of the beads. Under many common reaction conditions, however, these effects may not be very significant. General guidelines to identify these conditions have been developed.

A water-soluble torsion balance to study noncovalent interactions in aqueous media has been synthesized. The folding energies of new balances were found to be higher in water than in organic solvents. This increase can be partially attributed to hydrophobic forces. Aggregation and micelle formation were found to increase folding in water, indicating differences between microscopic and mesoscopic hydrophobic effects. The experimental data have been analyzed in the context of the Lum, Chandler and Weeks theory of hydrophobicity and evidences in its favor have been found. The hydrophobic response of a fluoromethyl group was found to be similar to a methyl group in two complementary torsion balances.

TABLE OF CONTENTS

1.0	POLYMER SUPPORTS FOR SOLID PHASE ORGANIC SYNTHESIS (SPOS) AND FACTORS EFFECTING REACTION KINETICS IN SPOS BEADS	1
1.1	IMPORTANT PHYSICAL CHARACTERISTICS OF POLYMER BEADS	2
1.2	IMPORTANT FACTORS THAT AFFECT REACTION KINETICS IN SPOS BEADS.....	5
1.2.1	Swelling.....	6
1.2.2	Diffusion.....	7
1.2.3	Bead size.....	8
1.2.4	Partition coefficient.....	8
1.2.5	Loading.....	9
1.2.6	Temperature.....	9
1.2.7	Activity.....	10
2.0	DIFFUSION CONTROLLED PROCESSES	12
2.1	DIFFUSION AND CHEMICAL REACTIONS	12
2.2	THE DIFFUSION-REACTION EQUATION AND RELEVANT PAST WORK.....	14

2.2.1	Diffusion and reaction in cylindrical fibers.....	15
2.2.2	Diffusion and reaction in a sphere immersed in a well stirred solution of limited size	16
2.3	SEMI-ANALYTICAL AND NUMERICAL METHODS FOR SOLVING THE DIFFUSION-REACTION EQUATION.....	17
2.3.1	The Danckwerts semi-analytical method	17
2.3.2	Numerical method applied in our model.....	18
2.4	DIFFUSION COEFFICIENTS OF SMALL MOLECULES IN SOLVENT SWOLLEN POLYMERS	20
2.4.1	Diffusion in restricted environments.....	20
2.4.2	The Mackie-Meares model.....	21
2.4.3	Measurement of diffusion coefficient in swollen polymers using pulsed-gradient spin-echo (PGSE) NMR.....	21
2.4.4	The Wilke-Chang correlation	23
3.0	EXPERIMENTAL AND COMPUTATIONAL INVESTIGATIONS IN BEAD BASED REACTION PROCESSES. UNDERSTANDING THE ROLE OF DIFFUSION AND REAGENT PARTITIONING.....	24
3.1	MATERIALS AND METHODS	25
3.2	DIFFUSION COEFFICIENT MEASUREMENTS	27
3.3	PARTITION COEFFICIENT MEASUREMENTS.....	28
3.4	RESULTS BASED ON OUR NUMERICAL MODELING.....	30
3.5	DATA ANALYSIS BASED ON A BIMOLECULAR MODEL	32
3.6	DIFFUSION-REACTION MODEL.....	35

3.7	EMPERICAL CORRELATION BETWEEN SIMPLE BIMOLECULAR AND DIFFUSION-REACTION REACTION RATES.....	38
4.0	EFFECTS OF NONCOVALENT INTERACTIONS AND SOLVATION ON MOLECULAR CONFORMATIONS AND THEIR COMPUTATIONAL MODELS.....	46
4.1	DISPERSION FORCES AND NONCOVALENT INTERACTIONS.....	46
4.2	COMPUTATIONAL METHODS FOR DISPERSION INTERACTIONS.....	48
4.3	SOLVATION EFFECTS IN WATER	49
4.3.1	The explicit and implicit solvation models of water.....	50
4.3.2	Estimations of γ – the microscopic surface tension of water.....	51
4.3.3	The Lum, Chandler and Weeks (LCW) theory of hydrophobic effects.....	52
4.4	STUDIES ON NONCOVALENT INTERACTIONS AND SOLVENT EFFECT USING THE WILCOX MOLECULAR TORSION BALANCE	55
4.5	COMPUTATIONAL STUDIES ON THE TORSION BALANCE	57
5.0	WATER SOLUBLE TORSION BALANCE.....	59
5.1	SYNTHESIS	60
5.2	SOLVENT AND SUBSTITUTENT EFFECT ON ROTATION RATE	66
5.3	FOLDING ENERGIES OF NEW TORSION BALANCES IN WATER.....	70
5.4	DIFFERENT EFFECTS ON FOLDING ENERGIES	76
5.4.1	Effect of concentration on folding ratios.....	76
5.4.2	Effect of denaturants, salting-in and salting-out agents	79
5.4.3	Effect of temperature on folding equilibrium.....	80
5.5	SELF CONSISTENCY OF FOLDING RATIOS.....	81
5.5.1	Solvent Accessible Surface Area (SASA) and γ calculations.	81

6.0	QUANTIFICATION OF C-F/π_H INTERACTION IN WATER.....	83
6.1	ELECTROSTATIC EFFECTS OF FLUORINATION.....	83
6.2	EVALUATION OF C-F/AMIDE INTERACTION USING THE TORSION BALANCE AND HUNTER’S DOUBLE MUTANT CYCLE.	84
6.3	TORSION BALANCE FOR QUANTIFICATION OF C-F/ π_F AND C-F/ π_H INTERACTIONS	86
6.4	TORSION BALANCE FOR C-F/ π_H INTERACTION IN WATER.....	87
7.0	CONCLUSIONS AND FUTURE DIRECTIONS.....	93
8.0	EXPERIMENTAL SECTION	95
	APPENDIX A.....	120
	BIBLIOGRAPHY	130

LIST OF TABLES

Table 2.1. Diffusion coefficients of cyclohexane in benzene swollen 1% CLP beads.	17
Table 3.1. Properties of polystyrene resins used in this study.	25
Table 3.2. Experimental and calculated values of diffusion coefficients in CH ₂ Cl ₂ .	28
Table 3.3. Simple bimolecular rate constants for three experiments on each bead size.	34
Table 3.4. Diffusion-reaction rate constants for three experiments on each bead size.	36
Table 3.5. The activity coefficients in beads on the basis of free volume theory.	37
Table 3.6. Reaction kinetics parameters from simulated data.	39
Table 3.7. Diffusion-reaction rate constants from Crank-Nicolson and the empirical correlation.	41
Table 4.1. Effect of Substituent on folding ratios.	55
Table 4.2. Folding ratio of a phenyl ester in different solvents.	56
Table 5.1. Rotation rates of methyl diester torsion balances in various solvents.	67
Table 5.2. Folding energies (kcal/mol) of new torsion balances at 298 K.	70
Table 5.3. Cohesive solvent effects on folding of isopropyl and cyclohexyl torsion balances at 298 K.	74
Table 5.4. Boltzmann averaged surface areas of minimum energy geometries (MMFF94x) in gas phase.	82
Table 6.1. C-F/amide interaction energies in different solvent.	85
Table 6.2. The folding energies of 36 and 37 .	86

Table 6.3. The folding energies of compounds 41 and 42 .	90
Table 6.4. Folding energies of hexafluoroisopropyl torsion balance 42b .	92

LIST OF FIGURES

Figure 1.1. Scanning Electron Micrograph of PEG-PS beads (Hudson, 1999).	2
Figure 1.2. Autoradiograph of a Merrifield resin.	3
Figure 1.3. Structures of Merrifield Resin and JandaJel.	4
Figure 1.4. Diffusion and Reaction of Dye in Macrobeads.	7
Figure 3.1. The experimental apparatus.	26
Figure 3.2. (a) Amine distribution, (b) isocyanate distribution, (c) reaction intensity inside a bead for various $(D/a^2)/(k \cdot n_0)$ values.	31
Figure 3.3. Representative fits for the homogeneous solution reaction model. The markers show the experimental data, and the solid lines are the best fits obtained using the simple second order bimolecular rate law. The rate constants, k_{bimol} , are $0.98 \text{ L mol}^{-1} \text{ sec}^{-1}$, $0.65 \text{ L mol}^{-1} \text{ sec}^{-1}$, $0.44 \text{ L mol}^{-1} \text{ sec}^{-1}$ for $110 \mu\text{m}$, $225 \mu\text{m}$ and $530 \mu\text{m}$ beads respectively.	33
Figure 3.4. Representative fits for the diffusion-reaction model. The markers show the experimental data, and the solid lines are the best fits obtained using the diffusion-reaction equation. The rate constants, k , are $1.12 \text{ L mol}^{-1} \text{ sec}^{-1}$, $0.98 \text{ L mol}^{-1} \text{ sec}^{-1}$, $0.74 \text{ L mol}^{-1} \text{ sec}^{-1}$ for $110 \mu\text{m}$, $225 \mu\text{m}$ and $530 \mu\text{m}$ beads respectively.	35
Figure 3.5. Empirical correlation between k_{bimol}/k and $(D/a^2)/(k \cdot n_0)$.	39
Figure 3.6. Linear empirical correlation between k_{bimol}/k and $k \cdot n_0 (D/a^2)$.	41
Figure 3.7. A simulated-diffusion reaction process for $(D/a^2)/(k \cdot n_0) = 0.0007$. (Above) diffusion-reaction equation fit, (below) a simple bimolecular rate law equation fit.	43
Figure 3.8. Simple bimolecular rate law fits for the reaction of $530 \mu\text{m}$ beads with 3-phenylpropylamine ($k_{bimol} = 0.54 \text{ L mol}^{-1} \text{ sec}^{-1}$), and 3,3-diphenylpropylamine ($k_{bimol} = 0.24 \text{ L mol}^{-1} \text{ sec}^{-1}$).	44
Figure 4.1. (A) Transfer of neopentane from its neat phase to water and (B) transfer of neopentane from gas phase into liquid neopentane phase. T_s and T_h represent temperatures	53

where the entropy and enthalpy of transfer are zero.

- Figure 4.2.** Excess chemical potential per unit area vs. solute radius. 54
- Figure 4.3.** Folded and unfolded conformations of the torsion balance. 55
- Figure 5.1.** Water soluble torsion balance: the “perfect” mutation. 59
- Figure 5.2.** NMR spectra of **21f** and **22f** in different solvents: (A) Acetone-d₆, (B) CD₃NO₂, (C) CD₃CN, (D) CDCl₃, (E) C₆D₆, (F) CD₃OD, (G) D₂O. 1 = **21f**, 2 = **22f**. 68
- Figure 5.3.** Adams’s model system for racemization studies. 69
- Figure 5.4a.** Model interactions of the 1-adamantyl and 2-adamantyl esters. 72
- Figure 5.4b.** X-ray crystal structures of compounds **21e** (top) and **22d** (bottom). 73
- Figure 5.5.** Torsion balances with large non polar surface areas. 75
- Figure 5.6.** Some alternatives to glutaric anhydride for water solubility enhancement. 76
- Figure 5.7.** NMR spectra in water: (A) **23c** at 0.1 mM (left) and 1.0 mM (right) concentrations, (B) **23d** at 0.1 mM (left) and 1.0 mM (right) concentrations. Spectra recorded in 25 mM K₂CO₃ in D₂O. 78
- Figure 6.1.** Torsion balances for C-F/ π _H and C-F/ π _F interactions in organic solvents. 86
- Figure 6.2.** NMR spectra of compound **42a** in water (25 mmol/L NaHCO₃ in D₂O) at 5 mmol/L (top), 1 mmol/L (middle) and 0.1 mmol/L (bottom) concentrations. The right peak represents the methyl ester in the *endo* position. 91

LIST OF SCHEMES

Scheme 3.1.	24
Scheme 5.1.	60
Scheme 5.2.	61
Scheme 5.3.	61
Scheme 5.4.	62
Scheme 5.5.	62
Scheme 5.6.	62
Scheme 5.7.	63
Scheme 5.8.	64
Scheme 5.9.	65
Scheme 5.10.	81
Scheme 6.1.	85
Scheme 6.2.	88
Scheme 6.3.	88
Scheme 6.4.	89

ACKNOWLEDGEMENT

I would like to express my gratitude to Prof. Craig Wilcox for giving me the wonderful opportunity to pursue exciting research under his supervision. I thank him for his patience, guidance, encouragement, and sharing his passion for science. From him, I learnt to think like a scientist.

I thank Professors Eric Borguet, David Waldek, David Pratt, Steven Weber, Dennis Curran, Christian Schafmeister, Toby Chapman and Karl Johnson for serving on my various different committees over the years, and contributing to my intellectual growth as a chemist.

I thank the Wilcox group members, past and present, for all their advice and help, and the interesting times. Special thanks to Mark Ams and Mike Martucci for the wonderful company. I wish them best of luck in their endeavors.

Thanks to the members of chemistry department's staff section, especially, Bill Valenta, Fran Nagy, Toni Weber, and Darlene Baltish, and to the facilities management, glass shop, machine shop, instrumentation labs, computing services and the rest for providing world-class infrastructure for chemical research.

Special thanks to Gami for her love and support.

I will always look forward to new research from the Wilcox group.

1.0 POLYMER SUPPORTS FOR SOLID PHASE ORGANIC SYNTHESIS (SPOS) AND FACTORS EFFECTING REACTION KINETICS IN SPOS BEADS

Solid phase organic synthesis (SPOS) has an important place in contemporary chemical synthesis.¹ Multistep synthesis can be performed in SPOS with molecules anchored to a polymer backbone and the final product may be obtained simply by cleaving the linker. Time consuming and expensive work up procedures such as column chromatography are reduced and large and complex molecules can be synthesized in high yields and purity. Solid phase synthesis is the foundation of modern combinatorial chemistry and has made it possible to generate huge libraries of biologically important compounds for drug discovery.

Solid phase synthesis originated with Merrifield's 1963 synthesis of a tetrapeptide appended to insoluble polystyrene.^{1a} Although, initially confined to peptide synthesis, SPOS gradually expanded in scope with introduction of diverse range of polymer bound linkers, reagents and scavengers,² and even multigram scale synthesis of complex natural products have been accomplished entirely using SPOS.³ SPOS has proved to be amenable to automation and even biologists can use it for peptide synthesis.

1.1 IMPORTANT PHYSICAL CHARACTERISTICS OF POLYMER BEADS

1.1.1 Shape and size distribution

Most commercially available SPOS resins are made by suspension polymerization, which results in beads of near perfect spherical shape and narrow size distributions.⁴ Their typical diameters are kept in the range of 100-500 μm , with 100-200 μm beads being most common. Merrifield found that the bead sizes are not normally, but log-normally distributed.⁵ During a SPOS synthesis, the bead sizes may increase as more and more linkages are attached. For example, Merrifield and Sarin observed an almost twofold increase in swollen bead size after 12 steps in a peptide synthesis process.⁵

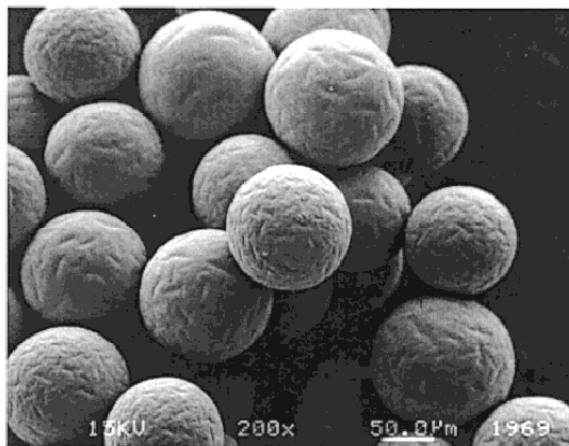


Figure 1.1. Scanning Electron Micrograph of PEG-PS beads (Hudson, 1999).⁶

1.1.2 Loading and reactive site distribution

The loading capacity of SPOS resins is defined as the moles of reactive sites per gram of beads. Commercial SPOS beads are usually densely functionalized and their loadings range from 0.1-2.0 mmol/g. For a loading capacity of ~ 1 mmol/g, almost every fourth monomer on the polymer backbone carries a reactive site, which makes it obvious that not all reactive sites can be present just on the surface of the beads. Merrifield established that $>99\%$ of the reactive sites lie inside a bead, which was also supported by autoradiographs of cross sections of peptide-resin beads with tritium labeled valine.⁴ Most of the reaction takes place inside the beads. However, not all sites in a bead may be equally reactive or accessible to a reactant and the final stages of a reaction can be extremely slow.⁷

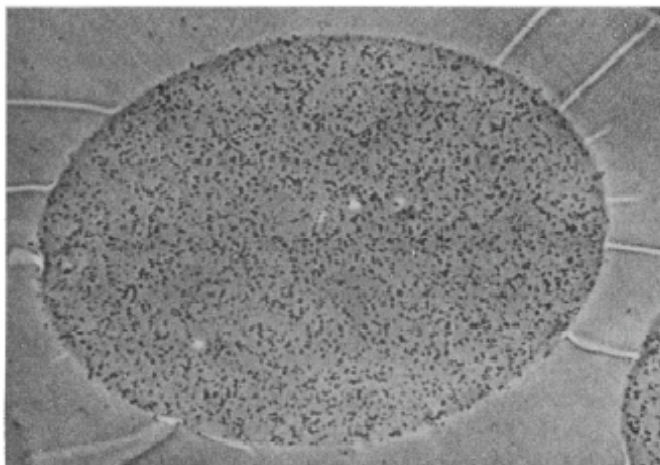


Figure 1.2. Autoradiograph of a Merrifield resin.⁴

1.1.3 Polymer matrix and cross-links

The natures of the polymer backbone and the cross-links define the most important physical characteristics of SPOS resins. Most commercially available functionalized polymer supports are made of cross-linked polystyrene (CLPS). The polymer matrix is homogeneous at the macroscopic scale, however, at microscopic level, it is inhomogeneous due to the presence of meta- and para- isomers of divinylbenzene, which react at different rates with styrene during resin synthesis.⁸ Although even a low cross-linked polymer matrix is basically motionless in the solid state, solvation by a good solvent can permit some thermal motion of the polymer chains. The glass transition temperature (T_g) of a polymer is a good indicator of the degree of its thermal motion. The T_g of swollen lightly cross-linked polystyrene in good solvents is significantly reduced compared to its solid state.⁹

The most common cross linking reagents are divinylbenzene (DVB, Merrifield resins) and 1,4-bis(vinylphenoxy)-butane (*JandaJel*).¹⁰ A third popular resin, *TentaGel*,¹¹ is a graft copolymer and consists of low cross linked polystyrene matrix on which poly(ethyleneglycol) is grafted.

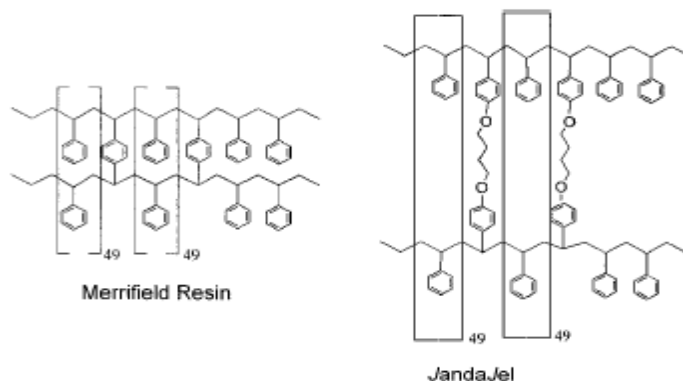


Figure 1.3. Structures of Merrifield Resin and JandaJel.⁴

Cross-links prevent any polymer from dissolving into a solvent and impart unique swelling properties, for example, Merrifield resins swell in organic solvents whereas *TentaGel* swells in water. At low cross-linking (1%), Merrifield resins can swell up to 3-5 times their original volume in common organic solvents where as at 10-20% cross-linking, their swelling is almost negligible.⁴ The swelling capacity of *JandaJels* is almost twice that of Merrifield resins; electron paramagnetic resonance studies showed that this was due to enhanced polymer-solvent interaction.¹² Cross-linking can also affect the mechanical strength of the beads; for example, polystyrene cross-linked with bis(vinylbenzyl)oligoethylene glycol is significantly more stable under magnetic stirring than polystyrene cross-linked with DVB.¹³

1.2 IMPORTANT FACTORS THAT AFFECT REACTION KINETICS IN SPOS BEADS

Some important factors that affect reaction progress in SPOS resins are – swelling, diffusion rate, loading, reagent partitioning, bead size, and temperature. Many of these factors may change during a reaction and often they are also interdependent. Several studies have been done to understand their importance in SPOS reaction kinetics and a few general trends that have been observed are discussed in the following sections.⁴

1.2.1 Swelling

Swelling allows a reactant to access the reactive sites inside a bead via diffusion and is a prerequisite for reaction and the most important factor influencing the reaction rate in a bead. Swelling ratio and swelling capacity of a resin describe the measure of swelling. Swelling ratio is the ratio of solvent swollen bead volume to the dry bead volume.

$$\text{Swelling ratio} = \text{volume of a swollen bead} / \text{volume of a dry bead}$$

Swelling capacity is the amount of solvent absorbed per gram of the swollen beads and it generally ranges from 4-8 mL/g. To allow for high swelling, cross-linking in most beads is kept low, at a low value of ~1%. Although good swelling is desirable because it enhances reaction rates,¹⁴ the polymer itself has been shown to be responsible for some surprising results. Janda *et al.* found highly cross-linked macroporous resins to be a more effective catalysts in Wacker oxidation of alkenes than low cross linked Merrifield resins.¹⁵ Gadek and Richter observed selective reaction of a phenol in the presence of a primary amine in a solid phase Mitsunobu reaction whereas no selectivity was observed under the homogeneous solution conditions.¹⁶

Swelling ratio may change during a reaction. In an interesting observation, Merrifield observed the swelling ratio in DMF to increase (where it was thought to decrease) with lengths of graft peptides.⁵ This was attributed to increase in free energy of solvation of the resin as peptide chains became longer.

1.2.2 Diffusion

Reactions in beads occur by diffusion. The most direct evidence of this comes from fluorescent dye experiments in large beads where the outer sites were found to react first.¹⁷ There was a gradual progression of reaction toward the center of the bead (Figure 1.4).

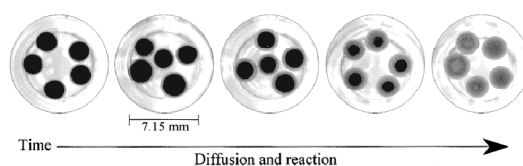


Figure 1.4. Diffusion and reaction of dye in macrobeads.¹⁷

Mass transfer calculations for forced convection also indicated diffusion to be the predominant mode of transport.¹⁸

Diffusion of a reagent in a bead can be affected by (1) physical obstruction by the polymer and (2) by interaction with attached functional groups.¹⁹ It can also be impeded by the turbulent hydrodynamic layer of solvent at a bead's surface.⁴ This motion can be significantly different from that of the bulk solvent. This turbulent layer is analogous to the Nernst layer at an electrode and its characteristics will depend on the rate of agitation. For example, a linear increase in reaction rate between 1-bromoacetone and aqueous sodium cyanide in toluene with speed of stirring in a triphasic (organic, polymer, aqueous) reaction was observed by Tomoi and Ford.²⁰

Diffusion and reaction are not independent, and the interplay between diffusion and reaction dictates the relative roles they ultimately play in observed reaction rates.

1.2.3 Bead size

Rates of reactions have been observed to decrease with the increase in bead size in many SPOS kinetic studies.^{14,21} Dependence of reaction rate on bead size is further evidence of the interplay between diffusion and reaction.

1.2.4 Partition coefficient

Partition coefficient is an important thermodynamic parameter defined as the equilibrium ratio of diffusant concentration inside a swollen bead to its concentration in the bulk solvent outside. It is determined by the difference in standard free energy of a diffusant in the swollen polymer matrix compared to free solvent.

$$\text{Partition coefficient} = [\text{solute}]_{\text{bead}} / [\text{solute}]_{\text{bulk}}$$

Large partition coefficients lead to enhanced reaction rates. Morphy et al. observed significant increases in yields in syntheses of tertiary amines when using perfluorous hydrocarbons as solvents despite their poor swelling properties.²² Organic compounds generally have poor solubility in fluoruous solvents.²³ In Morphy's case the reactants were forced by the solvent to concentrate inside the beads thereby increasing the partition coefficient and enhancing the reaction rate. While almost no products were obtained in DMF or DMSO, aliphatic perfluorous solvents gave >95% yields under the same conditions.

Pivonka and Palmer have developed “on-bead” IR techniques to measure partition coefficients by comparing the IR spectra of a single swollen bead held between two glass plates and the bulk solvent stream carrying the diffusant.²⁴ The partition coefficients of common organic reagents were determined for aminomethylstyrene beads swollen in three different solvents - DMF, THF and dichloromethane. They were found to be solvent dependent, and ranged between 0.2 – 1.2. The partition coefficients of homologous alcohols were found to decrease with the increase in chain length for all solvents.

1.2.5 Loading

The concentration of reactive sites in beads can be up to 1 M. The polystyrene backbone itself is inert and relatively non-polar, but the dense concentration of functional groups can significantly alter the chemical environment inside the beads. Neighboring functional groups, whether close by along the polymer chain or brought into a common space by accidents of folding, may interfere with each other during reaction. Leznoff found both ends of small diacyl chlorides reacted rapidly with the resin and could not be easily mono protected on Wang resins.²⁵

1.2.6 Temperature

The physical properties of the polymer and mobility of reactants change with temperature, thereby affecting reaction rates in ways not predicted for the homogeneous reactions. For peptide synthesis, a few contradictory results have been reported.

Merrifield (1974) found coupling yields of peptides to increase with increase in temperature.²⁶ Similar observations were also reported by Chen,²⁷ Raymond,²⁸ and Tam.²⁹ Contrary to these, Esko and Regnarson³⁰ reported a decrease in peptide coupling yield with temperature. Wang and Foutch³¹ found the activation energies for several peptide-coupling reactions to be in the range of 0.3 – 14 kcal/mol. Lower activation energy reactions are not very temperature sensitive. It is not clear whether these observations were influenced by temperature effects on swelling.

1.2.7 Activity

The volume available for the reaction inside the bead is not the same as the overall volume of the bead. How does one define ‘concentration’ and activity inside the bead? The question is relevant when comparing bimolecular rate constants determined in heterogeneous environments. We define the concentration of diffusant in the bead to be equal to the molar quantity of the diffusant divided by the total bead volume, taken to be the volume of a sphere of radius equal to the bead radius. The rate constants are initially derived using these concentrations and the assumption of unit activity. When comparing rate constants among different bead environments (different swelling, functional groups, or load capacity), or when comparing rate constants in the bead with rates in homogeneous media, reactant activities must be taken into account.³²

Effects that will influence reactant activities inside the polymer matrix may be divided into two categories. Specific effects on activity arise from the interaction of a solute with all other solutes present in solution and are often expressed by a virial equation that encompasses two-body, three-body, and higher interaction terms -

$$\ln \gamma_i = \sum_j B_{ij} C_j + \sum_j \sum_k B_{ijk} C_j C_k + \dots \quad (1.1)$$

Nonspecific effects on activity arise from the excluded volume effect, and may be estimated according to available volume theory (AVT).³³

$$\gamma_i = \frac{V_{total}}{V_{available,i}} = \frac{1}{f_{available,i}} \quad (1.2)$$

These two effects on activity (specific effects and excluded volume effects) can work in opposing directions. Two beads with identical loading factors and identical swelling are expected to have identical effects on solute activity coefficient. If the principle influence on activity coefficient is due to the attached functional groups, a higher loading factor will almost always lead to a lower activity for the solute due to the higher concentration of functional groups and consequent elevation of solute-polymer interactions. Lower swelling, at constant functional group concentration within the bead volume, will raise the activity coefficient due to the increase in the excluded volume effect. In the most common case to affect a synthesis - for example when a solvent change leads to a different swelling degree – higher swelling will reduce the volume concentration of functional groups (and thus raise the activity coefficient), but at the same time higher swelling will lower the excluded volume (and thus lower the activity coefficient). A complete understanding of reactivity in the polymer matrix or comparison of reactions in different polymer matrices would incorporate considerations of both of these effects.

2.0 DIFFUSION CONTROLLED PROCESSES

Diffusion is the spontaneous and random motion of matter arising from its thermal energy. Diffusion is ubiquitous in nature. Systematic scientific investigations on a diffusion process can arguably be said to have started with the discovery of the Brownian motion in 1827. Einstein developed the mathematical framework for Brownian motion on the basis of the atomic theory of matter in his seminal papers of 1905-1910,³⁴ which since then has found tremendous applications in physical, social, medical and economic sciences.

This work deals with role of diffusion in chemical processes³⁵ - an arena that came into existence immediately after Einstein's theory of Brownian motion.

2.1 DIFFUSION AND CHEMICAL REACTIONS

Consider a simple bimolecular reaction $A + B \rightarrow AB$ taking place under homogeneous conditions in well stirred solution. The rate law for the reaction can be written as

$$\frac{\partial[A]}{\partial t} = -k[A][B] \quad (2.1)$$

where $[A]$ and $[B]$ are the concentrations and k is the rate constant. Now imagine that stirring is stopped and the reactants allowed react under thermal diffusion. How are the

rates of events under diffusion control different from those under a homogeneous solution condition?

Smoluchowski was the first to study this question.³⁶ According to Smoluchowski's theory of colloidal aggregation under diffusion, particles of A can be assumed to be stationary, immersed in a sea of diffusing B's. A reaction occurs whenever a particle of B reaches the boundary of an A. The concentration of B's at the boundary of an A is zero and they diffuse toward A's obeying Fick's law of diffusion,

$$j = -DVC \quad (2.2)$$

where j is the flux of B's, $D = D_A + D_B$, the sum of diffusion coefficients of A's and B's. Under these conditions, Smoluchowski found that the steady state diffusion controlled bimolecular rate constant for the reaction (k_{rd}) is related to the homogeneous solution bimolecular rate constant (k_b) as -

$$\frac{k_{rd}}{k_b} = \frac{1}{1 + \frac{k_b}{4\pi R^* D N_A}} \quad (2.3)$$

where R^* , D and N_A are the reactions distance, sum of diffusion coefficients of A and B, and Avogadro's number, respectively. If in equation (2.3) $k_b \gg 4\pi R^* D N_A$, then $k_{rd} \ll k_b$, and the reaction is significantly affected by the diffusion rate. Under these conditions, chemical events are limited by encounter frequency (diffusion) of the reacting species and the reaction is said to be under "diffusion control". For reactions in common organic solvents ($D = \sim 10^{-5} \text{ cm}^2 \text{ sec}^{-1}$, $R^* = \sim 1 \text{ nm}$) to be under diffusion control $k_b = \sim 10^{10} \text{ L mol}^{-1} \text{ sec}^{-1}$, which means they must be extremely fast. Examples of such reactions include quenching of free radicals and strong acid-base reactions.³⁷ It must be pointed out that

achieving experimental conditions of absolute diffusion control can be challenging, as convectional currents due to thermal gradients can often exist.^{35e}

The organic reactions of current interest in solid phase synthesis are far slower than the reported diffusion controlled reactions; typical bimolecular rate constants for SPOS reactions would range from 0.1 – 1.0 L mol⁻¹sec⁻¹. It is therefore not the case that solid-phase reactions are under microscopic diffusion control.

There are puzzling aspects in Smoluchowski's model. For example, the concentration gradient of B's around an A is established after the reaction not before, and once the reaction has taken place, the established gradient loses its significance.³⁸ The activation energy of the reaction and formation of activated complex are also not considered.³⁸ More sophisticated models, however, lead to the same basic conclusions as Smoluchowski's theory and the theory has been successfully extended to more complex systems involving diffusion in the presence of electrostatic fields and van der Waals interactions.³⁹

2.2 THE DIFFUSION-REACTION EQUATION AND RELEVANT PAST WORK

The concentration profile, $C(r,t)$ (r and t are distance and time parameters), of a reactant undergoing simultaneous Fickian diffusion and a bimolecular chemical reaction with another reactant whose concentration is given by $n(r,t)$ can be described by a canonical diffusion-reaction equation^{35a}

$$\frac{\partial C(r,t)}{\partial t} = D\nabla^2 C(r,t) - kn(r,t)C(r,t) \quad (2.4)$$

where D is the diffusion coefficient and k is the reaction rate constant. The case of present interest is that where one of the reactants is immobile. This is the situation encountered in typical SPOS reactions; one of the reactive sites are held fixed, relative to a bead-based coordinate system, on the polymer backbone in the beads.

A few examples of applications of equation (2.4) that were followed closely by us in initiating our investigations are discussed in the following sections.

2.2.1 Diffusion and reaction in cylindrical fibers

In 1950, Katz, Kubo and Wakelin modeled the absorption of dye into wool fibers as a diffusion-reaction process with the diffusant (dye) diffusing from an infinite bath into cylindrical fibres (wool) of infinite length.⁴⁰ In their approach to the approximate solution of equation (2.4), the reaction term was ignored and the concentration profile calculated. The solution to (2.4) under these conditions can be given in terms of cylindrical Bessel functions

$$C(r,t) = C_0 - \frac{2C_0}{a} \sum_{l=1}^{\infty} e^{-D\alpha_l^2 t} \frac{J_0(r\alpha_l)}{\alpha_l J_1(r\alpha_l)} \quad (2.5)$$

where J 's are the Bessel functions.⁴¹ This concentration was then used within a bimolecular rate law to calculate reaction parameters.

At the same time, Reese and Eyring reported a similar method in modeling the reaction between hair fibers and chemical agents.⁴² In both these studies, the diffusion was assumed to occurring from an infinite bath, which is not the case in many practical

situations. The neglect of the reaction term in the solution to their equation makes this approach inappropriate for our work.

2.2.2 Diffusion and reaction in a sphere immersed in a well stirred solution of limited size

This is a more important case from our point of view as the SPOS beads are spherical and generally the amounts of reactants are finite. The solution to equation (2.4) for these boundary conditions *in absence of reaction* is given by equation 2.5^{41a}

$$\frac{M_t}{M_\infty} = 1 - \sum_{n=1}^{\infty} \frac{6\alpha(\alpha + 1)e^{-Dq_n^2 t/a^2}}{9 + 9\alpha + q_n^2 \alpha^2} \quad (2.5)$$

where

$$\tan(q_n) = \frac{3q_n}{3 + \alpha q_n^2} \quad (2.6)$$

In equation (2.5) M_t and M_∞ are the masses of of diffusant in the sphere at time t and infinity, respectively; a is the radius of the sphere; and α is the ratio of the volume of the solution (V) to the volume of the sphere, $\alpha = 3V/4\pi a^3$. If k is the ratio of concentration of diffusant inside the sphere to outside at equilibrium (the partition coefficient), then $\alpha = 3V/4\pi a^3 k$. Roucis and Ekerdt used the above equations to model diffusion of cyclic hydrocarbons in benzene swollen cross-linked polystyrene beads.¹⁸ They examined three types of beads, with swelling ratios that differed from 3.44 to 3.11 and 1.71. Known amounts of beads (2-7 g) were allowed to swell in 25 mL of benzene at 25 °C. The solution was stirred and the diffusant introduced to the suspension to produce an initial bulk concentration of ~0.06 M. Samples of the bulk solvent were withdrawn at

time intervals of ~20 sec, the concentration of the diffusant in the bulk was determined by GC, and equation (2.6) fitted to the data. The diffusion coefficients were found to decrease with decrease in swelling ratio (Table 2.1) and the changes matched those that were expected according to the Mackie-Mearns relation (*vide infra*).

Table 2.1. Diffusion coefficients of cyclohexane in benzene swollen 1% CLP beads.¹⁸

Entry	Polymer swelling ratio	Diffusion coefficient ($\text{cm}^2/\text{s} \times 10^6, \pm 12\%$)
1	3.44	5.89
2	3.11	5.37
3	1.71	0.82

2.3 SEMI-ANALYTICAL AND NUMERICAL METHODS FOR SOLVING THE DIFFUSION-REACTION EQUATION

2.3.1 The Danckwerts semi-analytical method

To solve for diffusion *and* reaction in a sphere, Danckwerts method can be used for unimolecular reactions.⁴³ Danckwerts discovered that if any solution S_0 for equation (2.7)

$$\frac{\partial C(r,t)}{\partial t} = D\nabla^2 C(r,t) \quad (2.7)$$

is known for given boundary conditions, then the solution S_1 for the equation (2.8)

$$\frac{\partial C(r,t)}{\partial t} = D\nabla^2 C(r,t) - kC(r,t) \quad (2.8)$$

is given by equation (2.9).

$$S_1 = k \int_0^t S_0 e^{-ky} dy + S_0 e^{-kt} \quad (2.9)$$

For our equation of interest, eq. (2.4), the Danckwerts method cannot be perfectly employed because $n(r,t)$ changes with time. A semianalytical solution is still possible if $n(r,t)$ is assumed to be constant for small time intervals and updated iteratively in a manner similar to that used Katz and Eyring. We implemented such an approach but found it to be inadequate because it required extremely small time steps to avoid convergence problems and to yield correct mass balances.

2.3.2 Numerical method applied in our model

Several numerical methods can be used to solve non-linear multivariate differential equations.^{41a} Of these, the implicit numerical methods are widely used in practical applications because they offer strong advantages of stability and rapid convergence, and require fewer computational efforts. We found the implicit Crank-Nicolson and Douglas methods to work excellently in our case.⁴⁴

Expressed in dimensionless units $T (=D t/a^2)$ and $R (=r/a)$, equation (2.4) in spherical coordinates can be written as equation (2.10)^{41a}

$$\frac{\partial C(R,T)}{\partial T} + kn(R,T)C(R,T) = \frac{\partial^2 C(R,T)}{\partial R^2} + \frac{2}{R} \frac{\partial C(R,T)}{\partial R} \quad (2.10)$$

Following the Douglas scheme,⁴⁴ Equation (2.10) can be expressed in a finite-difference form. (Equation 2.11)

$$2C_j^{N+1} + kn_j \delta T C_j^{N+1} - \left[\left(1 - \frac{1}{j-1}\right) \nu C_{j-1}^{N+1} - 2\nu C_j^{N+1} + \left(1 + \frac{1}{j-1}\right) \nu C_{j+1}^{N+1} \right] =$$

$$2C_j^N - kn_j \delta T C_j^N + \left[\left(1 - \frac{1}{j-1}\right) \nu C_{j-1}^N - 2\nu C_j^N + \left(1 + \frac{1}{j-1}\right) \nu C_{j+1}^N \right] \quad (2.11)$$

where

$$\nu = \frac{\delta T}{\delta R^2}$$

In this equation, the diffusant concentration distribution throughout the sphere at any time (C_j^N where N represent the present time and j is the radial position counter) is related to the diffusant concentration distribution at the next time increment (C_j^{N+1}). The reactive site concentration (n_j) is taken to be the average site concentration during the time increment. At the center of the sphere, a boundary condition applies. (Equation 2.12)

$$C_1^{N+1} \left(1 + \frac{k}{2} n_1^{N+1} \delta T + (3\nu - \frac{1}{2})\right) - (3\nu - \frac{1}{2}) C_2^{N+1} = \\ C_1^N \left(1 - \frac{k}{2} n_1^N \delta T - (3\nu + \frac{1}{2})\right) + (3\nu + \frac{1}{2}) C_2^N \quad (2.12)$$

Finally, a mass balance boundary condition applies at the surface and constrains the surface concentration (C_J). The inward flux of material from the external volume (V_0) must equal the rate of mass lost from the external volume. (Equation 2. 13)

$$\left[\frac{\nu}{2} \left(1 - \frac{1}{J-1}\right) - \frac{4\pi a^3}{V_0 \delta R} \right] (C_J^{N+1} - C_{J-1}^{N+1}) = \left[\frac{\nu}{2} \left(1 - \frac{1}{J-1}\right) + \frac{4\pi a^3}{V_0 \delta R} \right] (C_J^N - C_{J-1}^N) \quad (2.13)$$

Equations (2.11), (2.12) and (2.13) can be united to provide a set of simultaneous equations (expressible as a tridiagonal matrix)^{41a} that relates any current concentration distribution to the concentration distribution at a following time increment. A computer program running a 1.8 GHz microprocessor calculates all grid point concentrations for 200 radial points and 10,000 time increments in about 45 seconds.

2.4 DIFFUSION COEFFICIENTS OF SMALL MOLECULES IN SOLVENT SWOLLEN POLYMERS

The diffusion coefficient inevitably appears in any solution to the diffusion-reaction equation and knowledge of its magnitude is essential for calculating the effect of diffusion control in a reaction. Our data are influenced by the diffusion of small molecules in CLP resins. Studies on diffusion in polymers have been conducted in relation to drug delivery, membrane-based separation, and plasticization of polymers.⁴⁵ Traditional methods to determine diffusion coefficients in polymer solutions include dynamic light scattering, electron paramagnetic resonance (EPR), and nuclear magnetic resonance (NMR).^{45, 46} The best choice of technique is dictated by the actual problem at hand.

2.4.1 Diffusion in restricted environments

A polymer suspension is a heterogeneous environment – a relatively immobile polymer phase dispersed in a free solvent. Diffusion in a heterogeneous environment can be significantly different than diffusion in a homogeneous medium. In restricted environments, a random walker will interact with the boundaries where it may change its direction, reflect backwards, experience an interaction or become immobilized. The mathematical challenges of the analysis of restricted diffusion can be quiet interesting.⁴⁷ For example, Mitra has shown that diffusion coefficients in porous media are time dependent and the porosity of a medium can be determined from short time diffusion

coefficients.⁴⁸ In magnetic resonance imaging (MRI) restricted diffusion in tissues can yield useful physiological information.⁴⁹

Although swollen polymer gels and suspensions are heterogeneous, they are generally isotropic which makes calculation of diffusion coefficients somewhat simpler. Several models have been proposed for estimating the effect of rigid boundaries on the diffusion coefficient of a random walker in a heterogeneous isotropic medium. An early basic approach is the Mackie-Meares model,⁵⁰ which is still respected and which we have used in this study.

2.4.2 The Mackie-Meares model

Mackie and Meares proposed a random walk model in a polymeric ion exchange resin. According to Mackie and Meares, if D_0 is the diffusion coefficient of a solute in bulk solvent then the diffusion coefficient in presence of a polymer is given by equation 2.13

$$D = D_0 \left(\frac{1-V}{1+V} \right)^2 \quad (2.13)$$

where V is the volume fraction of polymer. The Mackie-Meares model has been shown to hold well for swollen polymer beads.¹⁸

2.4.3 Measurement of diffusion coefficient in swollen polymers using pulsed-gradient spin-echo (PGSE) NMR

Pulsed-gradient spin-echo (PGSE) NMR is a powerful tool to probe diffusive motion. The method is easy to employ and relatively nonperturbative. The longitudinal relaxation

time (T_1) and transverse relaxation time (T_2), and the diffusion coefficient can provide useful insights into the dynamics of a molecule and its interaction with the environment. A standard implementation of this method is to defocus the NMR bulk magnetization using a gradient magnetic field, allow for spins to diffuse for a set interval of time, apply a 180° pulse, and again refocus the magnetization. The echo signal after refocusing is related to the diffusion time and the gradient strength according to equation (2.14)

$$\frac{I(\delta)}{I(0)} = e^{-\gamma^2 \delta^2 G^2 D (\Delta - \frac{\delta}{3})} \quad (2.14)$$

where $I(\delta)$ and $I(0)$ are signal intensities in the presence and absence of the gradient, γ is the gyromagnetic ratio of the nucleus, G is the gradient strength, δ is the gradient duration interval, and Δ the time intervals between successive gradients. In a typical experiment, spectra are recorded at different gradient strengths (G) and the diffusion coefficient may be obtained by fitting the data to the above equation.

Using PGSE NMR, Pickup *et al.* found that the diffusion coefficient of toluene in swollen cross-linked polystyrene was almost the same as in a solution of linear polystyrene with the same weight fraction of polymer, and that cross-links had negligible effects.⁵¹ The diffusion coefficient decreased from $31.2 \times 10^{-6} \text{ cm}^2 \text{ sec}^{-1}$ to $1.25 \times 10^{-6} \text{ cm}^2 \text{ sec}^{-1}$ as the weight fraction of linear polystyrene increased from 0 to 0.7. The diffusion coefficient for Boc anhydrides of glycine, alanine, and phenylalanine decreased by a factor of two with respect to pure solvent in CLP beads with swelling ratio of 5.0.⁷ Ando *et al.* found diffusion of Boc protected amino acids in CLP resins to be much larger in THF than DMF.⁵² Janda *et al.* used an equivalent technique, diffusion ordered spectroscopy (DOSY), to measure diffusion coefficients of small molecules in a swollen CLP resin.¹⁹ They, too, found diffusion to be much slower in DMF than in toluene or

THF. Their diffusion coefficients mirrored the swelling ratios of their resins – an observation in accord with those made by Roucis and Ekerdt.¹⁸ The authors observed that the reactive sites inside the beads could affect the mobility of molecules by interacting with them. For example, the diffusion coefficient of free acid of Boc-glycine in amine functionalized resin was smaller than the Boc-glycine methyl ester in the same resin.

2.4.4 The Wilke-Chang correlation

The Stokes-Einstein relation for a spherical solute diffusing in a liquid can be expressed as equation (2.16)

$$\frac{T}{D\eta} = 1.004 \times 10^7 V^{1/3} \quad (2.16)$$

where T is the temperature, D diffusion coefficient, η the viscosity of the liquid and V the molal volume of solute at normal boiling point. On the basis of extensive experimental data, Wilke and Chang⁵³ recognized the group $T/D\eta$ to be largely independent of temperature and found a correlation between with the molal volume in the order of $V^{0.6}$.

The Wilke-Chang correlation is expressed in the equation (2.17)

$$D = 7.4 \times 10^{-3} \left(\frac{TM^{1/3}}{\eta V^{0.6}} \right) \quad (2.17)$$

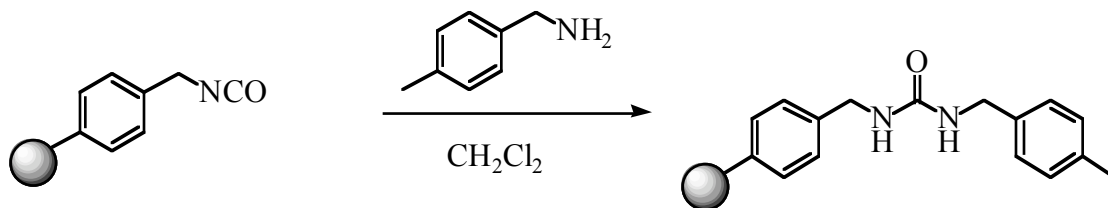
The above correlation was derived using the experimental data of 285 solute-solvent systems, and the calculated diffusion coefficient was found to be within 10% of the measured value in most cases. Such good accuracy makes the Wilke-Chang correlation a valuable tool, and it is extensively applied and cited in literature.

3.0 EXPERIMENTAL AND COMPUTATIONAL INVESTIGATIONS IN BEAD BASED REACTION PROCESSES. UNDERSTANDING THE ROLE OF DIFFUSION AND REAGENT PARTITIONING.

Our goal was to conduct a quantitative study of diffusion and reaction processes inside SPOS beads using experimental kinetic data and mathematical modeling. In developing our approach, we were most influenced by three previous reports – the 1982 paper by Roucis and Ekerdt¹⁸ on the measurement of diffusion coefficients inside polystyrene beads and the 1950 papers by Katz⁴⁰ and Eyring⁴² on mathematical modeling of diffusion and reaction in fibers. Our experimental setup is modeled on the experiments of Roucis and Eyring, with the added feature of *in situ* measurement of diffusant concentration using a UV-VIS probe.

Our prototype reaction is a reaction between polymer bound benzyl isocyanate and benzylamine (Scheme 3.1).

Scheme 3.1.



3.1 MATERIALS AND METHODS

Materials: The experiments employed 1% cross-linked polystyrene beads of three different diameters – 110, 225 and 530 μm . The smaller two sizes were used as supplied, the 530 μm beads were purchased as polymer bound benzylamine, which was converted to benzylisocyanate by treatment with phosgene. The observed swelling and loading capacities are described in Table 3.1. These bead properties did not always conform to the suppliers' specifications.

Table 3.1. Properties of polystyrene resins used in this study.

Entry	Dry bead diameter (μm)	Functional group	Supplier	Swelling capacity (mL/g)	Loading capacity (mmol/g)
1	530	Benzylamine	Rapp-polymer	8.3 ^a 8.3 ^b	8.2 ^a 5-5.5 ^b
2	225	Benzylisocyanate	Polymer Labs	5.5 ^a 4.8 ^b	1.4-1 ^a 1-0.8 ^b
3	110	Benzylisocyanate	Argonaut	8.5 ^a 4.5 ^b	1.4-0.8 ^a 0.9-1.1 ^b

^a Supplier's values, ^b Observed values. All beads were 1% CLP.

The swelling capacities were determined by taking a known weight of beads (~50 - 100 mg) in a 1 mL syringe (calibrated to ± 0.01 mL) and allowing them to swell in CH_2Cl_2 to their full capacity, (with gentle stirring to remove air bubbles). At least three measurements were performed for each bead size. The amines used were 4-methylbenzylamine, 3,3-diphenylbenzylamine and 3-phenylpropylamine. All amines were freshly distilled from CaH_2 and stored under nitrogen prior to use.

Methods: The apparatus used is presented in Figure 3.1. In a typical experiment, a 100 mL oven dried round bottom flask was charged with 65 mL of freshly distilled dichloromethane and ~50-75 mg beads (polymer bound isocyanate).

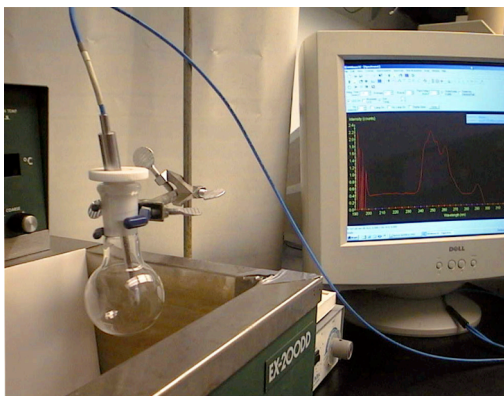


Figure 3.1. The experimental apparatus.

The flask was flushed with nitrogen, sealed with a rubber septum, and the beads were allowed to swell under nitrogen for at least an hour (110 μm beads swelled almost instantaneously). The flask was then transferred to a water bath maintained at a constant temperature of 25 ± 1 $^{\circ}\text{C}$ and the spectroscopic probe was inserted. The flask was then gently oscillated and a ~ 0.5 mL aliquot of amine in DMF was rapidly added. This created an initial bulk concentration of ~ 0.2 mmol/L, and automated spectra acquisition was started immediately after this addition. The molar extinction coefficient of the amine was separately calculated and the absorbance from bulk solution allowed us to calculate the concentration. We initially used a nylon net filter to keep the beads from entering the probe's optical path, but later experiments established that this was unnecessary.

3.2 DIFFUSION COEFFICIENT MEASUREMENTS

The diffusion coefficients of all amines were measured in CD_2Cl_2 using PGSE NMR. The diffusion coefficients inside the beads were also estimated by application of the Mackie-Meares equation.⁵⁰ The polymer volume fractions in swollen beads were determined using the observed swelling ratios and a packing fraction (volume occupied by beads/overall volume of bed of swollen beads) of 0.56.¹⁸

All diffusion experiments were performed on a Bruker 500 MHz NMR spectrometer at 25 ± 1 °C using the usual PGSE pulse sequence and with fixed times ($\Delta = 0.025$ sec) and gradients in the Z direction of up to 0.13 Tesla/m. For each experiment, at least six data acquisitions were performed with increasing gradient strength. The peaks were integrated to yield the relative echo intensities at each gradient, and the data were analyzed in accord with equation 2.14 to obtain the diffusion coefficients.

Our PGSE NMR diffusion coefficients in bulk solvent were in good agreement with the Wilke-Chang⁵³ correlation (Table 3.2). The polymer volume fraction in swollen beads required for the Mackie-Meares diffusion coefficient predictions were calculated using a packing fraction of 0.56,¹⁸ and our measured polymer density of 1.15 g/mL and led to the outcomes shown below:

Volume occupied by one gram of swollen beads:

110 and 225 μm beads: $0.56 \times 4.5 \text{ mL/g} = 2.56 \text{ mL/g}$.

530 μm beads: $0.56 \times 8.3 \text{ mL/g} = 4.65 \text{ mL/g}$.

Volume occupied by polymer in one gram of swollen beads:

$(1.0/1.15) \text{ mL} = 0.87 \text{ mL}$.

Volume fraction of polymer in a swollen bead:

110 and 225 μm beads: $0.87 \text{ mL}/2.56 \text{ mL} = \mathbf{0.34}$.

530 μm beads: $0.87 \times 4.65 \text{ mL} = \mathbf{0.2}$.

Mackie-Meares factors (equation 2.13):

110 and 225 μm beads: **0.25**.

530 μm beads: **0.5**.

Table 3.2. Experimental and calculated values of diffusion coefficients in CH_2Cl_2 .

Entry	Amine	D_{NMR} ($\times 10^{-5} \text{ cm}^2/\text{s}$)	$D_{\text{Wilke-Chang}}$ ($\times 10^{-5} \text{ cm}^2/\text{s}$)	$D_{\text{Mackie-Meares}}$ ($\times 10^{-5} \text{ cm}^2/\text{s}$)
1	4-Methylbenzylamine	2.4	2.4	1.2 ^a 0.6 ^b 0.6 ^c
2	3-Phenylpropylamine	2.2	2.2	1.1 ^a
3	3,3-Diphenylpropylamine	1.5	1.7	0.85 ^a

^a In 530 μm bead, ^b in 225 μm bead, ^c in 110 μm bead. $D_{\text{Mackie-Meares}}$ were calculated using $D_{\text{Wilke-Chang}}$ and equation 2.13.

3.3 PARTITION COEFFICIENT MEASUREMENTS

The partition coefficient ($\equiv [\text{amine}]_{\text{bead}}/[\text{amine}]_{\text{bulk}}$) of 4-methylbenzylamine was unity for all bead sizes in CD_2Cl_2 . It is essential that no free isocyanate groups be present in the beads during our partitioning experiments therefore the beads were pre-treated with methylamine. We recognize that this partition coefficient is therefore more representative of the partition coefficient effect in the later part of the experiment. The fact that the data ultimately fit well to our model promises that any change in partition coefficient during the reaction is not significant. In a typical experiment designed to measure partition coefficient, 5 μL of 4-methylbenzylamine was added to 1.0 mL CD_2Cl_2

and a 50 μL aliquot withdrawn. A 120 mg portion of dry 530 μm beads (pretreated with methylamine and thoroughly washed with aliquots of THF/toluene/dichloromethane and dried overnight under high vacuum) was then added, and the beads were allowed to swell for at least 2 h. A second 50 μL aliquot was withdrawn from this bead-treated sample. Concentrations of the two samples were compared by NMR spectroscopy. In the analysis, a 0.5 μL of benzyl alcohol (serving as an internal reference) was added to 0.7 mL CDCl_3 in an NMR tube, and the first sample aliquot was added after which the peak areas of the benzylic protons of the alcohol and the amine were recorded. To determine whether the beads had selectively absorbed any solute, the second aliquot was then added to the same NMR tube and the increase in the amine peak area was noted. This increase gave evidence of the concentration difference between the two samples. In control experiments, the peak intensities were found to increase linearly with concentration with an accuracy of 5%.

With all beads, the peak area of the amine doubled upon addition of the second aliquot, indicating that the bulk concentration remained unchanged after addition of the beads.

The relative partition coefficients of 3-phenylpropylamine and 3,3-diphenylpropylamine in 530 μm beads in CD_2Cl_2 were also determined. 5 μL of each were added to 2 mL of CD_2Cl_2 in an NMR tube and their relative peak intensities recorded. Dry beads (160 mg) were then added and allowed to swell to their maximum capacity in the NMR tube and the relative amine peak intensities recorded again. No changes in relative peak areas were observed, indicating identical partition coefficients for these amines, too.

3.4 RESULTS BASED ON OUR NUMERICAL MODELING

We believe that our numerical methods (presented in Section 3.2.2) can be used to demonstrate a valid mechanism through which diffusion will influence observed reaction rates within solid support polymer media. To support this, we will discuss three examples (Figure 3.2) that cover cases in which the rate of reaction is: (i) slow in comparison to the rate of diffusion-limited redistribution of reacting diffusant; (ii) comparable to the rate of diffusion-limited redistribution of reacting diffusant; and (iii) fast in comparison to the rate of diffusion-limited redistribution of reacting diffusant.

The relative rate of reaction and diffusion can be expressed quantitatively by the ratio $(D/a^2)/(k \cdot n_0)$,⁵⁴ which governs the concentration profiles of the diffusant inside the microsphere at any given time. This ratio is analogous to the Damkohler number (the ratio of residence time to reaction time) in combustion analysis.

Calculated distributions of amine and isocyanate within a bead (dry diameter 225 μm) are shown in Figure 3.2 for decreasing diffusion rates: (a) $D = 5 \cdot 10^{-5} \text{ cm}^2 \text{ sec}^{-1}$; (b) $D = 1 \cdot 10^{-5} \text{ cm}^2 \text{ sec}^{-1}$; (c) $D = 5 \cdot 10^{-6} \text{ cm}^2 \text{ sec}^{-1}$; (d) $D = 1 \cdot 10^{-6} \text{ cm}^2 \text{ sec}^{-1}$. In all cases $k = 0.6 \text{ L mol}^{-1} \text{ sec}^{-1}$, $n_0 = 0.45 \text{ M}$, and the bead radius, a , is 150 μm . Time increases clockwise around each circle. Each of 12 sectors is labeled with the mean reaction time represented by that sector. The third circular graph in the figure represents the product $[\text{RNH}_2][\text{RNCO}]$, a quantity that is proportional to the rate of reaction of reactants at any point. This quantity, normalized to vary from 0.0-1.0, represents the “reaction intensity” – the relative rate at which reactants are consumed at a given position at a given time

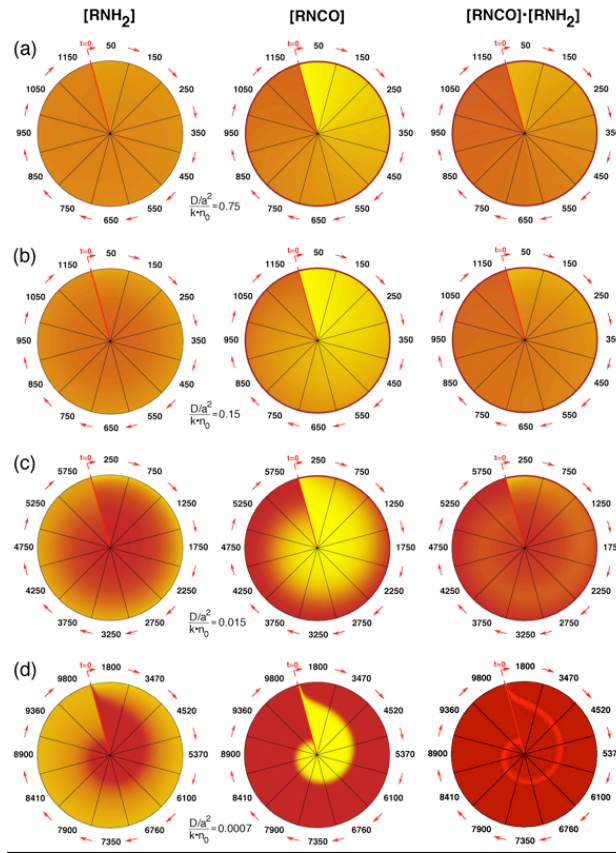


Figure 3.2. (a) Amine distribution, (b) isocyanate distribution, (c) reaction intensity inside a bead for various $(D/a^2)/(k \cdot n_0)$ values.

At the fastest diffusion rate, shown in the top row of Figure 3.2, and reading left to right, the reacting and diffusing amine (first circle) is evenly distributed throughout the bead at all times. Isocyanate (second circle) disappears evenly with time, and the reaction intensity (third circle) evenly and slowly subsides as isocyanate and amine concentrations decrease.

At the slowest diffusion rate, bottom row of Figure 3.2, amine is present only at the outer parts of the sphere and the domain, wherein amine is present, only slowly extends toward the center. At the same time, isocyanate (second circle, bottom row) is

being consumed, and there are clear domains of complete depletion of bound isocyanate (red) and unreacted isocyanate (yellow). The reaction is proceeding only in a shell of activity that moves toward the center – a ‘brushfire’ burning from the surface to the center. This burning front is illustrated in the third circle of the last row of Figure 3.2. Outside the circle, there are no available isocyanate groups. Inside the circle, there is no amine to react with the available isocyanate groups.

Technologists and commercial enterprises in the field of solid phase synthesis need guidelines for improving their products. We recommend that the factor $(D/a^2)/(k \cdot n_0)$ may be very useful; in this equation D is the diffusion rate of the reactant, a is the radius of the bead, k is the intrinsic reaction rate between the diffusing reactant, and n_0 is the concentration of the site within the bead. When this factor approaches or exceeds 1.0, diffusive mixing is faster than reaction, and the reaction process is unaffected by the presence of the polymer bead matrix. However, for fast reactions, or slow diffusion (caused, for example by lower swelling or larger diffusing reactants) the rate of consumption of any bead’s total capacity is controlled by two factors: the diffusion rate of the reacting molecule that is entering the bead, and the intrinsic reaction rate between the reacting molecule and the site within the bead.

3.5 DATA ANALYSIS BASED ON A BIMOLECULAR MODEL

We acquired data on reaction rates between amines and bead-bound isocyanate groups by measuring the concentration of amine in the external (bulk) solvent as a function of time. Our goal was to compare different size beads and to discover whether they consumed

external reactants at different rates. Data analysis (Table 3.3) using a simple bimolecular rate law assuming homogeneous solution conditions (in which all reactive components are evenly distributed throughout the available solvent volume) was applied to our concentration vs. time data and yielded rate constants (k_{bimol}) of $0.95 \pm 0.02 \text{ L mol}^{-1} \text{ sec}^{-1}$, $0.62 \pm 0.04 \text{ L mol}^{-1} \text{ sec}^{-1}$, and $0.4 \pm 0.07 \text{ L mol}^{-1} \text{ sec}^{-1}$ for 110, 225 and 530 μm beads, respectively (the uncertainties correspond to the 90% confidence intervals based on Student's t - distribution). Figure 3.3 shows representative data and best-fit predictions for the three different bead sizes.

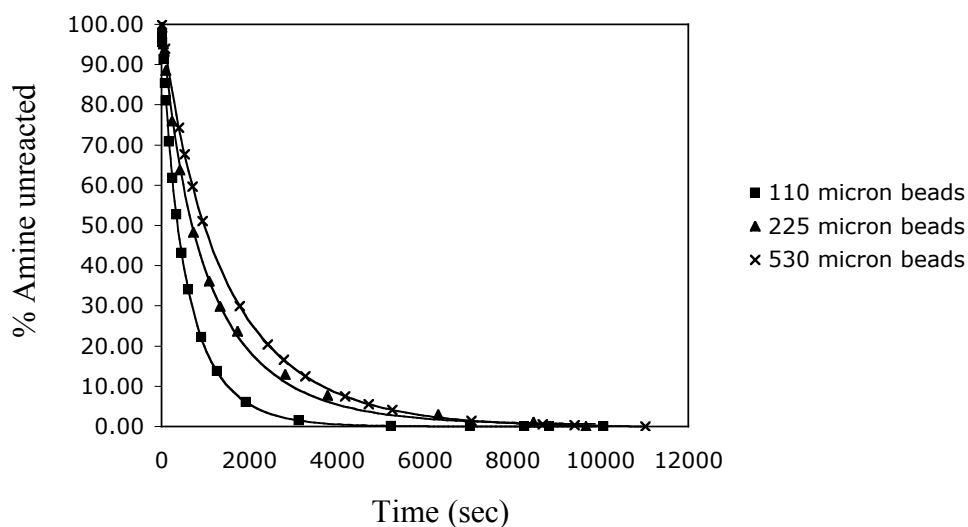


Figure 3.3. Representative fits for the homogeneous solution reaction model. The markers show the experimental data, and the solid lines are the best fits obtained using the simple second order bimolecular rate law. The rate constants, k_{bimol} , are $0.98 \text{ L mol}^{-1} \text{ sec}^{-1}$, $0.65 \text{ L mol}^{-1} \text{ sec}^{-1}$, $0.44 \text{ L mol}^{-1} \text{ sec}^{-1}$ for 110 μm , 225 μm and 530 μm beads respectively.

Table 3.3. Simple bimolecular rate constants for three experiments on each bead size.

Entry	Dry bead dia. (μm)	Resin loading capacity (mmol/g)	k_{bimol} ($\text{L mol}^{-1} \text{sec}^{-1}$)
1	110	1.1	0.96
2	110	1.1	0.96
3	110	1.14	0.94
4	225	0.96	0.65
5	225	0.96	0.6
6	225	1.0	0.6
7	530	0.55	0.35
8	530	0.6	0.46
9	530	0.57	0.4

In all cases the observed data fit adequately to a simple bimolecular model. Why do the same functional groups on similar polymer supports with the same solvent and temperature give different apparent reaction rates? Diffusion controlled mixing may be part of the answer. Partition coefficient or swelling differences cannot be the reason; the two smaller bead sizes had near identical swelling, partition coefficients, and load capacity.

The apparent good fit can hide the fact that the physical model is wrong. There are systematic deviations, but they will probably be obscured by random error. The ‘false’ bimolecular rate constant obtained in the above analysis is always smaller than the true (internal) bimolecular rate constant. Restricted mixing in the beads reduces the reaction rate by as much as 80% for small solutes and well-swollen beads. Larger

solutes, and less swollen beads will suffer greater rate diminishment. These issues are discussed in the next section.

3.6 DIFFUSION-REACTION MODEL

The rate constants obtained from a non-linear fit to the diffusion-reaction model would be more indicative of the true rate constants. Our data fit well with the diffusion-reaction equation (Figure 3.4) for our expected values of diffusion coefficients and rate constants.

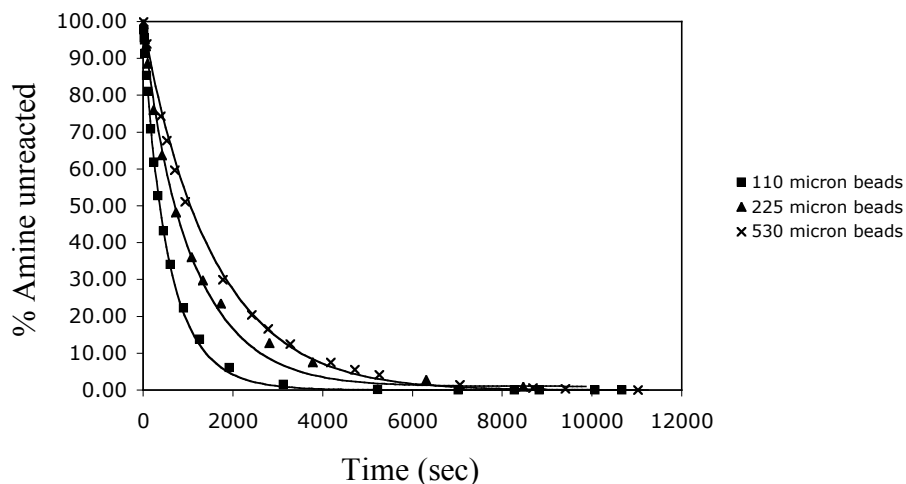


Figure 3.4. Representative fits for the diffusion-reaction model. The markers show the experimental data, and the solid lines are the best fits obtained using the diffusion-reaction equation. The rate constants, k , are $1.12 \text{ L mol}^{-1} \text{ sec}^{-1}$, $0.98 \text{ L mol}^{-1} \text{ sec}^{-1}$, $0.74 \text{ L mol}^{-1} \text{ sec}^{-1}$ for 110 μm , 225 μm and 530 μm beads respectively.

Table 3.4. Diffusion-reaction rate constants for three experiments on each bead size.

Entry	Dry bead dia. (μm)	Resin loading capacity (mmol/g)	$D_{\text{Mackie-Meares}}$ ($\times 10^{-5} \text{ cm}^2/\text{s}$)	k ($\text{L mol}^{-1} \text{ sec}^{-1}$)
1	110	1.1	0.6	1.17
2	110	1.1	0.6	1.13
3	110	1.1	0.6	1.12
4	225	0.96	0.6	1.05
5	225	0.96	0.6	0.93
6	225	1.0	0.6	0.97
7	530	0.55	1.2	0.47
8	530	0.6	1.2	0.7
9	530	0.57	1.2	0.56

For the diffusion coefficients estimated from the NMR data and Meares' formula (Table 3.2), the diffusion-reaction rate constants were $k = 1.14 \pm 0.03 \text{ L mol}^{-1} \text{ sec}^{-1}$, $k = 1.0 \pm 0.05 \text{ L mol}^{-1} \text{ sec}^{-1}$, and $k = 0.58 \pm 0.16 \text{ L mol}^{-1} \text{ sec}^{-1}$ for 110, 225 and 530 μm beads, respectively (Table 3.4). These rate constants are somewhat more consistent than k_{bimol} , especially for the smaller two beads, which had similar swelling. There also appears to be a correlation between the reaction rate constants and the loading capacities (Table 3.4). The loading can affect the reaction rate in two ways – first, higher loading will lead to a more polar environment and enhanced reaction rate. The neighboring ureas can also facilitate the reaction by forming hydrogen bonds. Secondly, it is possible that the reactivity of the isocyanate groups is non-uniform within a bead and especially for the largest bead, the most reactive sites have been destroyed before the reaction, giving it a

much lower loading and reaction rate. We don't know how much the neighboring groups affect the reaction rate, but second argument seems unlikely because it can be seen that our data fit quite well to the uniform reactivity model. Our simulations yielded consistent loading capacities for each size indicating the beads were stored properly and the experiments performed under identical conditions (Table 3.3 and 3.4). We have not yet corrected for non-specific (excluded volume) effects on activity. We will now address this effect.

Excluded volume effects on diffusant activities must be included when beads of different free solvent volumes are compared. As the fraction of polymer in the bead increases, excluded volume effects will increase the activity of the diffusant. We propose that to properly compare the internal rate constants among different swollen polymers, the concentrations should be corrected to unit activity. The excluded volume activity coefficients for the three beads are $1.53 \text{ L mol}^{-1} \text{ sec}^{-1}$, $1.53 \text{ L mol}^{-1} \text{ sec}^{-1}$, $1.25 \text{ L mol}^{-1} \text{ sec}^{-1}$, respectively (equation 1.2 and Table 3.5), and with this correction, the final rate constants we record for the three beads are 0.75 ± 0.02 , 0.65 ± 0.03 , and $0.47 \pm 0.13 \text{ L mol}^{-1} \text{ sec}^{-1}$, respectively.

Table 3.5. The activity coefficients in beads on the basis of available volume theory.

Entry	Dry bead dia. (μm)	Swelling capacity (mL/g in CH_2Cl_2)	Polymer volume fraction	Activity coefficient ^a (γ)
1	110	4.5	0.34	1.53
2	225	4.5	0.34	1.53
3	530	8.3	0.2	1.25

^a from equation 1.2.

Thus, when the effects of restricted mixing are incorporated, the supported isocyanate-amine reaction rate constants for the three different size beads are in closer agreement. The reaction rates are not exactly the same, but as mentioned earlier, there could be an affect from the loading capacity.

3.7 EMPIRICAL CORRELATION BETWEEN SIMPLE BIMOLECULAR AND DIFFUSION-REACTION REACTION RATES

The excellent fits from both the simple bimolecular and the diffusion-reaction rate equations leads to the following question. Under what conditions is the simple bimolecular rate law sufficient to describe the reaction kinetics and lead to an accurate measure of the internal rate constant. Generally these would be the conditions in which the effects of restricted mixing due to diffusion are minimized. To find this domain, fourteen different sets of data using the diffusion-reaction equation were created (calculated using our numerical methods) for various bead sizes and diffusion rates. The factor $(D/a^2)/(k \cdot n_0)$ (Section 3.4) varied from ~ 0.01 -3.0 (Table 3.6). The simple bimolecular rate law was fitted to these data sets and the diffusion-reaction and the simple bimolecular rate constants (k and k_{bimol}) were determined from these best-fit optimizations. The ratio of the false bimolecular rate constant to the true (internal) rate constant (k_{bimol}/k) vs. $(D/a^2)/(k \cdot n_0)$ is shown in Figure 3.5. The relationship is well expressed by the equation 3.1.

$$\frac{k_{bimol}}{k} = \frac{\frac{D/a^2}{k \cdot n_0}}{0.035 + \frac{D/a^2}{k \cdot n_0}} \quad (3.1)$$

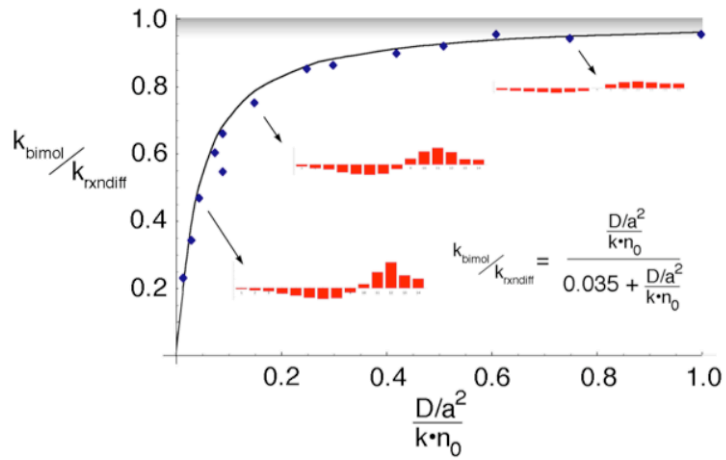


Figure 3.5. Empirical correlation between k_{bimol}/k and $(D/a^2)/(k \cdot n_0)$.

Table 3.6. Reaction kinetics parameters from simulated data.

Entry	a , cm	n_0 , mol/L	D (cm ² /s)	k_{bimol} (L mol ⁻¹ sec ⁻¹)	k (L mol ⁻¹ sec ⁻¹)	$(D/a^2)/(k \cdot n_0)$
1	0.0156	0.454	0.00001	0.473	0.6	0.15
2	0.0156	0.439	0.000001	0.194	0.667	0.014
3	0.0156	0.453	0.00016	0.593	0.6	2.43
4	0.0156	0.455	0.000003	0.323	0.60	0.045
5	0.0156	0.454	0.000034	0.558	0.6	0.51
6	0.0156	0.453	0.0005	0.572	0.6	0.76

Table 3.6 continued,

7	0.0156	0.454	0.000005	0.392	0.6	0.075
8	0.0076	0.453	0.00005	0.592	0.59	3.22
9	0.0369	0.454	0.00005	0.253	0.285	0.28
10	0.0156	0.454	0.000017	0.519	0.6	0.26
11	0.0156	0.454	0.000028	0.549	0.6	0.42
12	0.0076	0.454	0.000034	0.558	0.56	2.3
13	0.0369	0.455	0.000034	0.417	0.6	0.09
14	0.0076	0.454	0.00005	0.532	0.6	0.32
15	0.0369	0.431	0.00005	0.187	0.7	0.012
16	0.0156	0.455	0.00006	0.416	0.6	0.09

If k/k_{bimol} is plotted against $n_0 \bullet k/(D/a^2)$ (the relative rates of reaction and diffusion), the empirical correlation is obtained as a linear equation (equation 3.2 and Figure 3.6) as opposed to the hyperbola in equation 3.1. These simulations and empirical relationships can serve as a helpful guideline in deciding how accurate a simple homogeneous solution bimolecular model would be for a given set of conditions. It also lets one estimate the true internal rate constant (k) if D , a , n_0 , and the false homogeneous solution model rate constant k_{bimol} (which are mathematically easier to obtain) are known.

$$\frac{k}{k_b} = \frac{0.035n_0k}{D/a^2} + 1.0 \quad (3.2)$$

The results of application of equation 3.2 to our experimental data are shown in Table 3.7. For comparison, the intrinsic rate constants obtained from both the Crank-Nicolson method and the empirical correlation are shown.

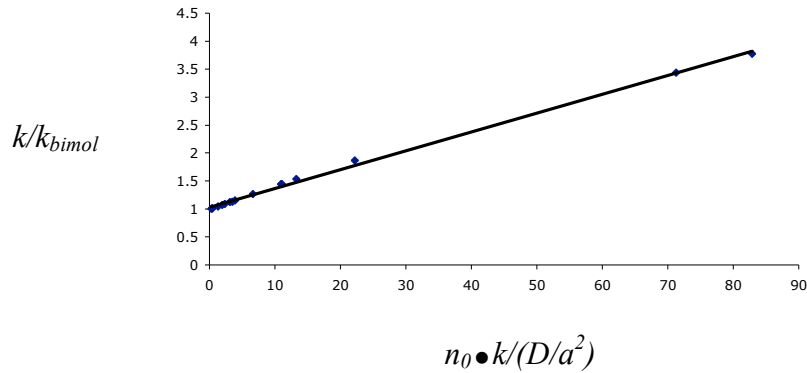


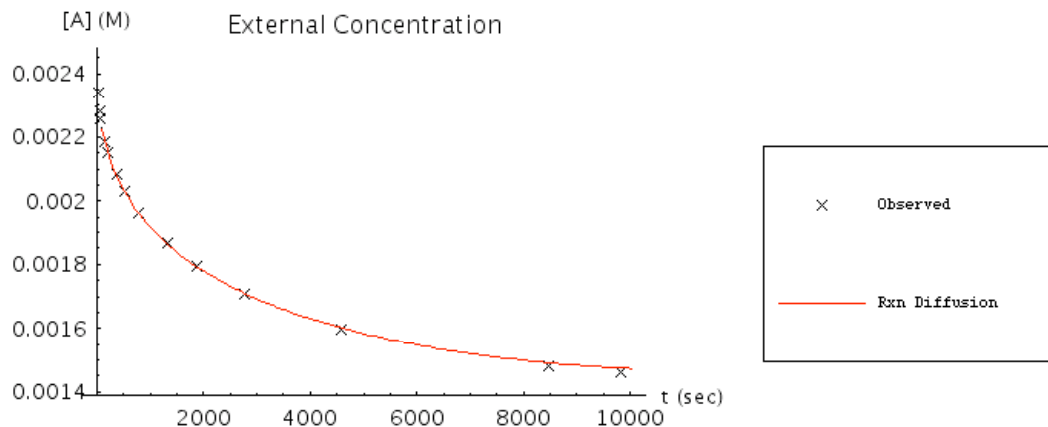
Figure 3.6. Linear empirical correlation between k/k_{bimol} and $n_0 \bullet k/(D/a^2)$.

Table 3.7. Reaction rate constants from Crank-Nicolson and the empirical correlation.

Entry	Swollen bead radius (a , cm)	Reactive site conc. (n_0 , mol/L)	D ($\times 10^{-5}$ cm ² /s)	k_{bimol} (L mol ⁻¹ sec ⁻¹)	k^a (L mol ⁻¹ sec ⁻¹)	k^b (L mol ⁻¹ sec ⁻¹)
1	0.0076	0.43	0.6	0.96	1.17	1.12
2	0.0076	0.44	0.6	0.96	1.13	1.12
3	0.0076	0.45	0.6	0.94	1.12	1.10
4	0.015	0.38	0.6	0.65	1.05	0.96
5	0.015	0.38	0.6	0.60	0.93	0.86
6	0.015	0.41	0.6	0.60	0.97	0.88
7	0.045	0.12	1.2	0.35	0.47	0.46
8	0.045	0.13	1.2	0.46	0.70	0.71
9	0.045	0.12	1.2	0.40	0.56	0.56

^a Crank-Nicolson rate constants, ^b empirical correlation rate constants from equation 3.2.

It can be seen that the diffusion-reaction rate constants calculated from the empirical correlation (column 7) are in good agreement with the Crank-Nicolson curve fitting (column 6). There is some error for the medium size bead, but that is probably because the simple bimolecular rate law did not fit well to the experimental data in this case. For the other two sizes, the agreement is excellent. Thus the empirical correlation allows one to calculate the true rate constants without any complicated calculations. In our simulations, the factor $(D/a^2)/(k \cdot n_0)$ varied from 0.01 - 3.0. It was found that the empirical correlation held good down to $(D/a^2)/(k \cdot n_0) \sim 0.008$, below which significant error was observed when large bead size (530 μm) was used. This happens because in this limit the reaction is significantly faster than diffusion and the data clearly deviate from the simple bimolecular rate law. Figure 3.7 below shows one such example where $(D/a^2)/(k \cdot n_0) = 0.0007$. It can be seen that a simple bimolecular rate law does not fit well to this reaction.



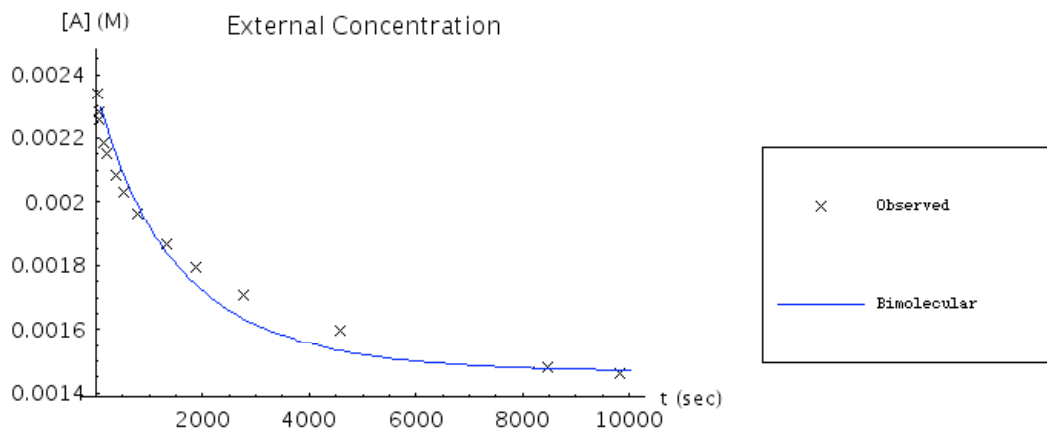


Figure 3.7. A simulated diffusion–reaction process for $(D/a^2)/(k \cdot n_0) = 0.0007$. (Above) diffusion-reaction equation fit, (below) a simple bimolecular rate law equation fit.

Thus, the empirical relationship can provide a quick calculation to determine how significant the effect of diffusion would be on a given simple bimolecular SPOS reaction without any complex calculations. (The rate constants obtained, however, are not corrected for any activity effects).

3.8 A DIRECT MEASUREMENT OF EFFECTS OF DIFFUSION ON REACTION RATES

So far our results indicate indirect evidence of diffusion control in the reaction between benzylamines and different beads. To obtain a direct evidence, two amines of different diffusion coefficients but similar reactivity – 3-phenylpropylamine and 3,3-diphenylpropylamine were chosen to react with the 530 μm beads. The largest size beads were chosen because effects of diffusion increase with size. These amines showed the same rate of reaction with benzylisocyanate in dichloromethane under well-stirred

homogeneous solution reaction conditions. This was established by adding 1.0 mmol of benzylisocyanate to a stirred solution (100 mL) of dichloromethane containing 1.0 mmol of each amine. The NMR spectrum the reaction mixture showed complete consumption of benzylisocyanate after 30 min and the peak integrations indicated both the amines to have been consumed in equal amounts. The partition coefficients of the two amines were also the same. The diffusion coefficients of these amines were measured to be 2.2×10^{-5} cm^2/s , and 1.5×10^{-5} cm^2/s in pure dichloromethane and agreed well with the Wilke-Chang correlation (Table 3.2). Our simulations indicated the difference in the diffusion coefficients of the two amines was large enough to give a detectable difference in their scavenging rates.

Figure 3.8 shows simple bimolecular rate law equation fits to the scavenging data of 3-phenylpropylamine and 3,3-diphenylpropylamine.

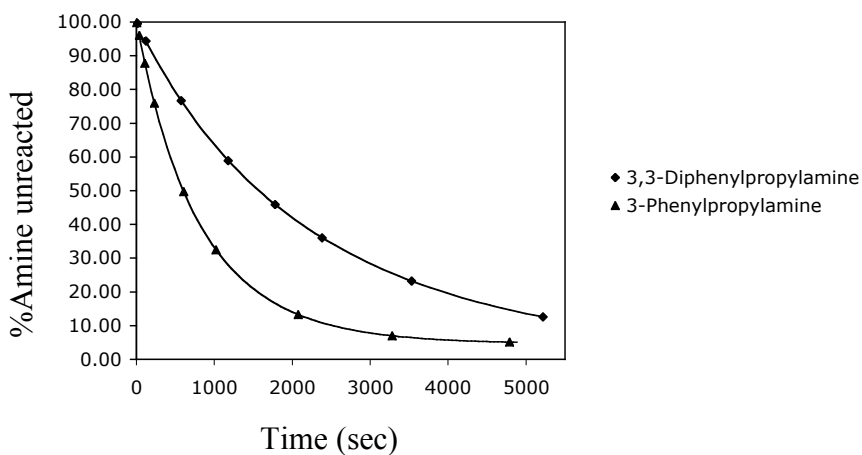


Figure 3.8. Simple bimolecular rate law fits for the reaction of 530 μm beads with 3-phenylpropylamine ($k_{bimol} = 0.54 \text{ L mol}^{-1} \text{ sec}^{-1}$), and 3,3-diphenylpropylamine ($k_{bimol} = 0.24 \text{ L mol}^{-1} \text{ sec}^{-1}$).

In the above example, the simple bimolecular rate constants obtained are $k_{bimol} = 0.54 \text{ L mol}^{-1} \text{ sec}^{-1}$, and $k_{bimol} = 0.24 \text{ L mol}^{-1} \text{ sec}^{-1}$. From our empirical correlation, the corresponding diffusion-reaction rate constants are $k = 0.77 \text{ L mol}^{-1} \text{ sec}^{-1}$ and $k = 0.32 \text{ L mol}^{-1} \text{ sec}^{-1}$. Crank-Nicolson simulations also yield similar values. Thus, the intrinsic reactivity of the larger amine inside the bead is lower, whereas it is same in homogeneous solution. This is probably due to nonspecific activity effects arising from interaction with polymer backbone. The specific activity effects will *increase* the activity of the bigger amine as lower free volume is available to the bigger amine. We have also not taken into account any kinetic barrier that may exist at the surface of the swollen bead (due to boundary layer effects) that may influence the mobility of the diffusants.

In conclusion, we developed the first mathematical model to quantitatively understand the factors affecting reaction rates in solid phase synthesis. Our theoretical and experimental investigations show that diffusion can be an important factor in SPOS reaction kinetics, and its influence increases with the bead size. The presence of polymer backbone affects the activity. Under many common reaction conditions, however, the presence of polymer may not have significant effects. General guidelines to identify these conditions have been developed. Our results will be useful to technologists working in the synthesis of solid supports who want to improve their products.

4.0 EFFECTS OF NONCOVALENT INTERACTIONS AND SOLVATION ON MOLECULAR CONFORMATIONS AND THEIR COMPUTATIONAL MODELS

4.1 DISPERSION FORCES AND NONCOVALENT INTERACTIONS

Noncovalent interactions between atoms, molecules, or aggregates can be broadly categorized as 1) Keesom forces - between permanent dipoles, 2) Debye forces - due to polarization caused by an external field, 3) London dispersion forces - due to interactions between correlated transient dipoles arising from the perpetual motion of charges because of their wave nature. A good review of these forces has been reported by Dr. Jaemoon Yang.⁵⁵

The London dispersion forces⁵⁶ (also called the van der Waals forces) are the weakest noncovalent interactions, and are always present, even among neutral atoms and molecules that are not influenced by Keesom or Debye forces. While individually these forces may be weak, they are additive, and can be significant for large molecules and aggregates, provided their separation is less than their sizes, and that's why for example, large alkanes are solid at room temperature – the dispersion interactions are strong enough to counter the thermal energy $k_B T$.⁵⁷ Hamaker extended London's theory to intermolecular attractions between macromolecules.⁵⁷ Casimir gave an alternative interpretation of these forces on the basis of electromagnetic fluctuations in vacuum.⁵⁸

Dispersion forces continue to be an active area of theoretical and experimental investigations.

Over the past century, several noncovalent interactions have been identified. These include the CH/ π ,⁵⁹ OH/ π ,⁶⁰ CH/O,⁶¹ ion/ π ,⁶² the venerable salt bridge,⁶³ various halogen bonds⁶⁴ and hydrophobic effects.⁶⁵ Several experimental and computational studies have suggested that dispersive forces have an important part in these interactions.⁶⁶ These interactions play a part in determining the structure of biological macromolecules where several of these interactions can operate simultaneously.

The CH/ π is a weak (<2 kcal/mol), neutral noncovalent interaction between a C-H and a π system such as an aromatic ring, C=C double or a C≡C triple bond, or convex surfaces of fullerenes and nanotubes.⁵⁹ It was first observed by Itaka⁶⁷ in the crystal structure of 1-(*p*-bromophenyl)ethyl *t*-butyl sulfoxide as an intramolecular interaction between the *tert*-butyl group and the phenyl ring and has since then been extensively studied with crystallographic and spectroscopic (IR, UV, NMR) techniques and computational methods. The CH/ π interaction can influence molecular recognition, protein folding, supramolecular chemistry, diastereoselective reactions, crystal packing, host guest chemistry, and self-assembly.^{59a} It may be distinguished from conventional hydrogen bonds by its dispersive origin, entropic favorability and weak directional constraints.⁵⁹

4.2 COMPUTATIONAL METHODS FOR DISPERSION INTERACTIONS

Although dispersion forces are theoretically well understood, they present a significant computational challenge, and an accurate *ab initio* calculation that properly represents dispersion effects can be difficult even for simple systems involving only a handful of atoms. Methods such as Hartree-Fock can be unreliable, and usually experimental data is used to parameterize computational methods. The experimentally measured enthalpy of formation of water dimers through hydrogen bonding was used to calibrate the AM1 and PM3 methods.⁶⁸ In a performance study of the AMBER94, MMFF94, and OPLS-AA force field models, Jorgensen and Kaminski found the parameterization of dispersion interactions to be the source of significant error in MMFF94 in modeling the physical properties of organic liquids.⁶⁹ The failure to accurately account for dispersive interactions can be especially problematic in predicting transition state geometries where these interactions can be more important than in the ground state.⁷⁰ As computational methods evolve, and computing power grows, good experimental data is needed for parameterization of methods used in our field and these data will allow us to test the accuracy of any computational method. The nature of the bottleneck in this area is well-described by Charles L. Brooks, III, an authority in computational methods, who wrote:

“In addition to the general difficulty that force fields optimized with high-level quantum mechanics are not directly transferable to solvent environments, there is a severe lack of direct experimental data on solvation energies of proteins as well as [on] the pairwise interactions between polar groups in solvent environments. As such, it appears that one has to resort to explicit water simulations and (indirect) experimental observables (e.g.,

thermodynamic stability and conformation equilibria of peptides and proteins) in the implicit solvent force field optimization efforts.” (C. L. Brooks, III; 2006)⁷¹

Our approach to meeting this need for experimental data is to synthesize minimal protein folding models that isolate pair-wise polar interactions, non-polar interactions, and hydrophobic (solvation-driven) interactions, and to study the behavior of these minimal models in aqueous and non-aqueous media.

4.3 SOLVATION EFFECTS IN WATER

Water is the medium of life and the most abundant solvent present in nature, and for these reasons, it is appropriate that water is also the most studied solvent in chemistry.⁷² The high polarity of water, the low polarizability of water, and the strongly hydrogen bonded network among water molecules contribute to water's exceptionally high polarity, dielectric constant, heat capacity, viscosity and cohesiveness. The cohesiveness of water and its low polarizability are responsible for hydrophobic effects, which greatly influence the shape and solubility of solutes, especially of non-polar macromolecules. A good review of structure of water and classical hydrophobic effects has been reported by Dr. Jaemoon Yang.⁵⁵ Hydrophobic and more general solvophobic effects appear in diverse contexts. To introduce our work we focus on two themes – the current state of computational models of aqueous solvation and the theory of hydrophobic effects developed by Lum, Chandler, and Weeks.⁷³ The data from our torsion balance experiments will be analyzed in the context of current computational approaches used to address these issues.

4.3.1 The explicit and implicit solvation models of water

The important chemical reactions in commerce and almost all chemical reactions in living systems, take place in a liquid phase or a liquid phase in contact with another (liquid or solid) phase. The effect of the solvent is undeniable. The incorporation of solvent effects upon any chemical agent in these phases is essential for the accurate modeling of our world.⁷⁴ For those who seek to predict the behavior of any real-world chemical system, the presence of solvent poses a significant computational challenge.

Solvation models have been divided into two categories – explicit and the implicit solvation models.⁶⁸ Explicit solvation models treat solvent as discrete molecules surrounding a solute. For example, in typical protein folding kinetics, water layers of 10 Å thick or more, which can contain thousands of discrete water molecules, are required. The molecular dynamic simulations are performed using chosen force fields and all interactions are considered explicitly. Due to the many degrees of freedom, explicit consideration of solvent is computationally expensive. In a 1998 study by Duan and Kollman, a one microsecond MD simulation of peptide containing 36 amino acids with explicit water representation required 6 months on a Cray T3D supercomputer.⁷⁵

Implicit solvent models were introduced as a more practical alternative. In these models, the solvent is considered as a statistical continuum that has its own potential functions. The first implicit solvation model was introduced by Still to model water and is known as the Born model.⁷⁶ In the Born model, solvation free energy is a sum of a solvent cavity energy, a solute-solvent van der Waals energy and a solute-solvent electrostatic polarization energy term.

$$G_{solvation} = G_{cavitation} + G_{vdW} + G_{polarization} \quad (4.1)$$

It had been known that the solvation free energy of saturated hydrocarbons in water is linearly related to the solvent accessible surface area and Still assumed

$$G_{cavitation} + G_{vdW} = \gamma \times ASA \quad (4.2)$$

where is the ASA is the solute's miscible surface area and γ is an empirical atomic solvation parameter, also recognized in the literature as microscopic surface tension.

4.3.2 Estimations of γ – the microscopic surface tension of water.

Lee and Richards (1973) introduced the concept of solvent accessible surface area in the context of the van der Waal's interaction between surfaces of proteins.⁷⁷ Lee et al., in their 1981 study, established a linear correlation between the percentage buried area of the amino acid residues in folded proteins and their transfer free energies from water to organic solvents.⁷⁸ The slope in their linear relationship was identified as γ and found to be $\sim 20 \text{ cal/mol}\cdot\text{\AA}^2$. This was the first empirical determination of microscopic contact free energy at the interface between water and hydrophobic groups. This was, however, in disagreement with the macroscopic contact free energy at the water-hydrocarbon interface which is $\sim 72 \text{ cal/mol}\cdot\text{\AA}^2$.^{79, 80} The discrepancies between and macroscopic and microscopic γ have been addressed by Dill and Honig as arising from uncertainties in activity coefficients in the transfer experiments.^{79, 80} They have proposed an updated value of $47 \text{ cal/mol}\cdot\text{\AA}^2$ by taking into account the solute and solvent sizes in the transfer experiments and correcting for the activity coefficients. The values of γ mentioned in literature range from 3 - $200 \text{ cal/mol}\cdot\text{\AA}^2$.⁸¹ Lum, Chandler, and Weeks proposed the interesting idea that γ is solute size dependent (*vide infra*).⁷³

4.3.3 The Lum, Chandler, and Weeks (LCW) theory of hydrophobic effects

Hydrophobic effects have unique thermodynamic features that have historically been measured by hydrocarbon-water partitioning experiments.⁷⁹ The partitioning of a hydrophobic molecule such as a hydrocarbon from its own neat phase to an aqueous phase is equated to the difference in chemical potential or the free energy of the solute in two phases. At equilibrium, the free energy change associated with the transfer is related to the concentrations of the solute in two phases by $\Delta G_{transfer} = RT \cdot \ln[C_1/C_2] = \Delta H_{transfer} - T\Delta S_{transfer}$, where C_1 and C_2 are the solute concentrations in two phases and $\Delta H_{transfer}$ and $\Delta S_{transfer}$ are the enthalpy and entropy of transfer. Early experiments in partitioning of hydrocarbons between water and their own neat phase revealed a large unfavorable entropic component in $\Delta G_{transfer}$.⁸² Further, both $\Delta H_{transfer}$ and $\Delta S_{transfer}$ were found to be strongly temperature and solute size dependent (Figure 4.1 below). The transfer of solute to water is generally accompanied by change in heat capacity of water, which can be determined by standard van't Hoff analysis (the application of equation 4.2 to the equilibrium constant versus temperature curve).⁸³

$$R \ln(k) = -\left(\frac{\Delta H_0}{T}\right) + \Delta C_p^0 \ln(T) + (\Delta S_0 - \Delta C_p^0) \quad (4.2)$$

The heat capacity change is an important experimental observable and is routinely measured calorimetrically in protein science and host-guest chemistry.

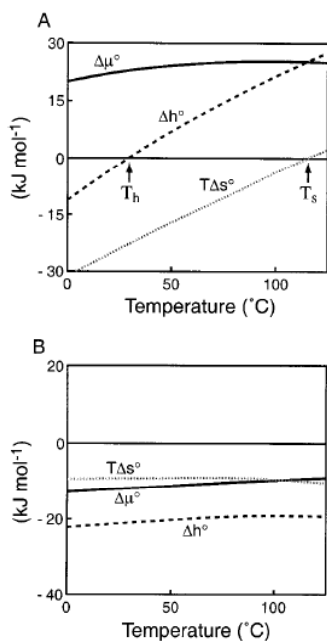


Figure 4.1. (A) Transfer of neopentane from its neat phase to water and (B) transfer of neopentane from gas phase into liquid neopentane phase. T_s and T_h represent temperatures where the entropy and enthalpy of transfer are zero.⁸²

On a molecular level, the observed solute size dependence of the hydrophobic effect has been rationalized on the basis of arguments first set forth by Stillinger: for small solutes, the hydrogen bond network in water is not significantly distorted, however, there is an entropic penalty due to decrease in available configuration space for the water molecules.⁸⁴ For large molecules, the hydrogen bond network is broken to accommodate the solute, and this results in an enthalpy of solvation. The density of water in the vicinity of the solute also decreases, causing a dewetting. The conditions when small-scale hydrophobic effects approach the large-scale hydrophobic effects are an active area of experimental and computational investigations. Recent computer simulations have shown that molecules as small as neopentane can induce a hydrophobic response similar to large hydrophobic surfaces.⁸⁵

Lum, Chandler and Weeks have developed a quantitative framework for these ideas. The LCW theory can predict the solute size and temperature dependence of the hydrophobic effect.⁷³ The implementation of LCW theory requires prior knowledge of the equation of state, surface tension and radial distribution function of water, which can be generally obtained from experimental data. As an illustration of LCW, Figure 4.2 shows the theoretical prediction of how the excess chemical potential depends upon the area of exposed surface.

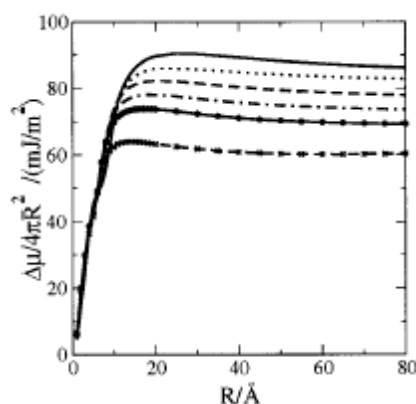


Figure 4.2. Excess chemical potential per unit area vs. solute radius.^{73b}

Despite the frequent application of the LCW theory, experimental studies have seldom been able to isolate and measure hydrophobic effects on folding,⁸⁶ and often, these studies focus on γ , the excess solvent free energy parameter. Chandler's LCW theoretical approach predicts that for spherical non-polar particles, γ rises steeply as the radius increases from 2 to 12 Å with a slope of approximately 7 cal/mol•Å² and at 298 K reaches a plateau at about 110 cal/mol•Å².

4.4 STUDIES ON NONCOVALENT INTERACTIONS AND SOLVENT EFFECT USING THE WILCOX MOLECULAR TORSION BALANCE

Wilcox and coworkers introduced the molecular torsion balance (Figure 4.3) in the 1990's.⁸⁷ It serves as a unique tool to quantitatively study weak interactions in well defined contexts. Kim and Paliwal examined the role of electron donating and electron withdrawing substituents on CH/ π and edge to face aromatic interactions, NH/ π , OH/ π , halogen/ π interactions and the effect of solvents on these interactions.^{88, 89} They found that these interactions were principally driven by London dispersion forces and aromatic substituents had little effect on CH/ π and edge to face interactions (Table 4.1). The average folding in organic solvents was ~ 0.3 kcal/mol for edge to face interactions and 0.5 kcal/mol for methyl-aryl interactions. The relevance of these results for biology is unclear because these studies were not conducted in water.

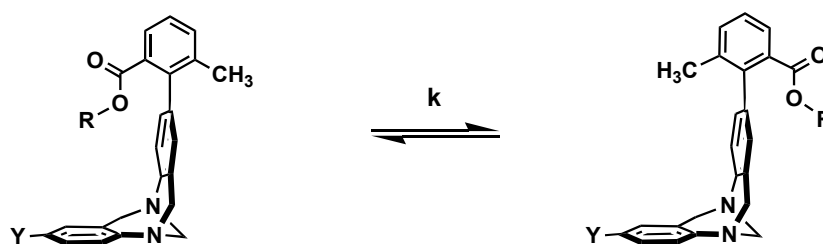


Figure 4.3. Folded and unfolded conformations of the torsion balance.

Table 4.1. Effect of substituent on folding ratios.⁸⁷

Entry	Y	ΔG_{fold}^0 ($\pm 10\%$) ^a		
		R = CH ₃	R = CH(CH ₃) ₂	R = C ₆ H ₅
1	NO ₂	0.11	-0.40	-0.10

Table 4.1 continued,

2	CN	0.06	-0.58	-0.24
3	I	-0.06	-0.52	-0.29
4	Br	0.02	-0.52	-0.24
5	H	-0.17	-0.52	-0.22
6	CH ₃	-0.04	-0.48	-0.31
7	OH	-0.03	-0.50	-0.26
8	NH ₂	-0.06	-0.40	-0.24

^a kcal/mol in CDCl₃ at 298 K.

The preference for the folded state was in a small part attributed to the change in net dipole moment of the molecule upon folding, in addition, the electron withdrawing substituents also slightly favored the folded state. This small folding energy due to dipolar effects had to be subtracted from the overall ΔG^0 to get the desired interaction energies. In the new torsion balance, the methyl group has been replaced by a methyl ester and this correction is not needed.

Paliwal reported the solvent effect on the folding equilibrium of phenyl ester (Table 4.2).⁸⁸ The polarity and the size of the solvent had a negligible effect on folding equilibrium. The range of solvents, however, does not include some important solvents such as fluorinated solvents, alcohols and water. The effects of these solvents on folding and rotation rates will be discussed in the present study.

Table 4.2. Folding ratios of a phenyl ester in different solvents.⁸⁸

Entry	Solvent	E _T (kcal/mol)	%Folded
-------	---------	---------------------------	---------

Table 4.2 continued,

1	CCl ₄	32.5	60
2	C ₆ D ₆	34.5	64
3	CDCl ₃	39.1	61
4	C ₂ Cl ₄	-	60
5	(CHCl ₂) ₂	39.4	62
6	DMSO	45.0	60
7	CD ₃ CN	46.0	62
8	CD ₃ NO ₂	46.3	62
9	CD ₃ OD	55.5	66

4.5 COMPUTATIONAL STUDIES ON THE TORSION BALANCE

Computational studies on the torsion balance have been reported by Houk,⁹⁰ Orozco,⁹¹ and Hunter.⁹² Houk and Nakamura performed computational analysis of the edge-to-face aromatic interactions in phenyl ester torsion balances using AMBER, MM2, MM3 and MMFF. The computations were done in both gas and liquid phase (using GB/SA model). They found that both gas phase and liquid phase simulations correctly showed a preference for the folded state, however, the gas phase tended to overestimate the folding energies by 1-3 kcal/mol. The preference for the folded state decreased in liquid phase because of stabilizing interactions with the solvent. These results are important because they highlight the role of solvent in folding. This will be especially important in the case

of water because it will solvate the torsion balance and it may encourage folding because of hydrophobic effects.

The effects of solvation have also been quantitatively evaluated by Hunter. According to Hunter, the solvent, the arene, and the ester interact with each other in a pair wise manner and folding equilibrium is guided by the discreet sum of all these interactions. Thus, if the H-bond interactions between the arene and the solvent are bigger than arene-ester interaction, the preference would tilt toward unfolded state. The magnitudes of these interactions were estimated using solubility parameters developed by Hunter. Hunter's explains why the edge-to-face interaction are independent of the substituent in the arene: in his view it is because chloroform has similar H-bond donor capabilities as the phenyl or the isopropyl group, and the balance of the interactions are independent of the properties of the face ring.

Orozco et al. studied the torsion balance with MP2 level quantum mechanical calculations. Similar to Houk, they also found that the gas phase tended to overestimate the folding energies. They made a unique observation that the hinge angle plays an important role in folding, especially when an electrostatic component (which is very distance sensitive) is present in the interactions. Thus, the aryl-aryl interactions, which have a bigger electrostatic component, are affected more than the aryl-alkyl interactions.

It can be seen that even for this relatively small system, several factors need to be considered to properly account for folding energies, and it makes the torsion balance an interesting and a challenging target for computational chemists.

5.0 WATER SOLUBLE TORSION BALANCE

Our objective is to further advance the field of weak interaction studies using the molecular torsion balance. We especially wanted to see the effect of water on folding. This required a new torsion balance design and synthesis strategy. Figure 5.1 shows the new torsion balance. It has a different ester on each side arm and a water-soluble group located symmetrically between the two esters. Because of symmetry, the water-soluble group should have no effect on the folding equilibrium. The presence of two esters ensures that folding is not driven by changes in dipole moment (ester position), as seen in previous cases. Furthermore, two different esters will allow direct comparisons between two different interactions.

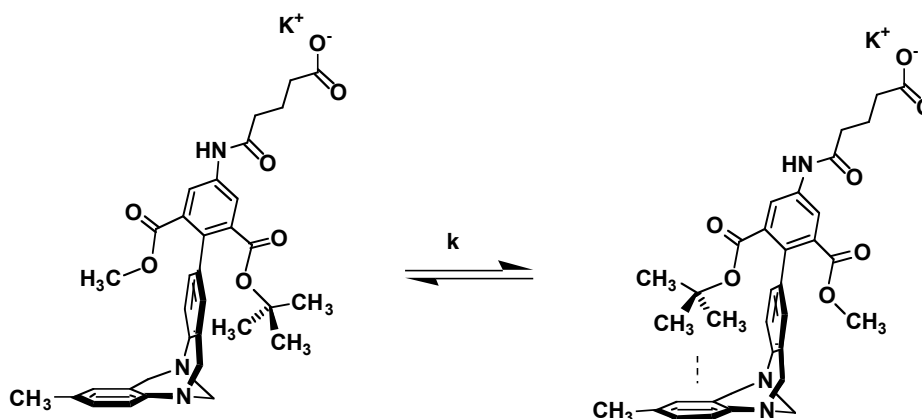
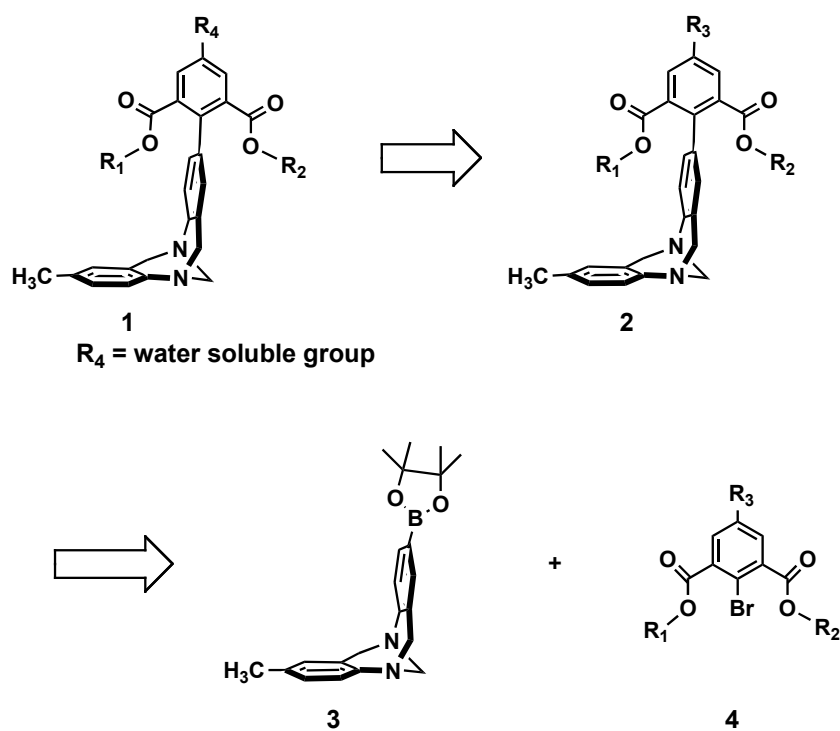


Figure 5.1. Water soluble torsion balance: the “perfect” mutation.

5.1 SYNTHESIS

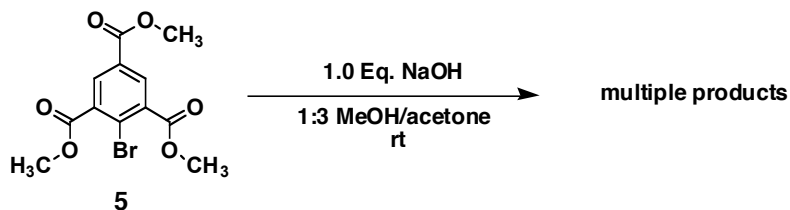
The retro-synthetic strategy for the new torsion balance is shown in Scheme 5.1. The pinacolborane ester of the Tröger's base **3**, and the diester **4** were synthesized in parallel and joined together via Suzuki reaction to yield **2**. Transformation of R_3 group in **2** into a water-soluble group R_4 furnished the desired compound **1**.

Scheme 5.1.



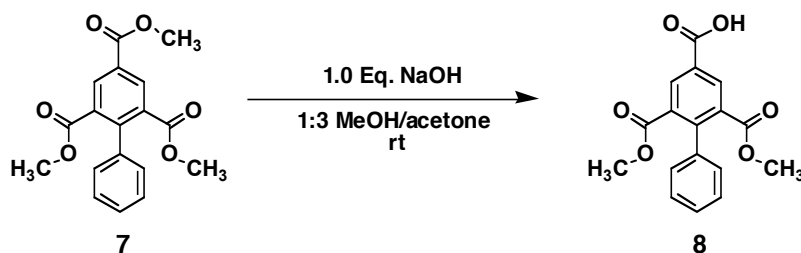
In the first attempt toward the synthesis, controlled hydrolysis of **5** (Scheme 5.2) was attempted using 1.0 equivalent of base. Compound **5** appeared to be a suitable choice as it could be easily synthesized from 2-bromomesitylene via permanganate oxidation and Fischer esterification in a straightforward manner in multi-gram quantities.⁹³

Scheme 5.2



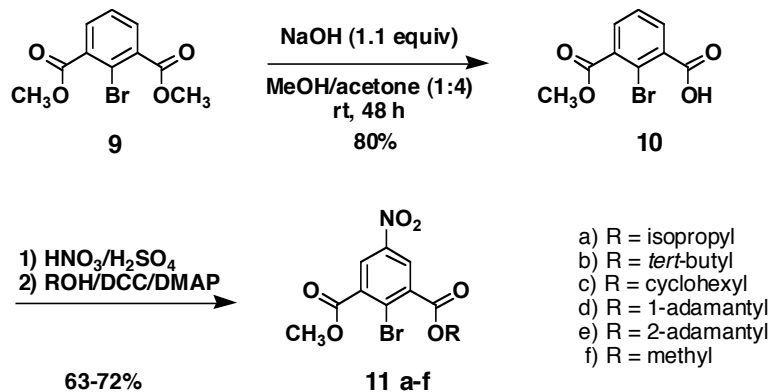
At room temperature, no significant selectivity for hydrolysis at the less hindered position (*para* to bromine) was observed and the reaction led to formation of multiple products that were difficult to isolate. We hypothesized that the central bromine atom did not provide enough steric hindrance to lead to exclusive *para* hydrolysis (Scheme 5.3). The selectivity increased (~ 50% *para* hydrolysis with one equivalent of hydroxide), when reaction was run at 0 °C. Lower temperatures led to inconvenient reaction times.

Scheme 5.3



Since mono-hydrolysis of **5** proved to be difficult, we turned toward a different and easily mutable functional group for the *para* position that might lead to a more selective synthesis. Toward this end, substrate **9**, synthesized on multi-gram scale in a straightforward manner, was chosen as the starting material.⁸⁹ Controlled hydrolysis^{93c} of **9** (Scheme 5.4) with one equivalent of base afforded hemiester **10**. Nitration of **10** occurred at room temperature without any further ester hydrolysis, and subsequent esterification was accomplished via the anhydride route to afford the unsymmetrical diesters **11 a-f**.

Scheme 5.4

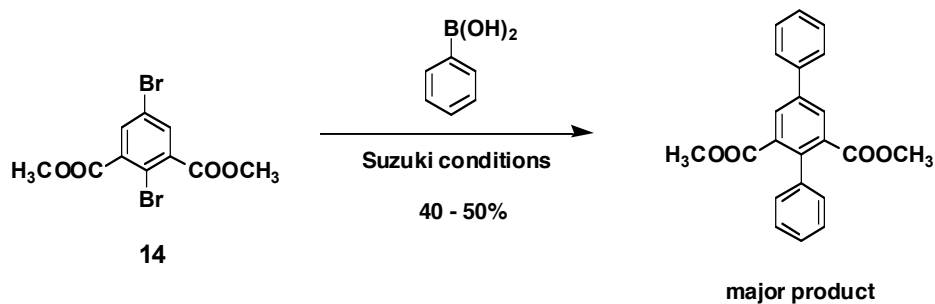


In an alternative approach (Scheme 5.5), **12** was brominated at the *para* position using Gelmont's method to yield **13**.⁹⁴ It was predicted that the less hindered bromine could be selectively replaced with a water-soluble group using one of the palladium catalyzed coupling reactions. However, coupling of dimethyl ester **14** with phenylboronic acid under several different reaction conditions⁹⁵ failed to show any selectivity toward the less hindered bromine, which limited the utility of this scheme.

Scheme 5.5

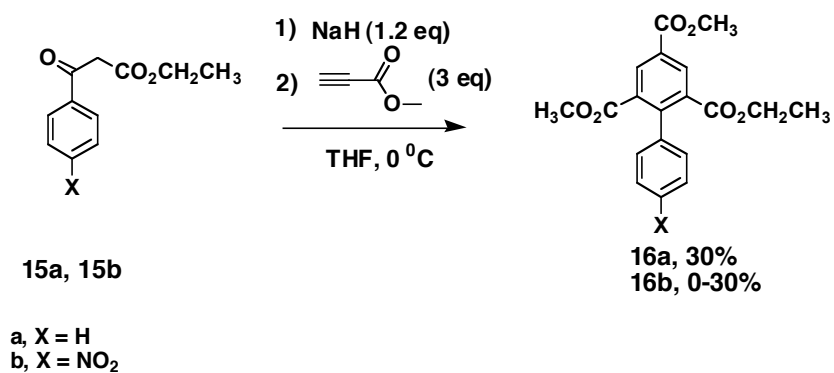


Scheme 5.6



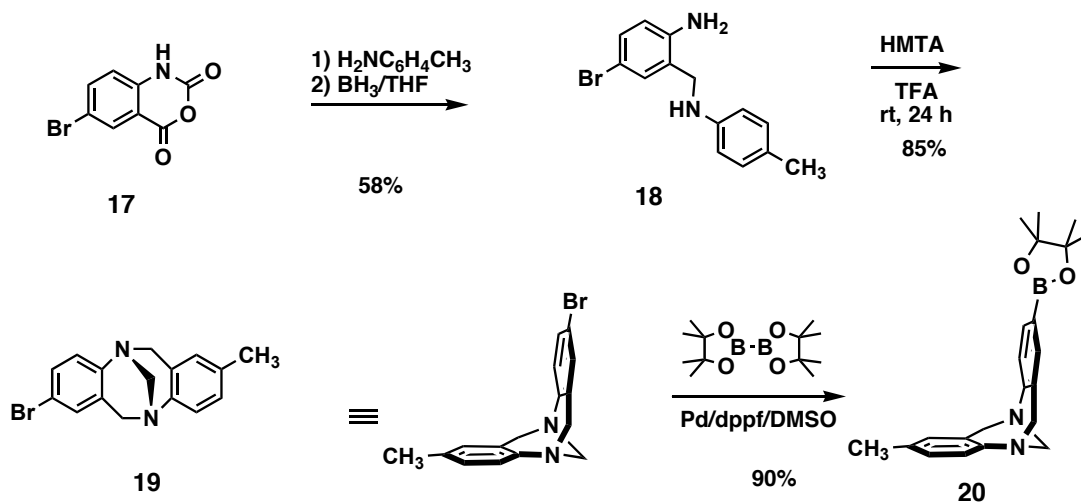
Synthesis of asymmetrical esters was also attempted via one pot double Michael addition of methyl propynoate to enolates and subsequent dehydration (Scheme 5.7), as described by Srikrishna et al.⁹⁶ Commercially available ethyl 4-nitrobenzoylacetate, **15b**, was chosen as the substrate. It was hoped that the aniline obtained after reduction of the nitro group could be made to undergo Tröger's base formation to furnish the torsion balance. Although we could reproduce the literature results (i.e. with **15a**), the reaction in presence of the nitro group gave uneven, low yields and multiple side products.

Scheme 5.7



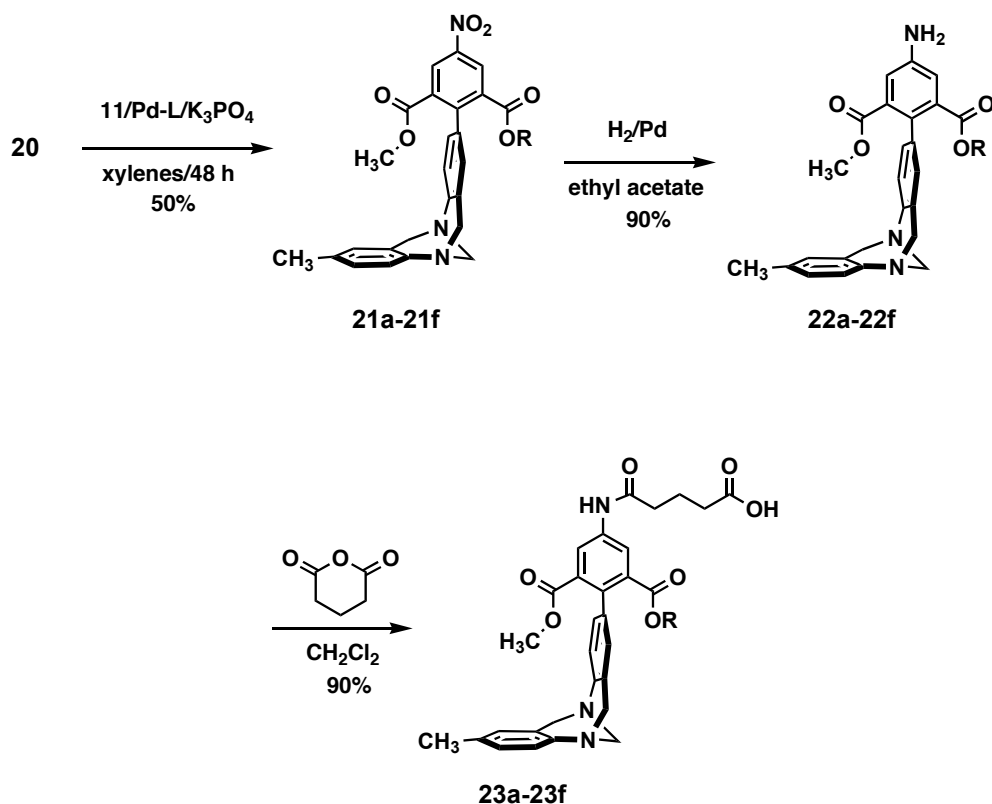
The Troger's base unit needed for our torsion balance was synthesized starting with commercially available 4-bromoisatoic anhydride **17**, using methods developed in our group.⁹⁷ Coupling of **17** with 4-methylaniline was achieved under reflux conditions (Scheme 5.8). The reduction of amide with BH₃.THF afforded the diamine **18**. The diamine **18** readily underwent the Troger's base formation using hexamethylenetetramine (HMTA) to yield dibenzodiazocene **19**, which was then converted to pinacolatoboronate **20**.⁹⁸

Scheme 5.8



The Suzuki coupling between pinacolboronate ester **20** and bromides **11a - 11e** (Scheme 5.9) proved to be difficult under traditional reaction conditions. Fortunately, the past 20 years have witnessed significant advances in Suzuki reaction technology especially with the introduction of N-heterocyclic carbene and trialkyl phosphine ligands in the catalysts, which react under mild conditions and exhibit good functional group tolerance.⁹¹ We tested several new catalysts and reaction conditions, and found Blaser's^{99, 91d} catalyst to be the most effective, consistently giving 50-60% product yields. The compound **11f** underwent the coupling most readily (~24 h), whereas, **11a - 11e** required longer reaction times (48 h). The substitution of one of the methyl esters with a phenyl ester in **11f** led to a decrease in yield (~20%), and substitution of both methyl esters with phenyl esters resulted in no reaction at all.

Scheme 5.9



Reduction of the nitro group (Scheme 5.9) furnished torsion balances **22a - 22f**, and subsequent treatment with glutaric anhydride furnished the final products **23a - 23f** in good yields.

Because our yields from the Suzuki coupling reaction were initially not good, it was decided that the nitro group be reduced and treated with the anhydride before coupling, so as to minimize the number of steps after the low yielding coupling reaction. The presence of three electron withdrawing groups, however, made **11a - 11f** very susceptible to debromination and the reduction of **11a** using standard reagents such as Zn/NH₄Cl, Pd-C/H₂, or SnCl₂, led to loss of bromine. Also, hydrolysis of **11a** using standard reagents such as LiOH, K₂CO₃ in methanol or NaCN in DMSO also led to

immediate debromination with the reaction mixture turning red. The esterification of the diacid of **11f** using BOP-Cl or alkyl halides under standard conditions also led to degradation of starting material. These results made it imperative for us to optimize the Suzuki coupling. We note that the hydrolysis of **11f** was eventually achieved in quantitative yield using trimethyltin hydroxide.¹⁰⁰

5.2 SOLVENT AND SUBSTITUTENT EFFECT ON ROTATION RATE

The solvent and substituent effects on the rotation rate about the biphenyl system were studied in detail on symmetrical dimethyl torsion balances **21f**, **22f**, and **23f**. The NMR peaks of new torsion balances were broader than the previous balances made in our group with only one ester and a methyl group in place of the second ester. The coalescence temperature the methyl ester peaks of **21f** in chloroform was 40 °C as opposed to 65 °C reported by Paliwal for the ortho-methyl-ortho'-ester. The rotation rate was solvent dependent (Table 5.1 and Figure 5.2), and in many common organic solvents such as THF-d₈, DMSO-d₆, pyridine, DMF-d₇, CD₃CN and CD₃NO₂, the rotation was so fast that distinct –OCH₃ signals could not be observed at room temperature.

The equilibrium exchange rate constants, *k*, were calculated using a dynamic NMR line fitting program (WINDNMR 7.1)¹⁰¹ and were highest in polar aprotic solvents (THF-d₈, DMSO-d₆, DMF-d₇, CD₃CN, CD₃NO₂), followed by halogenated solvents (CDCl₃, CD₂Cl₂, CCl₄, C₂D₄Cl₂), and lowest in protic solvents (CD₃OD, fluorinated alcohols, D₂O).

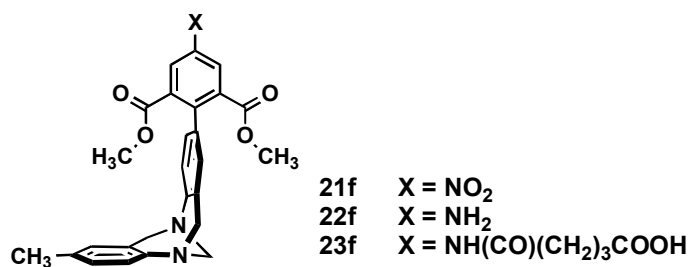


Table 5.1. Rotation rates of dimethyl ester torsion balances in various solvents.

Entry	Solvent	X	k (sec ⁻¹) ^a
1	CDCl ₃	NO ₂	135
2	CDCl ₃	NH ₂	200
3	Acetone-d ₆	NO ₂	650
4	Acetone-d ₆	NH ₂	1700
5	Acetone-d ₆	NH(CO)(CH ₂) ₃ COOH	850
6	C ₆ D ₆	NO ₂	200
7	C ₆ D ₆	NH ₂	2200
8	CD ₃ CN	NO ₂	350
9	CD ₃ CN	NH ₂	900
10	CD ₃ NO ₂	NO ₂	200
11	CD ₃ NO ₂	NH ₂	550
12	CD ₃ OD	NO ₂	135
13	CD ₃ OD	NH ₂	300
14	CD ₃ OD	NH(CO)(CH ₂) ₃ COOH	200
15	D ₂ O	NH(CO)(CH ₂) ₃ COO ⁻	50

^a Spectra were recorded on 500 MHz spectrometer at T = 298 °K. Rate constants were obtained from dynamic NMR line fitting.

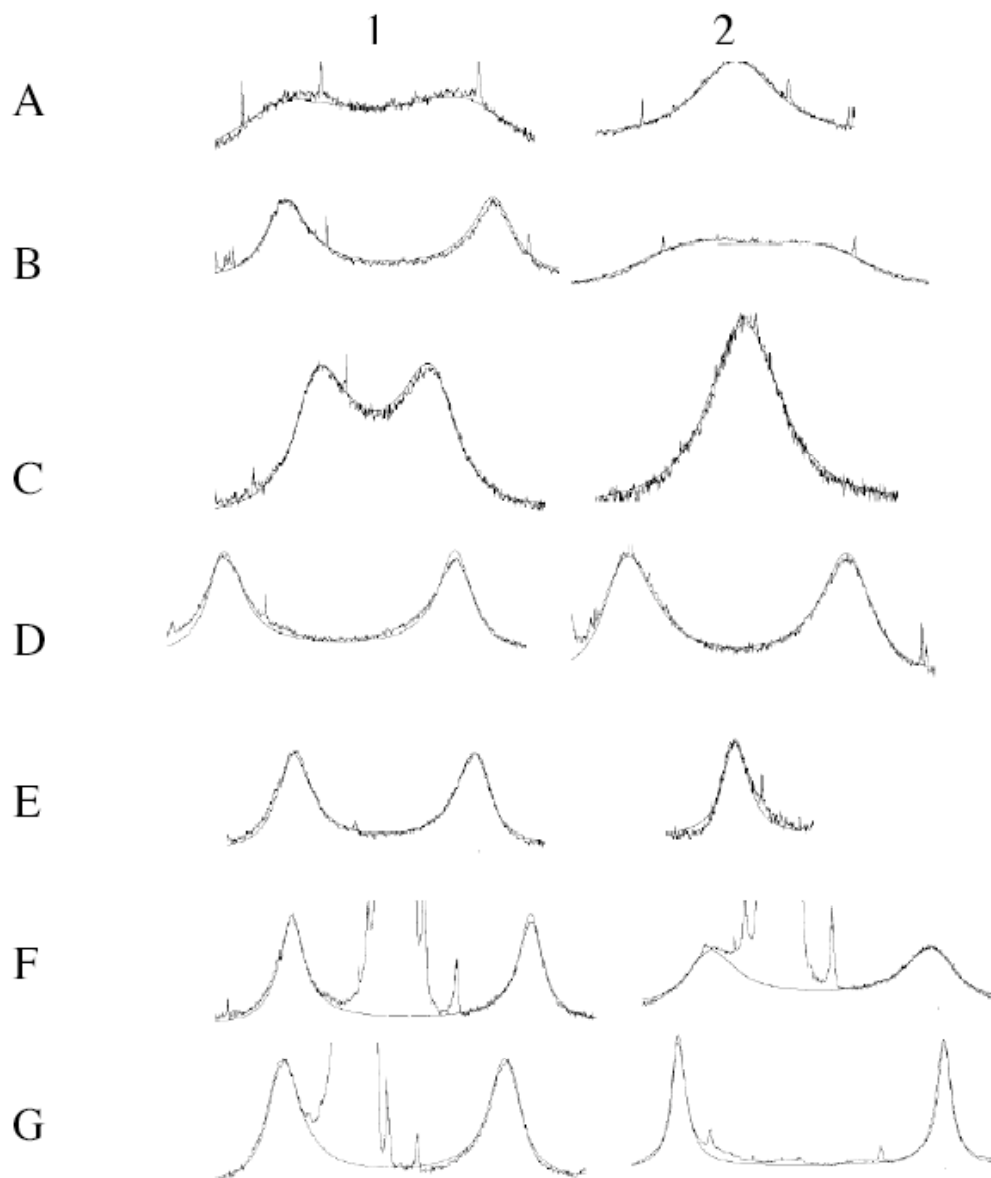


Figure 5.2. NMR spectra of **21f**, **22f**, and **23f** in different solvents: (A) Acetone- d_6 , (B) CD_3NO_2 , (C) CD_3CN , (D) $CDCl_3$, (E) C_6D_6 , (F) CD_3OD , (G) CD_3OD/D_2O . A1-F1 = **21f**, A2-F2 = **22f**, G1 = **23f** in CD_3OD , G2 = **23f** in D_2O .

Adams and coworkers studied the stereochemistry of chiral biphenyl compounds extensively in the 1930's. For 4' substituted chiral biphenyls **24a-24e** (Figure 5.3(a)), Adams and Hanford¹⁰² found that their stability towards racemization in acetone, chloroform, ethanol and water depended on the substituent at 4' in the following order:

$\text{CH}_3 < \text{OCH}_3 < \text{Cl} < \text{Br} < \text{NO}_2$. Evidently, electron withdrawing groups at 4' increased the barrier to rotation.

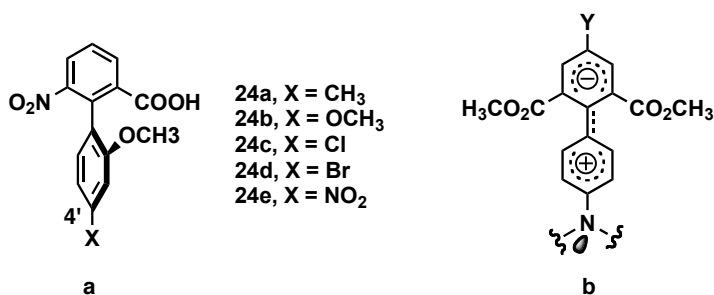


Figure 5.3. Adams's model system for racemization studies.

In our torsion balance, the 4' position in the biphenyl system is occupied by a tertiary nitrogen atom of the Troger's base whose lone pair is partially delocalized over the benzene ring. The availability of this lone pair for resonance will decrease if the nitrogen forms a hydrogen bond with the solvent, and the solvent would then decrease the rotation rate. The decrease in rotation barrier due to decreased electron donation at the 4' position can be explained on the basis of charge transfer in the transition state. In the transition state, the two benzene rings are coplanar and a charge transfer resonance structure may exist (Figure 5.3(b)) in which the lower ring has a partially positive charge. The lone pair of nitrogen can stabilize this positive charge, thereby stabilizing the transition state and increasing the rotation rate. Hydrogen bonding to the solvent would decrease this effect.

Although charge transfer may be one of the reasons why rotation is slower in hydrogen bonding solvents, it also implies that a nitro group on the upper ring should lead to a faster rotation rate compared to an amine. Our observation is however, the opposite. Another inexplicable feature in our data is the extraordinary difference in the

rotation rates between the nitro and amino torsion balances (entries 6 and 7) in presence of aromatic solvent benzene. We also did not observe any correlation between the solvent polarity and the rotation rate.


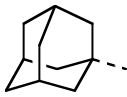
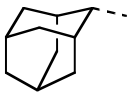
5.3 FOLDING ENERGIES OF NEW TORSION BALANCES IN WATER

The folding free energies of torsion balances are given in Table 5.2. In chloroform, the folding ratios of the isopropyl, *tert*-butyl and the cyclohexyl esters (0.5, 0.72 and 0.36 kcal/mol respectively, entries 1-9), were identical, within the error of measurement ($\pm 10\%$), with values reported previously by Paliwal and Kim. The introduction of the methyl ester side arm in place of the methyl group had no measurable effect on folding equilibria. Nitro and amino groups, as expected, did have a different influence on folding equilibrium.

Table 5.2. Folding energies (kcal/mol) of new torsion balances at 298 K.

Entry	Ester	R	$-\Delta G_{\text{fold}}^0$ (CDCl ₃ , $\pm 10\%$) ^a	$-\Delta G_{\text{fold}}^0$ (25 mM K ₂ CO ₃ in D ₂ O, $\pm 10\%$) ^a
1	21a	(CH ₃) ₂ HC-	0.50	i ^b
2	22a	"	0.50	i ^b
3	23a	"	0.50 ^c	0.72
4	21b	(CH ₃) ₃ C-	0.65	i ^b
5	22b	"	0.65	i ^b

Table 5.2 continued,

6	23b	"	0.65 ^c	0.92
7	21c		0.36	i ^b
8	22c	"	0.36	i ^b
9	23c	"	0.36 ^c	0.67
10	21d		0.36	i ^b
11	22d	"	0.36	i ^b
12	23d	"	0.36 ^c	0.68
13	21e		0.55	i ^b
14	22e	"	0.55	i ^b
15	23e	"	0.55 ^c	0.9
16	21f	H ₃ C-	0.0	i ^b
17	22f	"	0.0	i ^b
18	23f	"	0.0	0.0

^a Free energy change upon folding calculated from the observed equilibrium constant determined by integration and NMR line shape analysis. Samples were at 0.1 mM concentration. ^b Not sufficiently soluble. ^c Methyl ester of free acid was used.

The folding energies of the cyclohexyl (entries 7, 8) and the 1-adamantyl (entries 10, 11) esters were identical, although an adamantane has 3 internal rotational states that are identical to a cyclohexane. If the unfolded cyclohexyl has free rotation about the C-O bond, then the internal rotational entropy effects can make the folded state of the 1-adamantyl ester favorable over the cyclohexyl ester by a factor of $RT \ln 3$. However, if

the folded and unfolded states of the cyclohexyl ester have one major rotamer, then the adamantane would have no effect.

The 2-adamantyl ester folds more ($\Delta G_{\text{fold}}^0 = -0.55$ kcal/mol) than the 1-adamantyl ester ($\Delta G_{\text{fold}}^0 = -0.36$ kcal/mol), evidently, it makes a better contact with the arene. One reason for this may be that there are three 1,3-diaxial interactions in the 1-adamantyl ester as opposed to two in 2-adamantyl ester (Figure 5.4a). Fewer 1,3-diaxial interactions allow more flexibility in orientation thereby a better contact. X-ray crystal structures of **21e** showed the adamantyl ester to be in the conformation that minimized $A_{1,3}$ strain (Figure 5.4b). Unfortunately, the X-ray crystal structure of **21c** and **21d** could not be obtained for comparisons. The X-ray crystal structure of amino compound **22d** was obtained and showed an interesting effect - the adamantyl ester was found to be in the *exo* position, as opposed the favored *endo* position in solution. This result underlines the fact that a combinations of several factors determines crystal packing and the minimum energy conformation in a lattice may not always be the same as in solution. Further comparison between the X-ray structures of **21e** and **22d** show that in **21e**, one of the cyclohexyl rings of the adamantane (ring C27-C28-C29-C35-C33-C34) lies parallel to the arene, whereas in **21d**, only an edge of the adamantane (atoms C32 and C28) can face the arene. The parallel arrangements leads to a larger van der Waal's contact area between 2-adamantyl ester and the arene.

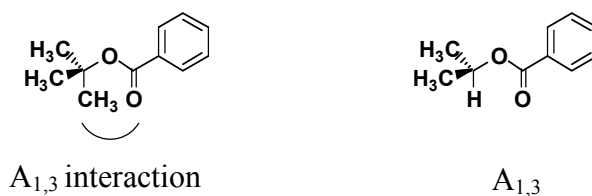


Figure 5.4a. Model interactions of the 1-adamantyl and 2-adamantyl esters.

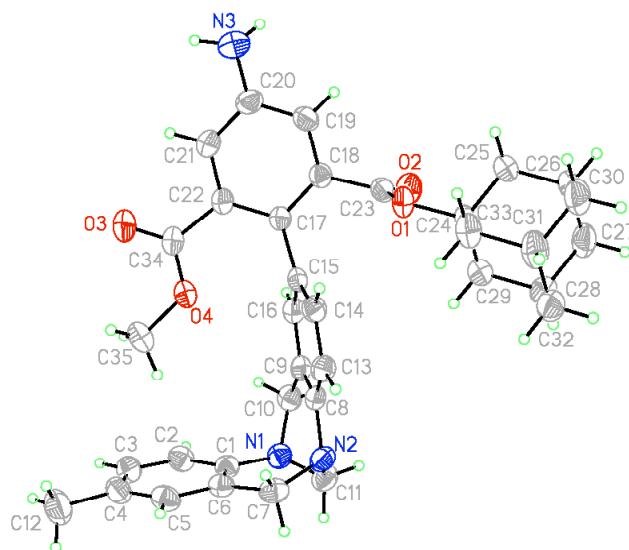
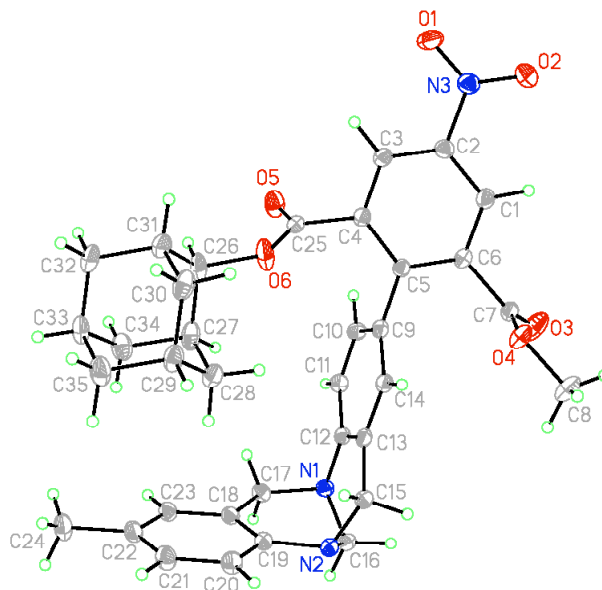


Figure 5.4b. X-ray crystal structures of compounds **21e** (top), and **22d** (bottom).

The folding ratios for all esters increased in water. We define the excess folding energy as $\Delta G^0_{\text{fold, water}} - \Delta G^0_{\text{fold, chloroform}}$, and it increased from 0.22 kcal/mol to 0.35 kcal/mol going from the smallest isopropyl to the bulkiest adamantyl ester. We attribute

the increase in folding in water to the microscopic hydrophobic effects arising from solvent cohesiveness. Previous studies found the solvent polarity to have little effect on the torsion balance folding equilibrium (Table 4.2), with the exception of methanol, which had the highest E_T (a measure of solvent cohesiveness) value among all solvents tested at that time. Taking a cue from this, folding ratios of the new torsion balances were determined as a function of solvent cohesive parameter for solvents with high E_T , and the results are shown in Table 5.3.

Table 5.3. Cohesive solvent effects on folding of isopropyl and cyclohexyl torsion balances at 298 K.

Entry	Solvent	$-\Delta G_{\text{fold}}$ (kcal/mol, $\pm 10\%$)		$E_T(30)$
		23a	23c	
1	D ₂ O	0.72	0.67	63
2	CF ₃ CD ₂ OD	0.53	0.50	59.4
3	CD ₃ OD	0.53	0.50	55.5
4	CDCl ₃ ^a	0.50	0.36	39.1
5	CS ₂ ^a	0.44	0.31	32.6

^a Methyl esters of free acids were used. Free energy change upon folding calculated from the observed equilibrium constant determined by integration and NMR line shape analysis. Samples were at 0.1 mM concentration.

The folding ratios increased with the solvent E_T values and bigger alkyl groups showed a higher response. These results show that the folding of non-polar alkyl groups is influenced by the solvent's cohesive strength in addition to the weak intramolecular interactions present in the folded state. Water is an exceptionally cohesive solvent due to its intermolecular hydrogen bonding network and can cause strong folding forces. In our

study we observed this extraordinary character of water, for example, the hydrophobic contribution to folding (~ 0.3 kcal/mol) for the cyclohexyl and 1-admantyl esters is almost as big as CH/ π interaction itself. In an effort to observe even larger hydrophobic contributions, torsion balance **25a-b** and **26a-b** (Figure 5.5) were synthesized. Computer modeling showed the contact areas between the arene and these bulky esters to be nearly 30% bigger than the adamantyl esters. Folding energies (ΔG^0_{fold}) of **25a** and **26a** in CDCl_3 were -0.09 kcal/mol and $+0.06$ kcal/mol respectively. These low preferences for the folded state are probably due to steric effects – the extra alkyl surface is too large for the folded position.

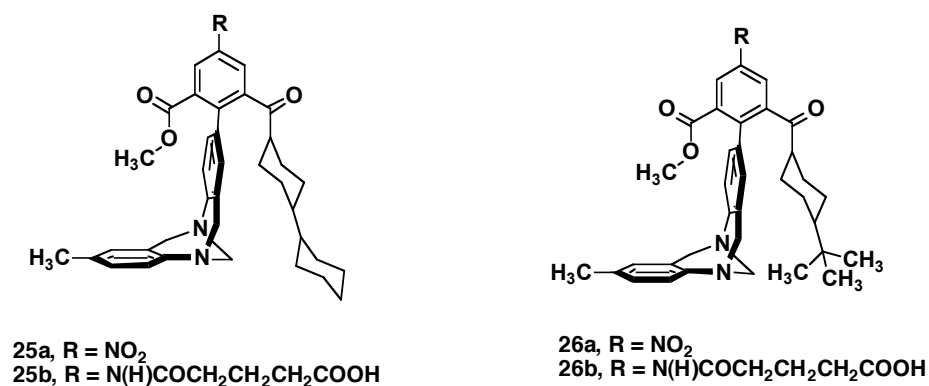


Figure 5.5. Torsion balances with large non-polar surface areas.

Unfortunately, the solubility of glutaramides **25b** and **26b** in water was not enough for NMR studies, and different water solvating groups were investigated. As an alternate to glutaric anhydride, anhydrides **27**, **28**, **29** and **30** (Figure 5.6) were tested, but without success, due to their unfavorable solubility properties (**28**, **29**) or overlapping NMR signals (**27**, **30**). Nevertheless, with appropriate modifications, these anhydrides can likely serve as water solubilizing groups for more advanced torsion balances.

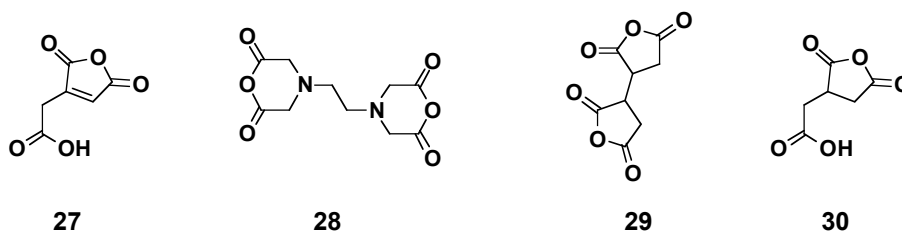


Figure 5.6. Some alternatives to glutaric anhydride for water solubility enhancement.

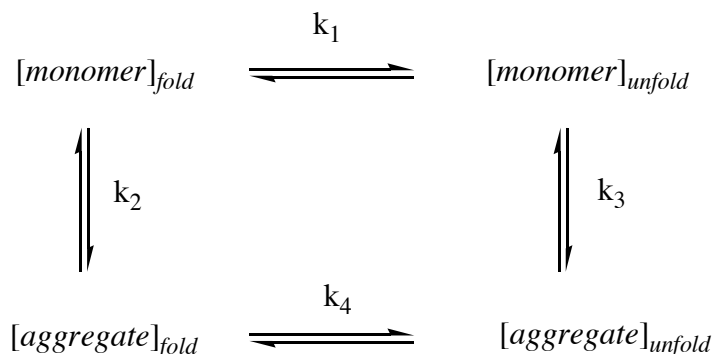
5.4 DIFFERENT EFFECTS ON FOLDING ENERGIES

5.4.1 Effect of concentration on folding ratios

Compounds **23a** - **23e** had limited solubility in water and tended to form micelles. Due to this, their folding ratios and NMR line widths in D_2O were concentration dependent. The critical micelle concentration below which the folding ratios were constant was ~ 0.1 mM for **23c** - **23e** and 0.5 mM for **23a** and **23b**. In contrast to water, in organic solvents such as $CDCl_3$, CD_3OD and CF_3CD_2OD the folding ratios of all torsion balances were concentration independent in the 0.1-10 mM range.

Lindman and coworkers studied the micelle formation in aqueous sodium hexanoate and sodium octanoate solutions using NMR and found that their experimental data fit well to a single micelle size model in which the micelles have a well-defined concentration dependent aggregation number.¹⁰³ This aggregation number was found to be between 5 - 35 for salt concentrations in 0.2 - 4 M range. Reasoning along these lines, we can assume our torsion balance molecules exists in an equilibrium between monomer

and aggregate states, and a folding equilibrium exists in both these states. This can be represented by a thermodynamic cycle shown below,



where $[monomer]$ and $[aggregate]$ represent the concentrations of monomers and the aggregates respectively. Folding ratio in micelles was found to be higher (Figure 5.7) than in monomers. If aggregation promotes folding, then bigger aggregates may lead to higher folding. The size of aggregates can be determined following Lindman's analysis, and increase in folding can in principal be realized as a function of the aggregate size. Such data will furnish invaluable information on effect of aggregation on hydrophobic forces, which is of fundamental importance in protein science.¹⁰⁴

At high concentrations (~ 1 mM) the aggregated adamantyl balance showed more folding than the cyclohexyl balance (Figure 5.7), although both had similar folding at 0.1 mM concentration. It could be that either the adamantyl balance aggregates more, or its folding is more sensitive to aggregation than the cyclohexyl balance. To determine which of these scenarios exists requires knowledge of the aggregation number and a further detailed and comprehensive study.

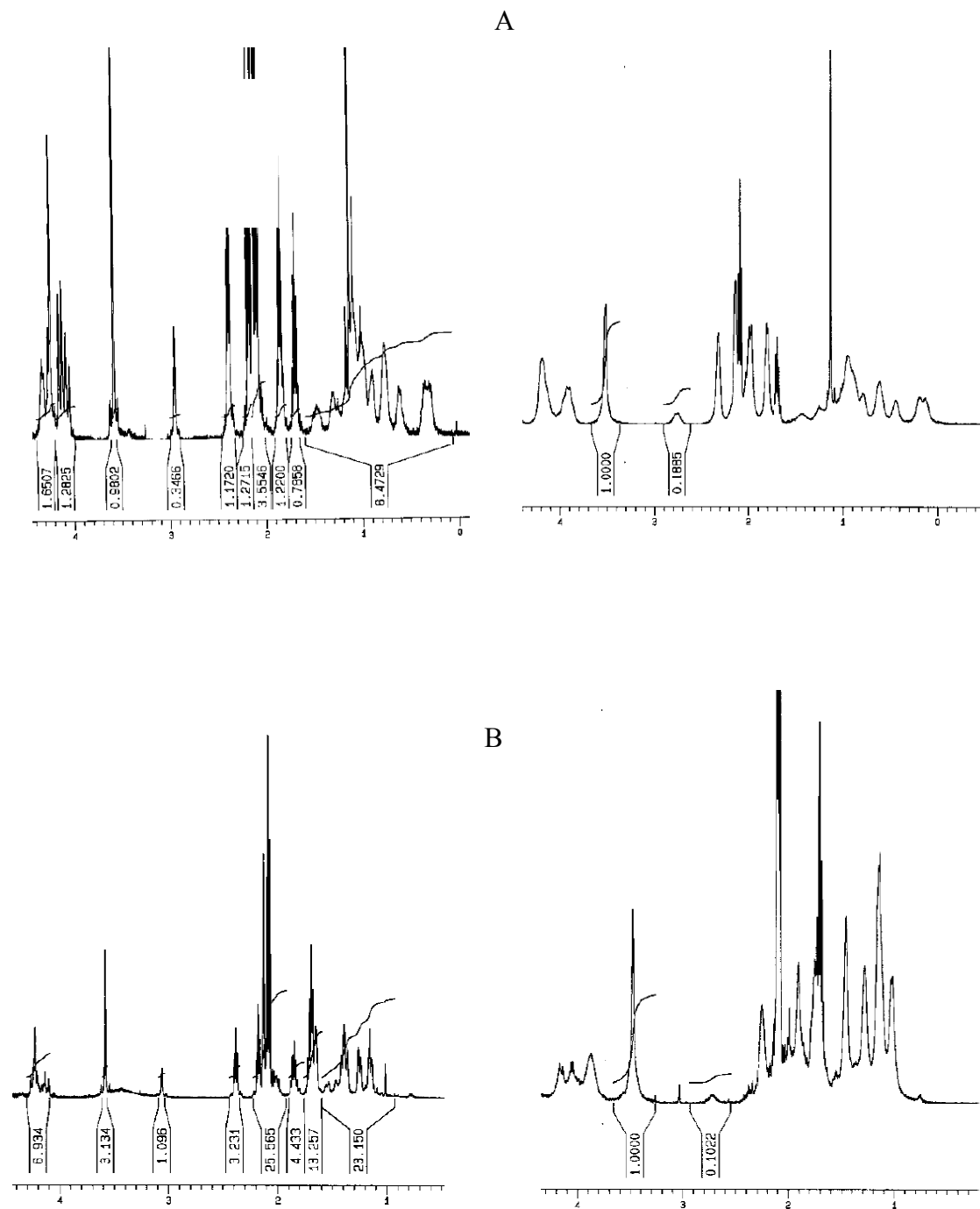


Figure 5.7. NMR spectra in water: (A) **23c** at 0.1 mM (left) and 1.0 mM (right) concentrations, (B) **23d** at 0.1 mM (left) and 1.0 mM (right) concentrations. Spectra recorded in 25 mM K_2CO_3 in D_2O .

A study of the concentration dependence of folding in a mixed solvent system led an interesting observation. A 1.0 mM solution of **21a** in CD₃OD was diluted with an equal amount of D₂O. Upon addition of D₂O, the clear CD₃OD solution turned turbid and the folding ratio increased. The quality of the NMR spectrum (line widths) however was unaffected. The turbidity and higher folding indicated aggregation. These results led us to avoid the addition of any co-solvents to increase the solubility of the torsion balances in water.

5.4.2 Effect of denaturants, salting-in and salting-out agents

Ionic salting-in and salting-out reagents, and organic denaturants such as urea influence the solubility and conformations of proteins and other biological macromolecules. Hofmeister performed one of the first studies of these phenomenon, and the relative efficiencies of different ionic salts in their ability toward salting-in and salting-out egg-white protein in water are called the Hofmeister series.¹⁰⁵ These phenomenon are not yet fully understood. It is controversial whether ion specific interactions between Hofmeister ions and peptides play a significant role or if these ions and organic denaturants act by disrupting the microscopic hydrogen-bonded structure of water.¹⁰⁶ The effects of denaturants on folding equilibrium in our torsion balances provide a unique opportunity for addressing these issues.

The folding ratio of the isopropyl ester torsion balance **23a** in D₂O was unchanged in 4.0 M urea (protein denaturant), 1.0 M Na₂SO₄ (denaturant) and 1.0 M LiCl (salting out agent) solutions. Similarly, for the cyclohexyl ester, **23c**, the folding ratios in

1.0 M LiCl (salting out agent) and 1.0 M LiClO₄ (salting in agent) were same as in our standard D₂O solutions.

Since folding in our systems is not driven by ionic interactions, it is reasonable that addition of ionic salts, which affect the electrostatic properties of water and significantly influence ionic interactions, causes no change in folding. How these ions specifically affect the van der Waals interactions and hydrophobic forces needs further computational and experimental investigations, but in the present case, no net influence of additives was observed. Recent computational studies suggest that effects of denaturants depend on the size of the hydrophobic solute.¹⁰⁷ Our data can be useful for computational chemists involved in such studies.

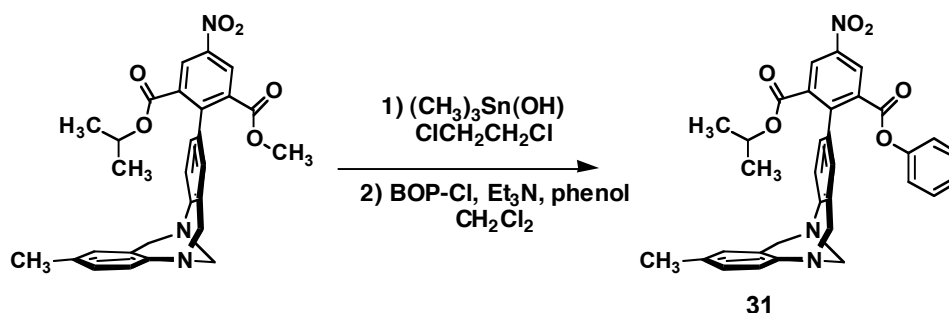
5.4.3 Effect of temperature on folding equilibrium.

No change was observed in the folding ratio of isopropyl torsion balance in 25 °C – 65 °C temperature range. Thus, $R\ln(k) = (\Delta H_{\text{fold}})/T - \Delta S_{\text{fold}}$ is independent of temperature. This implies that in the given temperature range, the folding is mainly entropy driven ($\Delta H_{\text{fold}} \sim 0$). This result is consistent with the fact that small changes in the hydrogen bond network of water are mainly entropic and can be accomplished without significant change in enthalpy.⁶⁵

5.5 SELF CONSISTENCY OF FOLDING RATIOS

Torsion balance **31** was synthesized (Scheme 5.11) to directly compare the CH/ π and the edge-to-face interactions.

Scheme 5.10



The folding was 0.25 kcal/mol in favor of the CH/ π interaction in CDCl_3 . The folding free energy of a phenyl ester with respect to a methyl ester is -0.19 ($\pm 10\%$) kcal/mol, and of an isopropyl ester with respect to a methyl ester (compound **21a**) is -0.5 ($\pm 10\%$) kcal/mol. The folding free energy of an isopropyl ester with respect to a phenyl ester (**31**) was found to be -0.3 ($\pm 10\%$) kcal/mol, which is consistent with the difference between the above two values.

5.5.1 Solvent Accessible Surface Area (SASA) and γ calculations.

The solvent accessible surface areas were calculated for energy minimized structures generated with force fields such as MMFF, Amber, CHARMM, Eng-Huber, OPLS-AA and the MNDO, AM1 and PM3 semi empirical methods. Depending on the nature of the model, 100 to 50000 starting geometries were generated and optimization carried out on each. Since a Boltzmann distribution of energies exists at a given

temperature, the ASA were Boltzmann averaged for lowest energy conformations lying within 1 kcal/mol of the global minimum. The values of γ generally ranged from 5 and 30 cal/mol $\cdot\text{\AA}^2$. The results of one such calculation are shown in Table 5.4. The program correctly predicted a similar change in ASA upon folding for the cyclohexyl and the adamantyl torsion balances.

Table 5.4. Boltzmann averaged surface areas of minimum energy geometries (MMFF94x) in gas phase.

Ester	ASA _{folded} (\AA^2)	ASA _{unfolded} (\AA^2)	ASA _{unfolded} - ASA _{folded} (\AA^2)	γ
Adamantyl	743	793	50	6.4
Cyclohexyl	715	760	45	6.8
Isopropyl	695	711	16	13.75

Although, our values of γ lie in the range expected based on prior work, the values from individual simulations showed a broad distribution (5 - 30 cal/mol $\cdot\text{\AA}^2$). One reason for such a broad variation in calculated γ 's is because for small molecules, small changes in geometry can lead to significant area differences. In folding of large molecules, these differences will probably average out yielding a more consistent γ . The Boltzmann averaged γ for cyclohexyl and adamantyl ester torsion balances is close to the LCW predicted value of ~ 7 cal/mol $\cdot\text{\AA}^2$ in many cases.

6.0 QUANTIFICATION OF C-F/ π_H INTERACTION IN WATER

Noncovalent interactions of fluorine in water are important from a biological perspective. Fluorine substitutions are often introduced in drug discovery where fluorination can render compounds resistant to oxidative metabolic pathways, increase their hydrophobicity and enhance interactions with substrates.¹⁰⁸ Fluorination is also important in catalysis where fluorine substitutions in benzene have been observed to have significant effects on stereoselectivity and reaction rates.¹⁰⁹

These facts make noncovalent interactions of fluorine an important area of study – an area where our torsion balance has already found application.^{64f}

6.1 ELECTROSTATIC EFFECTS OF FLUORINATION

A benzene ring has a negative electric potential at its centroid and a positive potential at its rim. Hexafluorbenzene on the other hand has a negative potential at the rim and a positive centroid. The magnitudes of their quadrupole moments are similar in magnitude but opposite in directions and these differences affect their electrostatic interactions.¹¹⁰

Recent computational studies have predicted an attractive interaction between the C-F bond and hexafluorobenzene (π_F) and a weak repulsive interaction between C-F and

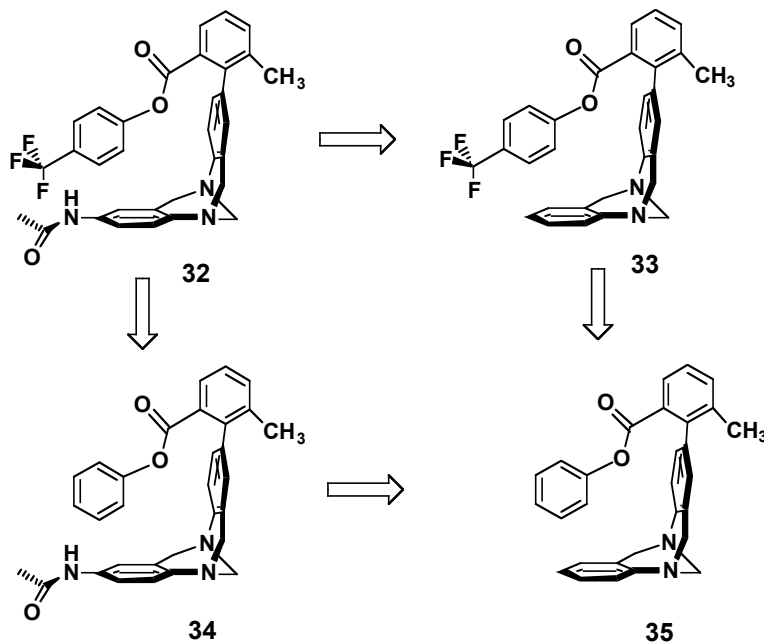
benzene (π_{H}).¹¹¹ Dougherty¹¹² and Danten¹¹³ have reported an attractive interaction between the lone pair of water and hexafluorobenzene in their computational studies. IR and Raman studies by Besnard and coworkers showed weak hydrogen bonding of water with benzene but not with hexafluorobenzene, indicating that a π_{F} system is not a good hydrogen-bond acceptor.¹¹⁴

A C-F group is a poor hydrogen-bond acceptor, this is one of the reasons that water and fluorinated hydrocarbons are immiscible. There are relatively few examples in the literature where an organofluorine may be regarded as accepting an intramolecular hydrogen-bond. However, an interesting example of N-H \cdots F-C hydrogen-bonding to form six membered rings (a driving force in itself) has recently been reported.¹¹⁵

6.2 EVALUATION OF C-F/AMIDE INTERACTION USING THE TORSION BALANCE AND HUNTER'S DOUBLE MUTANT CYCLE.

Diederich and coworkers attempted to measure the C-F/amide interaction energy in organic solvents using the Wilcox torsion balance and Hunter's double mutant cycle (Scheme 6.1).^{64f}

Scheme 6.1



The interaction energy was determined using equation (6.2)

$$\Delta G_{C-F\dots amide} = \Delta G_{32} - \Delta G_{33} - \Delta G_{34} + \Delta G_{35} \quad (6.2)$$

The interaction was found to be weak in CDCl_3 and C_6D_6 and essentially zero in CD_3OD (Table 6.1). The absence of interaction in methanol was attributed to its electrostatic effects.

Table 6.1. C-F/amide interaction energies at 298 K.

Entry	Solvent	ΔG_{fold}^0 (± 0.25 kJ/mol)
1	CDCl_3	-1.05
2	C_6D_6	-0.85
3	CD_3OD	-0.10

6.3 TORSION BALANCE FOR QUANTIFICATION OF C-F/ π_F AND C-F/ π_H INTERACTIONS

Torsion balances to study C-F/ π_H and C-F/ π_F interactions in organic solvents were synthesized by Wilcox and Paliwal (Figure 6.1).⁸⁸

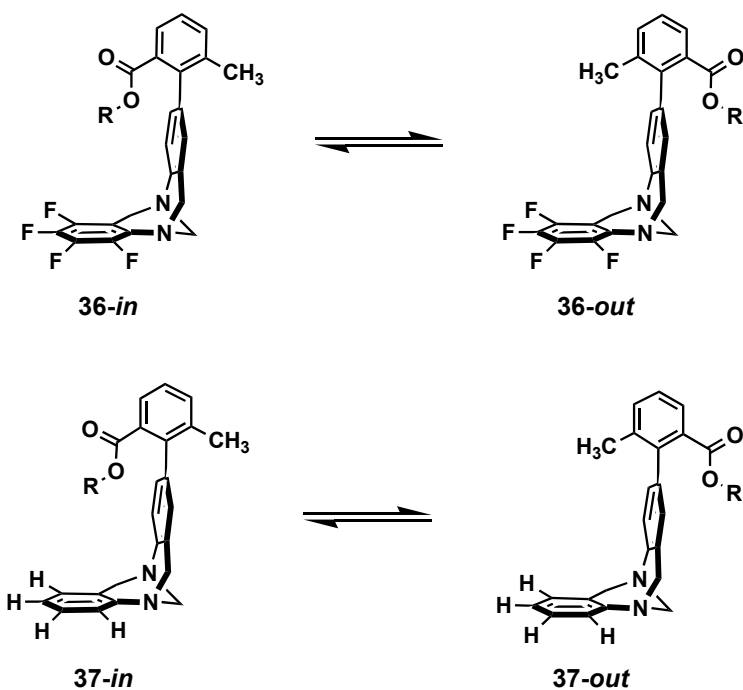


Figure 6.1. Torsion balances for C-F/ π_H and C-F/ π_F interactions in organic solvents.⁸⁸

Table 6.2. The folding energies of **36** and **37**.⁸⁸

Entry	R	ΔG_{fold}^0 ($\pm 10\%$) ^{a,b}	
		36	37
1	(CH ₃) ₂ H-	-0.56	-0.44
2	(CF ₃) ₂ CH-	-0.48	-0.03
3	C ₆ H ₅	-0.43	-0.27

^akcal/mol at 298 K.

^b $\Delta G_{\text{fold}}^0 = \Delta G_{\text{fold, ester}}^0 - \Delta G_{\text{fold, methyl ester}}^0$

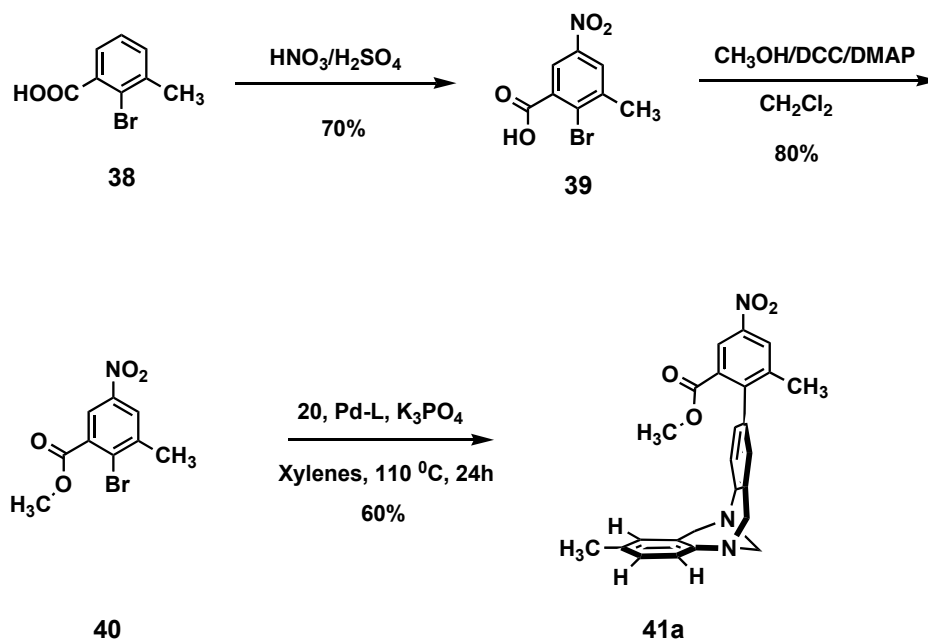
The folding energies of fluorinated torsion balances are presented in Table 6.2. The C-F/ π_{H} interactions (entry 2) were found to be weaker than C-H/ π_{H} interactions in chloroform (entry 1). The interaction between the hexafluoroisopropyl ester and the arene was very small (0.03 kcal/mol); it may be that any attractive dispersion forces in this case are countered by the electrostatic repulsion. The C-F/ π_{F} interactions were similar in magnitude to C-H/ π_{F} interactions, indicating that the aromatic perfluorocarbons interact with the C-F and C-H bonds in similar ways.

6.4 TORSION BALANCE FOR C-F/ π_{H} INTERACTION IN WATER

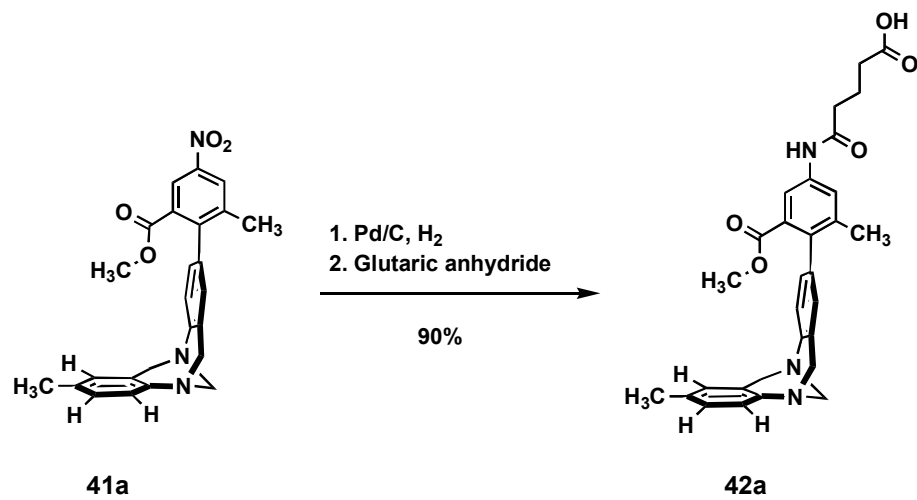
Studies conducted by Paliwal did not take into account any solvent effects. Our results for the C-H/ π_{H} interaction in water showed significant enhancement of folding in water, likely arising from hydrophobic effects. To study C-F/ π_{H} interaction in water, the biological solvent, we synthesized a water soluble fluorinated torsion balance containing a hexafluoroisopropyl ester.

Starting with commercially available 2-bromo-6-methylbenzoic acid **38** (Scheme 6.2), ester **40** was prepared via nitration and esterifications following procedures described in chapter 5. Torsion balance **41a** (Scheme 6.2) was synthesized via a Suzuki coupling between bromide **40** and boronic ester **20**. The methyl ester in **41a** was hydrolyzed, and the resulting acid esterified again with hexafluoroisopropanol to furnish the fluorinated torsion balance **41b** (Scheme 6.3). Reduction of the nitro groups and treatment with glutaric anhydride on compounds **41a** and **41b** (Schemes 6.3 and 6.4) were performed as described before to yield the desired torsion balances **42a** and **42b**.

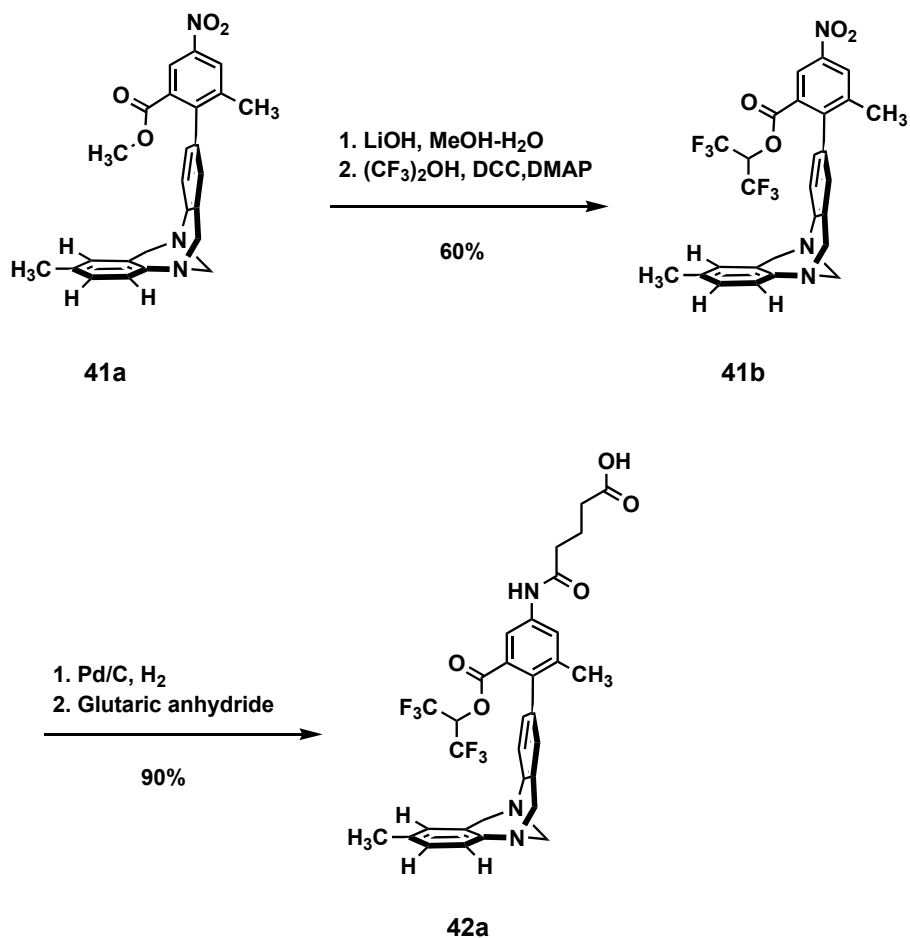
Scheme 6.2



Scheme 6.3



Scheme 6.4



The folding energies of the methyl ester and hexafluoroisopropyl ester torsion balances are given in Table 6.3. In chloroform, the folding energies of **41a** and **41b** were -0.056 kcal/mol and -0.11 kcal/mol respectively, indicating only a weak interaction between these esters and the arene. The methyl ester in **41a** is too far away from the arene for any significant van der Waals interaction, and steric and electrostatic effects diminish the folding of hexafluoroisopropyl ester **41b**. In water, the folding energy of the methyl ester torsion balance (-0.17 kcal/mol, entry 3) was higher than in chloroform. The

folding energy of **42b** in water was 0.31 kcal/mol, which is lower than the folding energy of the complementary C-H/ π_{H} torsion balance **23a** (Table 5.2).

Table 6.3. The folding energies of compounds **41** and **42**.

Entry	Compound	Solvent	$\Delta G^0_{\text{fold}} (\pm 10\%)^{\text{a}}$
1	41a	CDCl_3	-0.05
2	41b	CDCl_3	-0.11
3	42a	D_2O	-0.17 ^b
4	42b	D_2O	-0.32 ^b

^a kcal/mol at 298 K. ^b Spectra recorded in 25 mM NaHCO_3 in D_2O solution, sample concentration = 0.1 mmol/L.

The CMC of methyl ester **42a** in water (~ 0.1 mmol/L in 25 mmol/L NaHCO_3 in D_2O) was found to be much lower than that of methyl diester **23f** (~ 10 mmol/L). Evidently, the extra polar group in **23f** enhances water solubility. The folding ratio of **42a** in water was concentration dependent, and showed an interesting pattern. Figure 6.2 shows the NMR spectra of the methyl ester peaks of **42a** at three different concentrations: 5 mmol/L, 1 mmol/L and 0.1 mmol/L. Above the CMC (> 0.1 mmol/L), the folding ratio increased with concentration, and the ester preferred the *exo* position in which it is exposed to water. This fits well with the typical picture of micelles (such as in soap solutions) where hydrophobic groups aggregate inwards and polar groups are exposed to water. Below the CMC, the ester prefers the *endo* or the folded position, just like in organic solvents.

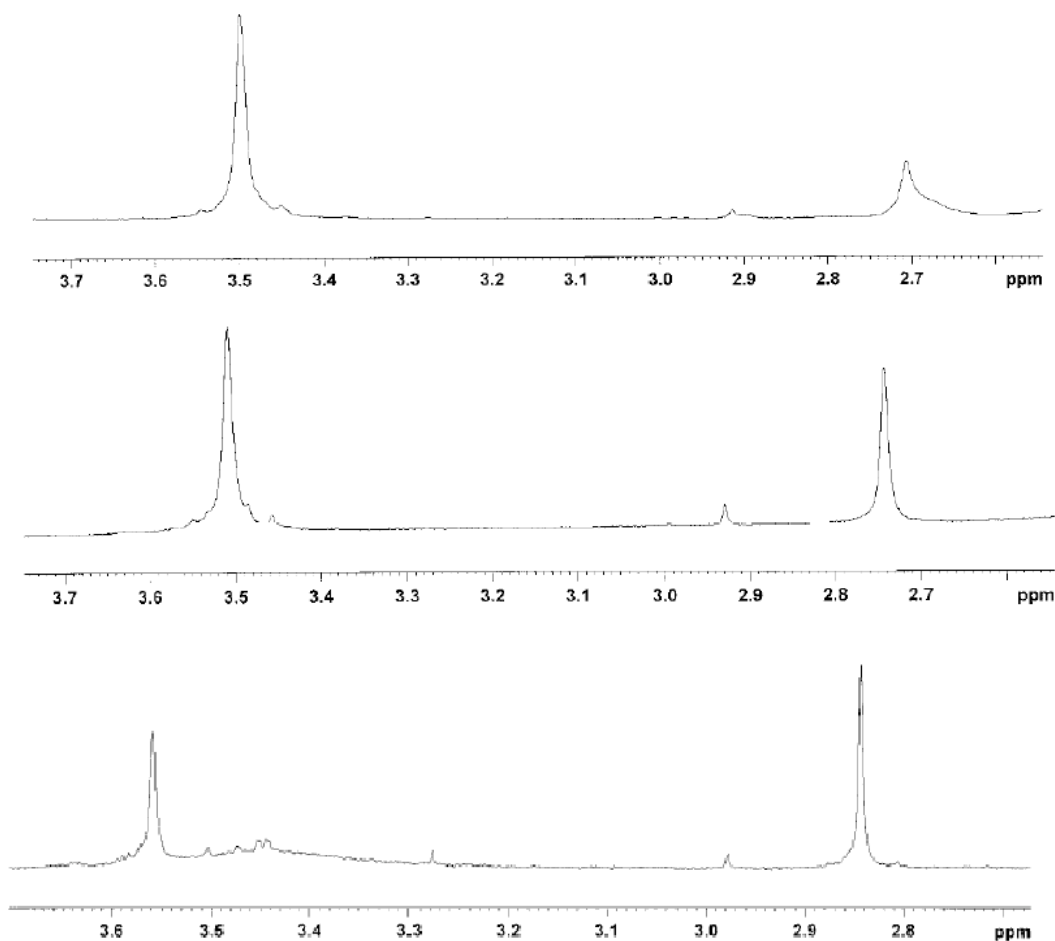


Figure 6.2. NMR spectra of compound **42a** in water (25 mmol/L NaHCO₃ in D₂O) at 5 mmol/L (top), 1 mmol/L (middle) and 0.1 mmol/L (bottom) concentrations. The right peak represents the methyl ester in the *endo* position.

The folding energy of hexafluoroisopropyl ester **42b** was higher in water compared to organic solvents (Table 6.4). This can be attributed to the hydrophobic effects. The excess folding energy ($\Delta G_{\text{fold, water}}^0 - \Delta G_{\text{fold, chloroform}}^0$) of **42b** in water is -0.1 kcal/mol, which is smaller than the excess folding energy of complementary unfluorinated torsion balance **23a** (-0.22 kcal/mol, Table 5.2). It must be pointed out,

however, that since only one isopropyl group comes in contact with the arene, the hydrophobic effects are only limited to that group.

Table 6.4. The folding energies of hexafluoroisopropyl torsion balance **42b**.

Entry	Compound	Solvent	ΔG_{fold}^0 ($\pm 10\%$) ^{a,b}
1	42b	CDCl ₃	-0.05 ^c
2	42b	Acetone-d ₆	-0.05
3	42b	DMSO-d ₆	-0.05
4	42b	CD ₃ OD	-0.05
5	42b	D ₂ O	-0.15

^a kcal/mol at 298 K. Sample concentration = 0.1 mmol/L. ^b $\Delta G_{\text{fold}}^0 = \Delta G_{\text{fold, ester}}^0 - \Delta G_{\text{fold, methyl ester}}^0$. ^c Methyl ester of free acid was used.

From our data, it is evident that the hydrophobic forces depend on the nature of solute. The microscopic surface tensions γ for a given cavity can be different for perfluorocarbons and hydrocarbons. These differences need to be considered in developing computational models of water, and our data can provide useful inputs toward these goals.

7.0 CONCLUSIONS AND FUTURE DIRECTIONS

The effects of diffusion, reagent partitioning and available free volume on reaction rates in SPOS polystyrene beads have been investigated experimentally and theoretically. The reaction between benzylamine and commercially available benzylisocyanate functionalized beads of three different sizes was used as a prototype reaction. The three bead sizes showed different reaction rates under similar reaction conditions. The rate of reaction was observed to decrease with increase in the bead size, which would not be expected if diffusion were not involved. To explain this difference, a mathematical model based on the diffusion-reaction equation has been proposed. Incorporation of diffusion yielded rate constants that were more consistent. Incorporation of proper activity coefficients based on free volume theory further improved the consistency.

The experimental data was also found to fit a simple bimolecular rate law with good fits. Mathematical modeling showed that for fast diffusion and slow reaction, a simple bimolecular rate law is sufficient to describe the reaction kinetics, and the discrepancy between the diffusion-reaction and homogeneous solution model increases as the rate of diffusion increases with respect to the rate of reaction. The error between the two models was found to follow a hyperbolic empirical correlation.

Our mathematical model showed that the reaction rate varies linearly with the partition coefficient of the diffusant, although the partition coefficient was found to be unity for the amines used.

Our results will be useful to technologists working in synthesis of solid supports who want to improve their products. Future goals of this project include studies on role of diffusion on reaction rates of large molecules such as triphenylphosphine and catalysts with bulky ligands. Solid phase reactions tend to slow down as peptides grow larger; our work can shed light on whether diffusion and reagent access may be causing these problems. To our knowledge this is the first study to explore solid phase kinetics both experimentally and theoretically and our procedures can be modified to study issues particular to individual reactions.

A water soluble torsion balance has been synthesized to study noncovalent interaction in aqueous media. In particular, the nature of CH- π interaction has been studied in water. The interaction was found to increase in water with hydrophobic effects playing an important part. Evidence suggests that this interaction in water has dispersive origin. The effects of concentration have also been studied. A torsion balance to investigate CF- π interaction was also synthesized. This interaction was also found to increase in water, with evidence of hydrophobic forces playing an important part. Future goals for this project include synthesis of torsion balances to study other noncovalent interactions such as halogen bonds and cation- π interaction in water. Our torsion balance can be further modified to study hydrophobic forces and the Lum-Chandler and Weeks theory of hydrophobicity.

8.0 EXPERIMENTAL SECTION

Experimental

General.

^1H and ^{13}C NMR spectra were recorded on Bruker Avance 300, 500 and 600 MHz spectrometers. The chemical shifts are given in parts per million (ppm) on the delta scale (δ), and the coupling constant values (J) are in Hertz. The solvent peak was used as the reference value. For ^1H spectra: $\text{CDCl}_3 = 7.26$ ppm; $\text{CD}_3\text{OD} = 3.30$ ppm; d_6 -acetone = 2.15; d_6 -DMSO = 2.49 ppm. For ^{13}C : $\text{CDCl}_3 = 77.0$ ppm; d_6 -DMSO = 39.5 ppm, d_6 -acetone = 29.0. The abbreviations in proton NMR data are: s = singlet; d = doublet; t = triplet; q = quartet; dd = doublet of doublets; sept = septet; m = multiplet; b = broad. High resolution mass spectra were recorded on a VG 7070 spectrometer. Infrared (IR) spectra were recorded on an Avatar 380 Nicolet FT-IR spectrometer. Melting points were determined using a Thomas Hoover capillary melting point apparatus and are uncorrected. Thin layer chromatography (TLC) was performed on E. Merck 60F 254 (0.25 mm) analytical glass plates. Dry solvents were obtained by distilling the solvents from appropriate drying agent under nitrogen atmosphere shortly before use. CDCl_3 was passed thru a column of basic alumina. Hexanes were stirred over concentrated H_2SO_4 , then over NaHCO_3 and then distilled. Dichloromethane (CH_2Cl_2) was distilled from CaH_2 and stored over 4Å molecular sieves. THF was distilled from sodium metal and

benzophenone. Ethyl acetate was stored over 4Å molecular sieves. Dry DMSO and xylenes were purchased from Aldrich and used as supplied. References to “removal of volatile components under reduced pressure” refer to rotary evaporation of the sample at 25-65 °C at a pressure of 18-25 mm Hg and then overnight under high vacuum (0.1 mm Hg) at room temperature. All percentage yields are for material of >95% purity as indicated by ¹H NMR spectra, unless stated otherwise.

2-Bromo-isophthalic acid monomethyl ester (10). To a solution of 6.31 g (23.2 mmol) of 2-bromo-isophthalic acid dimethyl ester (**9**) in 40 mL (3:1 acetone:methanol) was added solid NaOH (1.01 g, 25.42 mmol). The solution was stirred for 48 h at room temperature after which volatile components were removed under reduced pressure to yield a white slurry. The slurry was dissolved in 100 mL of 1 M NaHCO₃, washed twice with 25 mL ethyl acetate, organic layer was discarded, and aqueous layer acidified with 1 N HCl (to pH ~ 1) to yield a white precipitate. The precipitate was filtered, washed with water and dried to yield 4.8 g of crude product which according to ¹H NMR was mainly (85%) mono acid, (60-70% yield) and the rest diacid: ¹H NMR (500 MHz, CD₃OD) δ 7.76 (dd, 1H, *J* = 7.6 Hz and 1.6 Hz), 7.68 (dd, 1H, *J* = 7.6 Hz and *J* = 1.6 Hz), 7.49 (t, 1H, *J* = 7.6 Hz), 3.92 (s, 3H); ¹³C NMR (125MHz, d₆-DMSO) δ 52.79, 116.65, 127.98, 131.21, 131.49, 135.27, 136.73, 166.67, 167.57; HRMS calcd for C₉H₇BrO₄ 257.9528, found 257.9530. The product was used in the next step without further purification.

General procedure for synthesis of 11a-11f: *Step 1) Nitration:* To a stirred solution of 30 mL 98% sulfuric acid and 5 mL fuming nitric acid cooled in an ice bath

was added 4.7 g of crude **10** (~15 mmol monoacid) from the previous step. After 2 h at 0 °C and 12 h at room temperature, the reaction was quenched with cold water to yield a light yellow precipitate which was filtered and dried to yield 4.5 g of crude product which according to ¹H NMR, was ~85% monoacid (~12 mmol, ~80% yield) and ~15% diacid: ¹H NMR (300 MHz, d₆-DMSO) δ 8.57 (d, 1H, *J* = 2.7 Hz), 8.53 (d, 1H, *J* = 2.7 Hz); ¹³C NMR (75MHz, d₆-DMSO) δ 53.43, 124.33, 125.67, 125.74, 136.59, 137.97, 146.46, 165.018, 165.941; HRMS calcd for C₉H₆BrNO₆ 302.9378, found 302.9367. The product was used for esterification without further purification. **Step 2) Esterification:** To a stirred solution of 0.25 g of crude product (~0.7 mmol monoacid) from the previous step, 1.6 mmol of alcohol and 10 mg (0.08 mmol) of DMAP in 5 mL dichloromethane at -10 °C was added 1,3-dicyclohexylcarbodiimide (0.206 g, 1 mmol) in 5 mL dichloromethane, over 5 min under nitrogen. The reaction was allowed to stir for 3 h during which it warmed to room temperature. The precipitated urea was filtered off, volatile components removed under reduced pressure and the crude product was purified using flash chromatography (SiO₂, 20:80 Ethyl acetate:Hexanes) to give diesters **11a-11f** in 70-90% yield and 80-90% purity (mixtures of symmetrical and unsymmetrical diesters) as waxy solids. These diesters were used in the next step without further purification.

Isopropyl methyl 2-bromo-5-nitro isophthalate (11a): R_f = 0.7 (20:80 Ethyl acetate:Hexanes); ¹H NMR (300 MHz, CDCl₃) δ 8.52 (d, 1H, *J* = 2.7 Hz), 8.45 (d, 1H, *J* = 2.7 Hz), 5.32 (sept, 1H, *J* = 6.4 Hz), 4.0 (s, 3H), 1.41 (d, 6H, *J* = 6.4 Hz).

tert-Butyl methyl 2-bromo-5-nitro isophthalate (11b): $R_f = 0.72$ (20:80 Ethyl acetate:Hexanes); $^1\text{H NMR}$ (300 MHz, CDCl_3) δ 8.52 (d, 1H, $J = 2.7$ Hz), 8.41 (d, 1H, $J = 2.7$ Hz), 4.01 (s, 3H), 1.63 (s, 9H)

Cyclohexyl methyl 2-bromo-5-nitro isophthalate (11c): $R_f = 0.75$ (20:80 Ethyl acetate:Hexanes); $^1\text{H NMR}$ (500 MHz, CDCl_3) δ 8.54 (d, 1H, $J = 2.7$ Hz), 8.47 (d, 1H, $J = 2.7$ Hz), 5.1 (m, 1H), 4.0 (s, 3H), 2.03-1.2 (m, 10H).

1-Adamantyl methyl 2-bromo-5-nitro isophthalate (11d): $R_f = 0.75$ (20:80 Ethyl acetate:Hexanes); $^1\text{H NMR}$ (300 MHz, CDCl_3) δ 8.51 (d, 1H, $J = 2.7$ Hz), 8.4 (d, 1H, $J = 2.7$ Hz), 4.0 (s, 3H), 2.4-1.5 (m, 15H).

2-Adamantyl methyl 2-bromo-5-nitro isophthalate (11e): $R_f = 0.7$ (20:80 Ethyl acetate:Hexanes); $^1\text{H NMR}$ (300 MHz, CDCl_3) δ 8.54 (d, 1H, $J = 2.7$ Hz), 8.50 (d, 1H, $J = 2.7$ Hz), 5.28 (m, 1H), 4.0 (s, 3H), 2.2-1.5 (m, 15H).

Dimethyl 2-bromo-5-nitro isophthalate (11f): $R_f = 0.7$ (20:80 Ethyl acetate:Hexanes); $^1\text{H NMR}$ (300 MHz, CDCl_3) δ 8.5 (s, 2H), 4.0 (s, 3H).

2,5-Dibromo isophthalic acid (13): A 25 mL round bottom flask equipped with a magnetic stir bar was charged with 5.0 g (20.5 mmol) of diacid **12**, 3.1 g (19.6 mmol) bromine, 254 mg (1 mmol) iodine crystals and 7.5 mL fuming sulfuric acid (20% SO_3). The flask was tightly sealed with a glass stopper and heated at 100 $^\circ\text{C}$ in an oil bath for

24 h. After this time, the reaction was cooled to room temperature and slowly quenched with 100 mL 1M NaHSO₃ solution. The resulting precipitate was filtered and dried to yield 4.6 g (70%) of the product as a white powder. ¹H NMR (300 MHz, DMSO-d₆) δ 7.91 (s, 2H); ¹³C NMR (75 MHz, DMSO-d₆) δ 166.5, 138.6, 133.01, 120.6, 115.4; HRMS calcd for C₈Br₂H₄O₄ 321.8476, found 321.8472.

5-Bromo-2-amino-N-(4-tolyl)benzylamine (18). In a 50 mL round bottom flask, 2.0 g (8.2 mmol) 5-bromo-isatoic anhydride **17**, 2.0 g (18.7 mmol) 4-methylaniline and 10 mL dioxane were refluxed with stirring for 12 h. After this period, 25 mL of hot aqueous ethanol (ethanol:water = 80:20) was added and the reaction mixture heated under reflux until the precipitated solids redissolved. The reaction was then allowed to cool slowly to room temperature during which the desired amide precipitated. The precipitate was filtered and dried to yield 1.67 g (66%) of the product as a white flaky solid: R_f = 0.55 (40:60 Ethyl acetate:Hexanes); mp 178-180 °C; ¹H NMR (300 MHz, CDCl₃) δ 7.57 (b, 1H, *J* = 2.7 Hz), 7.55 (d, 1H, *J* = 2.2 Hz), 7.43 (d, 2H, *J* = 8.3 Hz), 7.32 (dd, 1H, *J* = 8.3 Hz and *J* = 2.2 Hz), 7.18 (d, 2H, *J* = 8.3 Hz), 6.61 (d, 1H, 8.3 Hz), 5.45 (b, 2H), 2.34 (s, 3H); ¹³C NMR (125 MHz, CDCl₃:d₆-DMSO = 9:1) δ 20.45, 106.61, 117.74, 118.22, 120.64, 128.78, 130.46, 133.19, 134.21, 135.57, 147.78, 166.44; IR (thin film) 3365, 3370, 3289, 1634, 1579, 1512, 1402, 1310, 1251, 1158 cm⁻¹; HRMS calcd for C₁₄H₁₃BrN₂O 304.0211, found 304.0213. **Amide Reduction:** 3.05 g (10.0 mmol) of the amide from previous step was placed in a 250 mL oven dried round bottom flask equipped with a stir bar and 20 mL dry THF added to it under nitrogen. The flask was cooled in an ice bath and 80 mL of 1.0 M BH₃•THF were slowly added over a period of

15 min with constant stirring. The ice bath was then removed, and the solution brought to reflux for 3 h. The reaction was then again cooled to 0 °C, quenched by drop wise addition of 50 mL 1M NaOH (*caution: vigorous gas evolution takes place*) and allowed to stir for an additional 2 h. The resulting solution was poured into 100 mL water and extracted with 2×50 mL ethyl acetate. The organic layers were combined, dried over MgSO₄, filtered and the volatile components removed under reduced pressure to yield 2.7 g (93%) of the desired amine as white solid which was >95% pure by ¹H NMR: R_f = 0.5 (40:60 Ethyl acetate:Hexanes); mp 76-78 °C; ¹H NMR (300 MHz, d₆-DMSO) δ 7.1 (d, 1H, *J* = 2.3 Hz), 7.02 (dd, 1H, *J* = 2.3 Hz and *J* = 8.3 Hz), 6.84 (d, 2H, *J* = 8.3 Hz), 6.55 (d, 1H, *J* = 8.3 Hz), 6.42 (d, 2H, *J* = 8.3 Hz), 5.85 (t, 1H, *J* = 5.7 Hz), 5.13 (s, 2H), 3.97 (d, 2H, *J* = 5.7 Hz), 2.1 (s, 3H); ¹³C NMR (125 MHz, CDCl₃) δ 145.62, 144.99, 132.39, 131.44, 129.85, 128.13, 125.06, 117.44, 113.96, 109.77, 47.24, 20.41; IR (thin film) 3366, 2915, 1614, 1518, 1487, 1284, 1245 cm⁻¹; HRMS calcd for C₁₄H₁₅BrN₂ 290.04186, found 290.04149.

2-Bromo-8-methyl-6H,12H-5,11-methanodibenzo[*b,f*][1,5]diazocine (19): To a 100 mL round bottom flask charged with 3.11 g (10.7 mmol) of **18** and 1.64 g (11.74 mmol) HMTA was added 40 mL TFA at room temperature over 5 minutes using a dropping funnel. The resulting solution was allowed to stir at room temperature for 14 hours, after which TLC indicated all the starting material to have disappeared. TFA was then distilled off (65 °C, 25 mm Hg) and the resulting thick brown oil diluted with 100 mL dichloromethane and 100 mL ice cold water, cooled in an ice bath and neutralized slowly with drop wise addition of 50 mL ice cold saturated ammonium hydroxide

solution. After a further addition of 50 mL dichloromethane and 50 mL water, the organic layer was separated, dried (MgSO₄), filtered, volatile components removed under reduced pressure and the resulting brown oil purified using flash chromatography (40:60 EtOAc:Hex) to yield 2.6 g (77%) of the desired product as a light yellow solid: R_f = 0.45 (40:60 Ethyl acetate:Hexanes); mp 195-200 °C; ¹H NMR (300 MHz, CDCl₃) δ 7.37-6.9 (m, 5H), 6.71 (s, 1H), 4.65 (dd, 2H, *J* = 7.2 Hz and *J* = 16.6 Hz), 4.27 (m, 2H), 4.11 (dd, *J* = 10.3 Hz and *J* = 16.6 Hz), 2.22 (s, 3H); ¹³C NMR (75 MHz, CDCl₃) δ 147.22, 144.99, 133.72, 130.32, 130.06, 129.71, 128.34, 127.19, 127.09, 126.69, 124.76, 116.46, 66.83, 58.69, 58.33, 20.82; IR (thin film) 2945, 2898, 1687, 1494, 1324, 1097, 1206, 947 cm⁻¹; HRMS calcd for C₁₆H₁₅BrN₂ 314.04186, found 314.04185.

2-Methyl-8-(4,4,5,5-tetramethyl-[1,3,2]dioxaborolan-2-yl)-6H,12H-5,11-methanodibenzo[*b,f*][1,5]diazocine (20): A 50 mL round bottom flask was charged with 0.50 g (1.58 mmol) of **19**, 10 mL DMSO, 0.97 g (2.34 mmol) potassium acetate, bis(pinacolato)diboron (0.5 g, 2 mmol), and dichlorobis[methylene-bis(diphenylphosphine)]-dipalladium-dichloromethane adduct (19.6 mg, 0.024 mmol). The reaction mixture was degassed by freeze pump thaw cycle (×2) and heated at 80 °C for 16 hours under nitrogen. The flask was then cooled to room temperature, diluted with 100 mL dichloromethane and washed twice with 100 mL brine. The organic layer was dried (MgSO₄) and concentrated under reduced pressure to yield a dark brown oil which was purified using flash chromatography (SiO₂, 60:40 EtOAc:Hex) to yield 0.4 g (70%) of **20** as a light brown solid: R_f = 0.5 (60:40 Ethyl acetate:Hexanes); mp 225-227 °C, ¹H NMR (300 MHz, CDCl₃) δ 7.58 (d, 1H, *J* = 7.9 Hz), 7.38 (s, 1H), 7.12 (d, 1H, *J* = 7.9

Hz), 7.1-6.9 (m, 2H), 6.68 (s, 1H), 4.66 (d, 2H, $J = 16.6$ Hz), 4.31 (s, 2H), 4.15 (d, 2H, $J = 16.6$ Hz), 2.19 (s, 3H), 1.28 (s, 12H); ^{13}C NMR (75 MHz, CDCl_3) δ 151.14, 145.1, 133.88, 133.42, 128.16, 127.32, 127.14, 124.71, 124.24, 83.58, 66.89, 58.71, 58.53, 24.75, 20.76; IR (thin film) 2976, 1609, 1360, 1145, 1115, 947 cm^{-1} ; HRMS calcd for $\text{C}_{22}\text{H}_{27}\text{BN}_2\text{O}_2$ 362.2166, found 362.2155.

Representative method for synthesis of torsion balances 21a-21f: A 25 mL pear shaped flask equipped with a magnetic stir bar was charged with 475 mg (1.5 mmol) of diester **11f**, 362 mg (1 mmol) **20**, 636 mg (3 mmol) potassium phosphate (thoroughly grounded with a mortar and pestle), 28 mg (0.05 mmol) chloro(di-2-norbornylphosphino)(2'-dimethylamino-1,1'-bi-phenyl-2-yl)palladium (II), and 5 mL xylenes. The flask was sealed with a rubber septum, flushed with nitrogen, degassed twice using the freeze pump thaw cycle, and heated at 110 °C with vigorous stirring for 48 h. The flask was then cooled to room temperature, 20 mL dichloromethane added, and the reaction mixture filtered to yield a dark brown solution which was concentrated under reduced pressure and purified using flash chromatography (SiO_2 , 60:40 EtOAc:Hex) to yield the desired product **21f** as a yellow foam in 50% (235 mg, 0.5 mmol) yield.

Isopropyl methyl 4'-nitro-2-phenyl-8-methyl-6H,12H-5,11-methanodibenzo [b,f][1,5] diazocine-3',6'-dicarboxylate (21a): By the general procedure, 650 mg (~1.5 mmol) of crude diester **11a**, 362 mg (1 mmol) **20**, 636 mg (3 mmol) potassium phosphate and 28 mg (0.05 mmol) chloro(di-2-norbornylphosphino)(2'-dimethylamino-1,1'-bi-phenyl-2-yl)palladium (II) afforded 300 mg (60%) of **21a** after chromatography (SiO_2 ,

60:40 Ethyl acetate:Hexanes) as a yellow foam: $R_f = 0.3$ (60:40 Ethyl acetate:Hexanes); ^1H NMR (500 MHz, CDCl_3) δ 8.63 (m, b, 2H), 7.14 (d, 1H, $J = 8.2$ Hz), 7.1-6.8 (m, 5H), 5.2-4.4 (b, 1H), 4.7 (d, 2H, $J = 16.6$ Hz), 4.36 (b, 2H), 4.13 (m, 2H, $J = 16.6$ Hz), 3.7/2.99 {s, (2.1/0.9)H}, 2.2 (s, 3H), 1.07/0.34 {s/d, (1.8/4.2)H}; ^{13}C NMR (75 MHz, CDCl_3) δ 19.9, 20.61, 52.72, 58.68, 59.04, 66.95, 69.77, 124.25, 124.54, 125.67, 125.89, 126.44, 127.01, 127.158, 127.58, 128.13, 132.56, 133.28, 134.04, 136.1, 144.97, 146.11, 146.17, 148.37, 165.96; IR (thin film) 2941, 2850, 1720, 1600, 1530, 1493, 1440, 1348, 1321, 1245, 1205; HRMS calcd for $\text{C}_{28}\text{H}_{27}\text{N}_3\text{O}_6$ 501.1899, found 501.1883.

***tert*-Butyl methyl 4'-nitro-2-phenyl-8-methyl-6H,12H-5,11-methanodibenzo [*b,f*][1,5]diazocine-3',6'-dicarboxylate (21b):** By the general procedure, 700 mg (~1.5 mmol) of crude diester **11b**, 362 mg (1 mmol) **20**, 636 mg (3 mmol) potassium phosphate and 28 mg (0.05 mmol) chloro(di-2-norbornylphosphino)(2'-dimethylamino-1,1'-biphenyl-2-yl)palladium (II) afforded 270 mg (52%) of **21b** after chromatography (SiO_2 , 60:40 Ethyl acetate:Hexanes) as a yellow foam: $R_f = 0.3$ (60:40 Ethyl acetate:Hexanes); ^1H NMR (500 MHz, CDCl_3) δ 8.56 (m, 2H), 7.14 (d, 1H, $J = 8.3$ Hz), 7.1-6.8 (m, 5H), 4.69 (d, 2H, $J = 16.6$ Hz), 4.36 (b, 2H), 4.13 (m, 2H, $J = 16.6$ Hz), 3.68/3.02 {s, (2.3/0.7) H}, 2.21 (s, 3H), 1.28/0.68 {s, b, (2.8/9.2)H}; ^{13}C NMR (75 MHz, CDCl_3) δ 166, 165.56, 148.37, 146.23, 145.86, 145.06, 133.36, 132.88, 128.23, 127.66, 127.25, 127.02, 126.51, 125.75, 125.43, 124.67, 124.36, 82.68, 66.94, 59.16, 58.75, 28.92, 26.73, 20.66; IR (thin film) 2949, 1716, 1600, 1530, 1493, 1439, 1351, 1322, 1292, 1250, 1157; HRMS calcd for $\text{C}_{29}\text{H}_{30}\text{N}_3\text{O}_6$ 516.2135, found 516.2140.

Cyclohexyl methyl 4'-nitro-2-phenyl-8-methyl-6H,12H-5,11-methanodibenzo [b,f][1,5]diazocine-3',6'-dicarboxylate (21c): By the general procedure, 750 mg (~1.5 mmol) of crude diester **11c**, 362 mg (1 mmol) **20**, 636 mg (3 mmol) potassium phosphate and 28 mg (0.05 mmol) chloro(di-2-norbornylphosphino)(2'-dimethylamino-1,1'-bi-phenyl-2-yl)palladium (II) afforded 310 mg (58%) of **21c** after chromatography (SiO₂, 60:40 Ethyl acetate:Hexanes) as a yellow foam: R_f = 0.35 (60:40 Ethyl acetate:Hexanes); ¹H NMR (300 MHz, CDCl₃) δ 8.60 (b, 2H), 7.14 (d, 1H, *J* = 8.2 Hz), 7.1-6.9 (m, 3H), 6.72 (m, 2H), 4.7-4.3 (b, 1H), 4.68 (m, 2H, *J* = 16.8 Hz), 4.31 (b, 2H), 4.12 (m, 2H, *J* = 16.8), 3.68/2.99 {s, (1.95/1.05)H}, 2.2 (s, 3H), 2-0.2 {b, 11H}; ¹³C NMR (75 MHz, CDCl₃) δ 20.71, 23.19, 24.55, 24.80, 24.97, 25.39, 30.76, 52.5, 58.84, 66.88, 74.66, 74.91, 124.51, 124.75, 125.61, 125.92, 126.47, 126.99, 127.16, 127.27, 127.68, 128.22, 132.66, 133.47, 134.84, 135.79, 145.18, 145.99, 146.31, 148.65, 152.83, 165.87, 166.47; IR (thin film) 2940, 2857, 1722, 1600, 1530, 1493, 1439, 1348, 1322, 1245, 1206; HRMS calcd for C₃₁H₃₁N₃O₆ 541.2212, found 541.2198.

1-Adamantyl methyl 4'-nitro-2-phenyl-8-methyl-6H,12H-5,11-methano dibenzo[b,f][1,5]diazocine-3',6'-dicarboxylate (21d): By the general procedure, 750 mg (~1.5 mmol) of crude diester **11d**, 362 mg (1 mmol) **20**, 636 mg (3 mmol) potassium phosphate and 28 mg (0.05 mmol) chloro(di-2-norbornylphosphino)(2'-dimethylamino-1,1'-bi-phenyl-2-yl)palladium (II) afforded 350 mg (59%) of **21d** after chromatography (SiO₂, 60:40 Ethyl acetate:Hexanes) as a yellow foam: R_f = 0.35 (60:40 Ethyl acetate:Hexanes); ¹H NMR (500 MHz, CDCl₃) δ 8.58 (m, b, 2H), 7.14 (d, 1H, *J* = 8.2 Hz), 7.1-6.7 (m, 5H), 4.68 (m, 2H), 4.31 (b, m, 2H), 4.12 (m, 2H), 3.67/3.07 {s,

(1.92/1.08) H}, 2.19 (s, 3H), 2.2-0.9 {m, b, 15H}; ¹³C NMR (75 MHz, CDCl₃) δ 20.47, 20.74, 20.96, 21.37, 24.82, 30.6, 30.83, 35.82, 40.61, 52.38, 58.67, 60.31, 66.89, 74.93, 83.13, 123.86, 124.49, 124.76, 125, 125.28, 125.56, 126.52, 126.94, 127.02, 127.18, 127.4, 127.6, 128.1, 128.2, 132.83, 133.4, 133.5, 134.56, 137.15, 145.3, 145.7, 146.31, 148.67, 165.17, 166.45; IR (thin film) 2911, 1719, 1600, 1529, 1493, 1439, 1351, 1324, 1245, 1207; HRMS calcd for C₃₅H₃₅N₃O₆ 593.2525, found 593.2527.

2-Adamantyl methyl 4'-nitro-2-phenyl-8-methyl-6H,12H-5,11-methanodibenzo[*b,f*][1,5]diazocine-3',6'-dicarboxylate (21e): By the general procedure, 750 mg (~1.5 mmol) of crude diester **11e**, 362 mg (1 mmol) **20**, 636 mg (3 mmol) potassium phosphate and 28 mg (0.05 mmol) chloro(di-2-norbornylphosphino)(2'-dimethylamino-1,1'-bi-phenyl-2-yl)palladium (II) afforded 325 mg (55%) of **21e** after chromatography (SiO₂, 60:40 Ethyl acetate:Hexanes) as a yellow foam: R_f = 0.35 (60:40 Ethyl acetate:Hexanes); ¹H NMR (300 MHz, CDCl₃) δ 8.58 (b, 2H), 7.14 (d, 1H, *J* = 8.2 Hz), 7.1-6.7 (m, 5H), 5.0-4.8 (b, 1H), 4.68 (m, 2H), 4.29 (b, 2H), 4.12 (b, 2H), 3.66/2.96 {s, (2.1/0.9) H}, 2.2 (s, b, 3H), 2-0.2 {b, 15H}; ¹³C NMR (125 MHz, CDCl₃) δ 166.72, 148.89, 147.21, 146.26, 145.4, 135.0, 133.58, 132.67, 128.3, 127.91, 127.27, 127.09, 126.35, 125.96, 125.51, 124.91, 79.46, 74.97, 66.59, 58.67, 58.1, 52.74, 36.93, 35.99, 31.45, 30.8, 26.68, 24.82, 20.9; IR (thin film) 2911, 1719, 1600, 1529, 1494, 1439, 1351, 1324, 1250, 1200; HRMS calcd for C₃₅H₃₅N₃O₆ 593.2525, found 593.2546.

Dimethyl 4'-nitro-2-phenyl-8-methyl-6H,12H-5,11-methanodibenzo[*b,f*][1,5]diazocine-3',6'-dicarboxylate (21f): ¹H NMR (300 MHz, CDCl₃) δ 8.63 (b, 2H), 7.14

(d, 1H, $J = 8.1$ Hz), 7.1-6.83 (m, 3H), 6.71 (s, 2H), 4.69 (d, 2H, $J = 16.6$ Hz), 4.39 (m, 2H), 4.13 (dd, 2H, $J = 16.6$ Hz and $J = 10.3$ Hz), 3.7/2.88 {s, (1.5/1.5) H}, 2.19 (s, 3H); ^{13}C NMR (125 MHz, CDCl_3) δ 166.5, 148.48, 146.64, 146.3 145.03, 133.42, 132.47, 128.21, 127.84, 127.35, 127.25, 127.03, 126.62, 126.15, 124.6, 124.34, 67.31, 59.35, 59.05, 52.24, 20.67; IR (thin film) 2949, 1726, 1600, 1529, 1493, 1439, 1350, 1312, 1244; HRMS calcd for $\text{C}_{26}\text{H}_{23}\text{N}_3\text{O}_6$ 473.1586, found 473.1597.

Representative method for synthesis of torsion balances 22a-22f. A 25 mL round bottom flask equipped with a magnetic stir bar was charged with 100 mg (0.2 mmol) of **21a**, 21.1 mg (0.01 mmol) 5% palladium on carbon and 10 mL, ethyl acetate. The flask was sealed with a rubber septum and the heterogeneous solution was stirred under H_2 (using a balloon) for ~12 h. After this time TLC indicated all the starting material to have disappeared. The catalyst was filtered off using a short (1'') column of silica gel and eluting with ethyl acetate (50 mL). Removal of solvent under reduced pressure afforded 85 mg (90%) of **22a** as a white foam, which was >95% pure by ^1H NMR.

Isopropyl methyl 4'-amino-2-phenyl-8-methyl-6H,12H-5,11-methanodibenzo [b,f][1,5]diazocine-3',6'-dicarboxylate (22a): $R_f = 0.15$ (60:40 Ethyl acetate:Hexanes); ^1H NMR (300 MHz, CDCl_3) δ 7.1-6.9 (m, 6H), 6.65(b, 2H), 5.2-4.4 (b, 1H), 4.64 (d, 2H, $J = 16.6$ Hz), 4.36 (m, 2H), 4.12 (m, 2H, $J = 16.6$ Hz), 3.88 (b, 2H), 3.54/2.87 {s, (2.1/0.9)H}, 2.17 (s, 3H), 0.97/0.28 {s/d, (1.8/4.2)H}; ^{13}C NMR (75 MHz, CDCl_3) δ 168.45, 146.57, 145.39, 145.14, 135.15, 134.95, 133.54, 133.11, 129.86, 128.21, 127.99,

127.37, 127.26, 126.99, 126.77, 126.68, 124.54, 123.65, 117.37, 117.1, 68.45, 67.06, 58.96, 58.77, 51.72, 20.56; IR (thin film) 3374, 2950, 1700, 1607, 1460, 1348, 1254, 1208, 1150; HRMS calcd for C₂₈H₂₉N₃O₄ 471.2158, found 471.2155.

***tert*-Butyl methyl 4'-amino-2-phenyl-8-methyl-6H,12H-5,11-methanodibenzo[*b,f*][1,5]diazocine-3',6'-dicarboxylate (22b):** Following the general method, 100 mg (0.2 mmol) of **21b** and 21 mg (0.01 mmol) 5% palladium on carbon afforded 85 mg (90%) of **22b** as a white foam: R_f = 0.15 (60:40 Ethyl acetate:Hexanes); ¹H NMR (300 MHz, CDCl₃) δ 7.1-6.8 (m, 6H), 6.67 (m, 2H), 4.68 (d, 2H, *J* = 16.3 Hz), 4.35 (m, 2H), 4.12 (m, 2H), 3.82 (s, 2H), 3.6/2.91 {s, (2.4/0.6)H}, 2.2 (s, 3H), 1.1-0.6 (b, 12H); ¹³C NMR (75 MHz, CDCl₃) δ 167.95, 149.37, 146.68, 146.48, 145.3, 145.05, 135.52, 135.31, 133.32, 132.69, 129.81, 128.36, 128.16, 127.42, 127.32, 127.24, 127.05, 126.84, 126.75, 124.68, 123.88, 123.82, 117.46, 117.07, 116.96, 116.45, 115.99, 81.35, 67.01, 59.09, 58.82, 52.22, 28.94, 28.09, 26.82, 20.67; IR (thin film) 3374, 2949, 1709, 1607, 1461, 1348, 1254, 1204, 1157; HRMS calcd for C₂₉H₃₁N₃O₄ 485.2315, found 485.2393.

Cyclohexyl methyl 4'-amino-2-phenyl-8-methyl-6H,12H-5,11-methanodibenzo[*b,f*][1,5]diazocine-3',6'-dicarboxylate (22c): Following the general method, 100 mg (0.18 mmol) of **21c** and 21 mg (0.01 mmol) 5% palladium on carbon afforded 90 mg (96%) of **22c** as a white foam: R_f = 0.15 (60:40 Ethyl acetate:Hexanes); ¹H NMR (300 MHz, CDCl₃) δ 7.1-6.9 (m, 6H), 6.69 (b, 2H), 4.7-4.3 (b, 1H), 4.69 (dd, 2H, *J* = 16.6 Hz and *J* = 5.5 Hz), 4.32 (b, m, 2H), 4.12 (m, 2H, *J* = 16.6 Hz), 3.85 (s, 2H), 3.55/2.87 {s, (1.95/1.05) H}, 2.19 (s, 3H), 2-0.5 (b, 11 H); ¹³C NMR (75 MHz, CDCl₃) δ

168.68, 146.79, 145.21, 135.16, 134.09, 133.33, 130, 128.21, 128.1, 127.37, 127.02, 126.84, 124.74, 123.97, 117.52, 117.18, 73.48, 66.86, 58.89, 58.67, 51.73, 30.86, 27.8, 25.09, 24.83, 23.27, 20.76; IR (thin film) 3374, 2941, 1713, 1607, 1494, 1463, 1354, 1258, 1204, 1119; HRMS calcd for C₃₁H₃₃N₃O₄ 511.2471, found 511.2472.

1-Adamantyl methyl 4'-amino-2-phenyl-8-methyl-6H,12H-5,11-methano dibenzo[*b,f*][1,5]diazocine-3',6'-dicarboxylate (22d): Following the general method, 100 mg (0.17 mmol) of **21d** and 21 mg (0.01 mmol) 5% palladium on carbon afforded 95 mg (98%) of **22d** as a white foam: R_f = 0.15 (60:40 Ethyl acetate:Hexanes); ¹H NMR (500 MHz, CDCl₃) δ 7.2-6.8 (m, 6H), 6.7 (b, 2H), 4.67 (m, 2H, *J* = 16.3 and *J* = 7.5 Hz), 4.29 (b, 2H), 4.11 (m, 2H), 3.87 (b, 2H), 3.53/2.95 {s, (1.92/1.08)H}, 2.18 (s, 3H), 2-0.5 (b, 15 H); ¹³C NMR (125 MHz, CDCl₃) δ 168.78, 167.53, 146.74, 145.23, 136.11, 135.37, 133.8, 133.47, 133.31, 129.64, 128.36, 128.05, 127.79, 127.21, 126.99, 126.65, 124.96, 124.71, 123.89, 117.25, 116.79, 81.43, 66.81, 58.59, 51.78, 40.51, 35.88, 30.47, 24.77, 20.7; IR (thin film) 3368, 2900, 1711, 1607, 1496, 1466, 1359, 1262, 1196, 1119; HRMS calcd for C₃₅H₃₇N₃O₄ 563.2784, found 563.2764.

2-Adamantyl methyl 4'-amino-2-phenyl-8-methyl-6H,12H-5,11-methano dibenzo[*b,f*][1,5]diazocine-3',6'-dicarboxylate (22e): Following the general method, 100 mg (0.17 mmol) of **21e** and 21 mg (0.01 mmol) 5% palladium on carbon afforded 95 mg (98%) of **22e** as a white foam: R_f = 0.15 (60:40 Ethyl acetate:Hexanes); ¹H NMR (300 MHz, CDCl₃) δ 7.2-6.9 (m, 6H), 6.72 (m, 2H), 4.8-4.3 (b, 1H), 4.67 (m, 2H), 4.29 (s, 2H), 4.12 (m, 2H), 3.87 (s, 2H), 3.53/2.81 {s, (2.1/0.9)H}, 2.19 (s, 3H), 2-0.5 (b,

15H); ^{13}C NMR (75 MHz, CDCl_3) δ 169.1, 147.01, 145.48, 145.23, 135.23, 134.62, 133.37, 129.67, 128.76, 128.16, 127.54, 127.1, 127.05, 125.05, 124.88, 124.25, 117.59, 117, 78.31, 75, 66.93, 66.18, 58.67, 51.69, 37.15, 36.17, 31.89, 31.59, 31.04, 26.89, 24.86, 20.87; IR (thin film) 3369, 2906, 1711, 1608, 1494, 1464, 1359, 1262, 1196, 1120; HRMS calcd for $\text{C}_{35}\text{H}_{37}\text{N}_3\text{O}_4$ 563.2784, found 563.2809.

Dimethyl 4'-amino-2-phenyl-8-methyl-6H,12H-5,11-methanodibenzo[*b,f*][1,5]diazocine-3',6'-dicarboxylate (22f): Following the general method, 100 mg (0.21 mmol) of **21f** and 21 mg (0.01 mmol) 5% palladium on carbon afforded 95 mg (99%) of **22f** as a white foam: $R_f = 0.15$ (60:40 Ethyl acetate:Hexanes); ^1H NMR (300 MHz, CDCl_3) δ 7.1-6.9 (m, 6H), 6.67 (m, 2H), 4.66 (dd, 2H, $J = 16.6$ Hz and $J = 5.6$ Hz), 4.38 (m, 2H), 4.11 (dd, 2H, $J = 16.6$ Hz and $J = 9.5$ Hz), 3.86 (s, 2H), 3.57/2.77 {s, (1.5/1.5) H}, 2.17 (s, 3H); ^{13}C NMR (75 MHz, CDCl_3) δ 168.75, 146.7, 145.29, 135.01, 133.22, 130.57, 128.18, 128.07, 127.6, 127.27, 127.03, 124.62, 123.8, 117.63, 67.45, 59.34, 59.2, 51.6, 20.68; IR (thin film) 3375, 2948, 1720, 1608, 1493, 1435, 1351, 1261, 1202, 1118; HRMS calcd for $\text{C}_{26}\text{H}_{25}\text{N}_3\text{O}_4$ 443.1845, found 443.1837.

Representative procedure for synthesis of torsion balances 23a-23f. A 10 mL round bottom flask was charged with 47 mg (0.1 mmol) of **22a**, 22.8 mg (0.2 mmol) of glutaric anhydride and 1 mL of dichloromethane. The resulting solution was allowed to sit for 24 h after which TLC indicated all the starting material to have disappeared. The solvent was removed under reduced pressure and then under high vacuum to yield a white foam which according to ^1H NMR consisted of the desired product **23a**

(quantitative yield) and the unreacted glutaric anhydride only. The unreacted glutaric anhydride was removed by carefully washing the crude product with small amount of dichloromethane, however, some loss of the product occurred during this process. After washing, 20 mg (35%) of **23a** was obtained as a white foam.

Isopropyl methyl 4'-(4-carboxybutyrylamino)-2-phenyl-8-methyl-6H,12H-5,11-methanodibenzo[*b,f*][1,5]diazocine-3',6'-dicarboxylate (23a): ^1H NMR (500 MHz, D_2O) δ 7.9/7.84 {s, (0.77/0.23)H}, 7.79/7.75 {s, (0.23/0.77)H}; 7.07 (d, 1H, $J = 8.2$ Hz), 6.95 (m, b, 2H), 6.87 (d, 1H, $J = 8.2$ Hz), 6.73 (s, 1H), 6.68 (s, 1H), 4.58-4.51 (m, 2H), 4.25 (b, 2H), 4.08 (d, 1H, $J = 17.1$ Hz), 4.03 (d, 1H, $J = 17.1$ Hz), 3.54/2.93 {s, (2.3/0.7)H}, 2.32 (t, 2H, $J = 7.4$ Hz), 2.12 (t, 2H, $J = 7.4$ Hz), 2.07 (s, 3H), 1.8 (q, 2H, $J = 7.4$ Hz), 0.85/0.15 {m/m ($J = 6.1$ Hz), (0.7/2.3)H}, ^{13}C NMR (125 MHz, d_6 -acetone) δ 174.09, 171.29, 167.73, 167.28, 147.67, 145.83, 139.86, 138.72, 134.75, 134.09, 134.03, 133.66, 132.51, 127.84, 127.66, 127.37, 127.05, 124.61, 123.87, 121.08, 120.83, 68.26, 66.87, 58.75, 58.59, 51.2, 35.69, 32.9, 20.49, 19.9; IR (thin film) 3325, 2978, 1710, 1593, 1526, 1460, 1323, 1252, 1203, 1103; HRMS calcd for $\text{C}_{33}\text{H}_{35}\text{N}_3\text{O}_7$, 585.2475, found 585.2486.

***tert*-Butyl methyl 4'-(4-carboxybutyrylamino)-2-phenyl-8-methyl-6H,12H-5,11-methanodibenzo[*b,f*][1,5]diazocine-3',6'-dicarboxylate (23b):** Following the general procedure, 48 mg (0.1 mmol) of **22b** and 22.8 mg (0.2 mmol) of glutaric anhydride afforded 22 mg (36%) of **23b** as a white foam: ^1H NMR (500 MHz, D_2O) δ 7.96/7.88 {s, (0.83/0.17)H}, 7.84/7.78 {s, (0.17/0.83)H}; 7.07 (d, 1H, $J = 8.2$ Hz), 6.95

(m, b, 2H), 6.84 (d, 1H, $J = 8.2$ Hz), 6.75 (s, 1H), 6.65 (s, 1H), 4.6-4.5 (m, 2H), 4.29 (b, 2H), 4.07 (d, 1H, $J = 17.2$ Hz), 3.99 (d, 1H, $J = 17.2$ Hz), 3.58/2.88 {s, (2.5/0.5)H}, 2.38 (t, 2H, $J = 7.4$ Hz), 2.17 (t, 2H, $J = 7.4$ Hz), 2.11 (s, 3H), 1.84 (q, 2H, $J = 7.4$ Hz), 1.13/0.5 {s/s, (2/10)H}, ^{13}C NMR (75 MHz, $\text{d}_6\text{-DMSO}$) δ 174.01, 171.26, 167.28, 166.8, 147.24, 145.3, 138.14, 135.56, 133.49, 132.77, 132.2, 127.63, 127.39, 127.2, 126.9, 126.78, 124.39, 123.76, 120.75, 120.39, 80.9, 66.44, 58.54, 58.3, 51.83, 35.33, 32.82, 26.64, 20.31, 20.21; IR (thin film) 3320, 2979, 1709, 1590, 1525, 1460, 1323, 1250, 1203, 1103; HRMS calcd for $\text{C}_{34}\text{H}_{37}\text{N}_3\text{O}_7$, 599.2631, found 599.2602.

Cyclohexyl methyl 4'-(4-carboxybutyrylamino)-2-phenyl-8-methyl-6H,12H-5,11-methanodibenzo[*b,f*][1,5]diazocine-3',6'-dicarboxylate (23c): Following the general procedure, 51 mg (0.1 mmol) of **22c** and 22.8 mg (0.2 mmol) of glutaric anhydride and afforded 15 mg (24%) of **23c** as a white foam: ^1H NMR (500 MHz, D_2O) δ 7.93-7.84 (m, 2H), 7.11 (d, 1H, $J = 8.3$ Hz), 7.01 (m, b, 2H), 6.94 (d, 1H, $J = 8.3$ Hz), 6.82 (s, 1H), 6.73 (s, 1H), 4.6-4.2 (m, 4H), 4.13 (d, 1H, $J = 17$ Hz), 4.16 (d, 1H, $J = 17$ Hz), 3.58/2.95 {s, (2.25/0.75)H}, 2.38 (t, 2H, $J = 7.5$ Hz), 2.17 (t, 2H, $J = 7.5$ Hz), 2.13 (s, 3H), 1.86 (q, 2H, $J = 7.5$ Hz), 1.6-0.1 {m, 11H}; ^{13}C NMR (75 MHz, $\text{d}_6\text{-acetone}$) δ 174.01, 171.27, 167.89, 167.25, 147.8, 145.92, 138.7, 134.66, 134.15, 134.01, 133.88, 132.57, 127.76, 127.66, 127.59, 127.37, 126.94, 126.87, 124.7, 124.04, 123.31, 121.1, 120.8, 72.95, 70.33, 66.71, 58.45, 58.37, 51.15, 43.29, 32.77, 30.55, 24.42, 22.89, 20.51, 19.95; IR (thin film) 3300, 2970, 1709, 1590, 1530, 1455, 1323, 1250, 1200, 1113; HRMS calcd for $\text{C}_{36}\text{H}_{39}\text{N}_3\text{O}_7$ 625.2788, found 626.2763.

1-Adamantyl methyl 4'-(4-carboxybutyrylamino)-2-phenyl-8-methyl-6H, 12H-5,11-methanodibenzo[*b,f*][1,5]diazocine-3',6'-dicarboxylate (23d): Following the general procedure, 56 mg (0.1 mmol) of **22d** and 22.8 mg (0.2 mmol) of glutaric anhydride and afforded 10 mg (15%) of **23d** as a white foam: ^1H NMR (500 MHz, D_2O) δ 7.92-7.7 {m, 2H}; 7.18 (d, 2H, $J = 8.4$ Hz), 7.0 (m, 3H), 6.85 (s, 1H), 6.76 (s, 1H), 4.7-4.3 (m, 2H), 4.22-4.1 (m, 4H), 3.58/3.06 {s, (2.3/0.7)H}, 2.38 (t, 2H, $J = 7.4$ Hz), 2.16 (t, 2H, $J = 7.4$ Hz), 2.11 (s, 3H), 1.84 (q, 2H, $J = 7.4$ Hz), 1.5-0.5 {m, 15H}, ^{13}C NMR (125 MHz, $\text{d}_6\text{-DMSO}$) δ 174.1, 171.36, 167.52, 166.51, 147.44, 145.52, 138.18, 135.44, 133.46, 133.13, 132.28, 127.61, 127.49, 127.08, 126.92, 124.51, 123.95, 120.61, 120.36, 80.96, 66.5, 58.04, 51.9, 35.38, 32.87, 32.77, 29.92, 20.41, 20.27, 19.96; IR (thin film) 2913, 1708, 1595, 1533, 1496, 1460, 1343, 1249, 1203; HRMS calcd for $\text{C}_{40}\text{H}_{43}\text{N}_3\text{O}_7$ 677.3101, found 678.3193.

2-Adamantyl methyl 4'-(4-carboxybutyrylamino)-2-phenyl-8-methyl-6H, 12H-5,11-methanodibenzo[*b,f*][1,5]diazocine-3',6'-dicarboxylate (23e): Following the general procedure, 56 mg (0.1 mmol) of **22e** and 22.8 mg (0.2 mmol) of glutaric anhydride and afforded 9 mg (14%) of **23e** as a white foam: ^1H NMR (500 MHz, D_2O) δ 7.96-7.83 {m, 2H}, 7.15-6.9 (m, 4H), 6.87 (s, 1H), 6.85 (s, 1H), 4.7-4.3 (m, 2H), 4.22 (s, 2H), 4.16 (d, 1H, $J = 17$ Hz), 4.09 (d, 1H, $J = 17$ Hz), 3.58/2.94 {s, (2.4/0.6)H}, 2.38 (t, 2H, $J = 7.4$ Hz), 2.19 (s, 3H), 2.17 (t, 2H, $J = 7.4$ Hz), 1.84 (q, 2H, $J = 7.4$ Hz), 2-0.1 (m, 15H); ^{13}C NMR (75 MHz, $\text{d}_6\text{-DMSO}$) δ 174.02, 171.31, 167.75, 167.19, 147.44, 145.43, 138.18, 134.17, 133.77, 133.3, 132.29, 127.62, 127.35, 127.11, 126.92, 126.38, 124.53, 1124.15, 120.83, 120.46, 77.55, 57.9, 52.1, 36.46, 35.45, 35.35, 32.82, 32.7, 30.94, 30.45,

26.17, 24.89, 20.48, 20.21, 19.91; IR (thin film) 3331, 2878, 1710, 1589, 1525, 1455, 1320, 1249, 1200, 1110; HRMS calcd for C₄₀H₄₃N₃O₇ 677.3101, found 677.3175.

Dimethyl 4'-(4-carboxybutyrylamino)-2-phenyl-8-methyl-6H,12H-5,11-methanodibenzo[*b,f*][1,5]diazocine-3',6'-dicarboxylate (23f): Following the general procedure, 44 mg (0.1 mmol) of **22f** and 22.8 mg (0.2 mmol) of glutaric anhydride and afforded 28 mg (56%) of **23f** as a white foam: ¹H NMR (300 MHz, D₂O) δ 7.9-7.7 {m, b, 2H}, 7.01(d, 1H, *J* = 8.3 Hz), 6.96 (m, b, 2H), 6.78(d, 1H, *J* = 8.3 Hz), 6.73 (s, 1H), 6.56 (s, 1H), 4.54 (d, 1H, *J* = 7.3 Hz), 4.48 (d, 1H, *J* = 7.3 Hz), 4.28 (s, 2H), 4.04 (d, 1H, *J* = 12 Hz), 3.98 (d, 1H, *J* = 12 Hz), 3.55/2.71 {s, (1.5/1.5)H}, 2.34 (t, 2H, *J* = 7.4 Hz), 2.14 (t, 2H, *J* = 7.4 Hz), 2.03 (s, 3H), 1.8 (q, 2H, *J* = 7.4 Hz), ¹³C NMR (125 MHz, DMSO-*d*₆) δ 174.14, 171.42, 168.1, 167.7, 147.24, 145.34, 138.23, 133.91, 133.09, 132.27, 127.76, 127.66, 127.41, 126.98, 126.72, 124.41, 123.86, 121.04, 66.58, 58.54, 58.42, 51.78, 35.38, 32.84, 32.75, 20.35, 20.25, 19.96; IR (thin film) 3307, 2949, 1716, 1594, 1558, 1496, 1458, 1338, 1249, 1203, 1120; HRMS calcd for C₃₁H₃₁N₃O₇ 557.2162, found 557.2142.

***trans*-4-Cyclohexylcyclohexyl methyl 4'-nitro-2-phenyl-8-methyl-6H,12H-5,11-methanodibenzo[*b,f*][1,5]diazocine-3',6'-dicarboxylate (25a):** By the general procedure, ~1.5 mmol of crude diester, 362 mg (1 mmol) **20**, 636 mg (3 mmol) potassium phosphate and 28 mg (0.05 mmol) chloro(di-2-norbornylphosphino)(2'-dimethylamino-1,1'-bi-phenyl-2-yl)palladium (II) afforded 350 mg (51%) of **25a** after chromatography (SiO₂, 60:40 Ethyl acetate:Hexanes) as a yellow foam: R_f = 0.4 (60:40 Ethyl

acetate:Hexanes); ^1H NMR (500 MHz, CDCl_3) δ 8.60 (b, 2H), 7.16-6.9 (m, 4H), 6.72 (m, 2H), 4.66 (m, 2H), 4.32 (b, 2H), 4.14 (m, 2H), 3.68/3.0 {s, (1.65/1.35) H}, 2.2 (s, 3H), 2-0.2 (b, 21H); ^{13}C NMR (125 MHz, CDCl_3) δ 166.33, 164.53, 157.39, 156.28, 148.69, 146.25, 145.13, 135.21, 134.58, 133.43, 132.60, 128.23, 127.63, 127.32, 126.99, 125.91, 125.73, 124.78, 124.51, 75.78, 74.97, 58.63, 52.73, 42.46, 41.90, 31.13, 30.30, 30.13, 27.51, 26.68, 24.81, 20.82; IR (thin film) 2925, 2852, 1724, 1600, 1530, 1493, 1439, 1350, 1325, 1244, 1147; HRMS calcd for $\text{C}_{37}\text{H}_{42}\text{N}_3\text{O}_6$ 624.3074, found 624.3041.

***trans*-4-*tert*-Butylcyclohexyl methyl 4'-nitro-2-phenyl-8-methyl-6H,12H-5,11-methanodibenzo[*b,f*][1,5]diazocine-3',6'-dicarboxylate (26a):** By the general procedure, ~1.5 mmol of crude diester, 362 mg (1 mmol) **20**, 636 mg (3 mmol) potassium phosphate and 28 mg (0.05 mmol) chloro(di-2-norbornylphosphino)(2'-dimethylamino-1,1'-bi-phenyl-2-yl)palladium (II) afforded 320 mg (50%) of **26a** after chromatography (SiO_2 , 60:40 Ethyl acetate:Hexanes) as a yellow foam: $R_f = 0.4$ (60:40 Ethyl acetate:Hexanes); ^1H NMR (500 MHz, CDCl_3) δ 8.60 (b, 2H), 7.2-6.9 (m, 4H), 6.72 (m, 2H), 4.68 (m, 2H), 4.31 (b, 2H), 4.14 (m, 2H), 3.68/2.99 {s, (1.4/1.6)H}, 2.2 (s, 3H), 2-0.2 (b, 19H); ^{13}C NMR (150 MHz, CDCl_3) δ 167.57, 146.32, 145.16, 133.46, 132.6, 131.33, 128.25, 127.68, 127.41, 127.23, 127.01, 126.65, 125.9, 125.73, 125.05, 124.8, 124.5, 75.86, 66.92, 58.71, 46.85, 32.25, 31.52, 27.55, 25.28, 24.86; IR (thin film) 2950, 1725, 1600, 1530, 1493, 1439, 1349, 1325, 1245, 1206; HRMS calcd for $\text{C}_{35}\text{H}_{39}\text{N}_3\text{O}_6$ 597.2838, found 597.2825.

Isopropyl phenyl 4'-nitro-2-phenyl-8-methyl-6H,12H-5,11-methanodibenzo [b,f][1,5]diazocine-3',6'-dicarboxylate (31): A 10 mL flask was charged with a magnetic stir bar, 100 mg (0.2 mmol) of **21a**, 110 mg (0.6 mmol) (CH₃)₃Sn(OH), and 5 mL 1,2-dichloroethane. The flask was septum sealed and heated at 80 °C for 72 h after which TLC indicated only a faint spot for the starting material. A portion of 20 mL 1,2-dichloroethane was then added and the reaction mixture washed with 25mL 1 M HCl and then with brine. The organic layer was dried over MgSO₄, filtered and concentrated under reduced pressure. The crude product was dissolved in 5 mL dichloromethane and to this solution was added bis(2-oxo-3-oxazolidinyl)phosphinic chloride (102 g, 0.4 mmol), phenol (94 mg, 1mmol) and triethylamine (0.11 mL, 0.8 mmol). The reaction mixture was stirred for 4 h at room temperature, diluted with 25 mL dichloromethane and washed with successively with 25 mL 1 M HCl, 25 mL 1 M NaHCO₃ and brine. The organic layer was dried over MgSO₄, filtered, concentrated under reduced pressure and purified using column chromatography (SiO₂, 60:40 ethyl acetate/hexanes) to yield 40 mg (0.07 mmol, 35% yield) of the desired product as a yellow foam: ¹H NMR (300 MHz, CDCl₃) δ 8.73 (m, b, 2H), 7.4-6.7 (m, 5H), 6.24 (b, 0.3 H), 5.2-4.4 (b, 1H), 4.8-3.9 (m, 6H), 2.23 (b, 3H), 1.08/0.4 {s/d, (2.3/3.7)H}; ¹³C NMR (125 MHz, CDCl₃) δ 165.76, 164.41, 150.11, 148.56, 146.57, 146.17, 144.5, 136.19, 134.14, 132.96, 129.49, 128.56, 127.6, 127.22, 127.02, 126.76, 126.44, 125.98, 124.69, 120.96, 69.99, 67.02, 59.02, 30.0, 29.67, 21.33, 20.8, 20.55, 20.21; IR (thin film) 2925, 1716, 1590, 1530, 1493, 1440, 1346, 1303, 1239, 1207, 1169, 1129; HRMS calcd for C₃₃H₃₀N₃O₆ 564.2135, found 564.2146.

2-Bromo-3-methyl-5-nitro-benzoic acid (39): To a stirred solution of 15 mL 98% sulfuric acid and 2.5 mL fuming nitric acid cooled in an ice bath was added **38** (2.13 g, 10 mmol) in small portions over 15 min. After 2 h at 0 °C and 12 h at room temperature, the reaction was quenched with cold water to yield a light yellow precipitate which was filtered, washed with distilled water, and dried to yield 1.9 g (75%) of compound **39** as a white solid. ¹H NMR (300 MHz, CD₃OD) δ 8.34 (d, 1H, *J* = 2.7 Hz), 8.31 (d, 1H, *J* = 2.7 Hz), 2.62 (s, 3H).

2-Bromo-3-methyl-5-nitro-methyl benzoate (40): To a stirred solution of 0.26 g (1 mmol) **39**, 0.1 mL methanol (3 mmol) and 10 mg (0.08 mmol) DMAP in 5 mL dichloromethane was added 1,3-dicyclohexylcarbodiimide (0.206 g, 1 mmol) in 5 mL dichloromethane, over 5 min at -10 °C. The reaction was allowed to stir for 3 h during which it warmed to room temperature. The precipitated urea was filtered off, volatile components removed under reduced pressure and the crude product purified using flash chromatography (SiO₂, 10:90 Ethyl acetate:Hexanes) to give 0.24 g (90%) of **40** as a white solid. ¹H NMR (300 MHz, CDCl₃) δ 8.34 (d, 1H, *J* = 2.72 Hz), 8.20 (d, 1H, *J* = 2.72 Hz), 3.98 (s, 3H), 2.58 (s, 3H).

Methyl 4'-nitro-6'-methyl-2-phenyl-8-methyl-6H,12H-5,11-methanodibenzo [b,f][1,5]diazocine-2'-carboxylate (41a): By the general procedure, 410 mg (1.5 mmol) **40**, 362 mg (1 mmol) **20**, 636 mg (3 mmol) potassium phosphate and 28 mg (0.05 mmol) chloro(di-2-norbornylphosphino)(2'-dimethylamino-1,1'-bi-phenyl-2-yl)palladium (II) afforded 325 mg (55%) of **41a** after chromatography (SiO₂, 60:40 Ethyl acetate:Hexanes)

as a yellow foam: $R_f = 0.35$ (60:40 Ethyl acetate:Hexanes); ^1H NMR (300 MHz, CDCl_3) δ 8.44/8.37 {s, (0.48/0.52)H}, 8.2/8.19 {s, (0.52/0.48)H}, 7.18 (d, 1H, $J = 8.3$ Hz), 7.1-6.9 (m, 3H), 6.76/6.71 {s, (0.48/0.52)H}, 6.67/6.64 {m, (0.48/0.52)H}, 4.69 (dd, 2H, $J = 16.8$ Hz and $J = 4.6$ Hz), 4.35 (d, 2H, $J = 21.7$ Hz), 4.69 (m, 2H), 3.64/2.91 {s, (1.44/1.56) H}, 2.27/2.26 {s, (1.56/1.44)H}, 2.2/2.14 {s, 3H}; ^{13}C NMR (150 MHz, CDCl_3) δ 167.39, 166.89, 148.1, 147.91, 147.48, 147.14, 146.47, 146.35, 145.39, 145.01, 139.8, 139.39, 134.0, 133.46, 128.21, 128.07, 127.86, 127.49, 127.33, 127.2, 127.05, 126.83, 126.75, 126.43, 124.96, 124.63, 121.85, 82.9, 75.0, 67.33, 66.76, 59.26, 58.99, 58.55, 58.32, 52.43, 51.47, 24.83, 24.56, 21.13, 20.93, 20.86, 20.7; IR (thin film) 2946, 1722, 1524, 1493, 1439, 1350, 1294, 1205, 1160; HRMS calcd for $\text{C}_{25}\text{H}_{23}\text{N}_3\text{O}_4$ 429.1667, found 429.1688.

Methyl 4'-(4-carboxybutyrylamino)- 6'-methyl-2-phenyl-8-methyl-6H,12H-5,11-methanodibenzo[*b,f*][1,5]diazocine-2'-carboxylate (42a): Compound **41a** 100 mg (0.23 mmol) was reduced following the general procedure. After reduction, the product was treated with 46 mg (0.4 mmol) of glutaric anhydride in 1 mL CH_2Cl_2 for 12 h. After this time, TLC (100% ethyl acetate) showed all the starting material to have disappeared. The crude product was purified using flash chromatography (SiO_2 , 20:80 isopropanol:ethyl acetate) to yield 55 mg (43% overall yield) of **42a** as a white foam: ^1H NMR (300 MHz, DMSO-d_6) δ 10.02 (s, 1H), 7.77 (b, 1H), 7.57 (b, 1H), 7.07 (d, $J = 8.2$ Hz, 1H), 7-6.8 (m, 3H), 6.75 (s, 1H), 6.62 (s, b, 1H), 4.57 (d, $J = 16.5$ Hz, 2H), 4.3-4.0 (m, $J = 16.5$ Hz, 4H), 3.5/2.8 {s, (1.4/1.6)H}, 2.33 (t, $J = 7.4$ Hz, 2H), 2.26 (t, $J = 7.4$ Hz, 2H), 2.14 (s, b, 3H), 1.78 (q, $J = 7.4$ Hz, 2H); ^{13}C NMR (150 MHz, $\text{CD}_3\text{OD}:\text{DMSO-d}_6 =$

8:2) δ 175, 172.13, 169.23, 169.09, 147.02, 145.42, 138.61, 138.1, 137.9, 137.71, 136.2, 135.52, 133.53, 133.2, 130.37, 128.94, 128.82, 128.39, 128.27, 128.14, 127.93, 127.61, 127.47, 127.32, 126.8, 124.88, 124.5, 123.84, 123.61, 123.29, 123.05, 118.06, 117.66, 117.18, 67.11, 66.75, 58.55, 51.1, 36.47, 35.84, 33.59, 33.26, 33.13, 32.93, 32.61, 32.47, 32.28, 21.81, 20.89, 20.53, 20.38, 20.15; IR (thin film) 2945, 1713, 1520, 1494, 1439, 1350, 1294, 1215, 1160; HRMS calcd for C₃₀H₃₁N₃O₅ 513.2264, found 513.2282.

2'',2'',2''-Trifluoro-1'-trifluoromethyl 4'-(4-carboxybutyrylamino)-6'-methyl-2-phenyl-8-methyl-6H,12H-5,11-methanodibenzo[*b,f*][1,5]diazocine-2'-carboxylate (42b): Compound **41b** 100 mg (0.17 mmol) was reduced following the general procedure. After reduction, the product was treated with 46 mg (0.4 mmol) of glutaric anhydride in 1 mL CH₂Cl₂ for 12 h. After this time, TLC (100% ethyl acetate) showed all the starting material to have disappeared. The crude product was purified using flash chromatography (SiO₂, 20:80 isopropanol:ethyl acetate) to yield 60 mg (54% overall yield) of **42b** as a white foam: ¹H NMR (600 MHz, D₂O) δ 7.9/7.82 {s, (0.35/0.65)H}, 7.58/7.52 {s, (0.65/0.35) H}, 7.22 (d, 1H, *J* = 8.3 Hz), 7.2-7.0 (m, 3H, *J* = 8.2 Hz), 6.88 (s, 1H), 6.8/6.73 {s, (0.65/0.35)H}, 6.25/5.97 {m, (0.35/0.65)H}, 4.4 – 4.0 (m, 6H, *J* = 16.9 Hz), 2.43 (t, 2H, *J* = 7.5 Hz), 2.19 (s, 3H), 2.17 (t, 2H, *J* = 7.5 Hz), 2.03(s, 3H), 1.91 (q, 2H, *J* = 7.5 Hz); ¹³C NMR (75 MHz, acetone-d₆) δ 173.49, 173.41, 171.03, 164.81, 164.46, 148, 146.02, 138.92, 138.68, 138.59, 136.82, 134.13, 132.85, 129.05, 128.84, 128.31, 128.1, 127.94, 127.85, 127.67, 127.59, 127.13, 127.05, 124.87, 124.6, 117.74, 66.71, 66.36, 58.33, 58.26, 35.73, 32.54, 32.37, 20.5, 20.23, 20.14, 20; IR (thin film)

2960, 1710, 1597, 1534, 1496, 1354, 1231, 1200, 1110; MS (ES) calcd for $C_{32}H_{29}N_3O_5F_6$
650.20, found 650.20.

APPENDIX A

A.1 CRYSTAL STRUCTURE DATA FOR COMPOUND 21E

Identification code	bb1026t	
Empirical formula	C ₃₅ H ₃₅ N ₃ O ₆	
Formula weight	593.66	
Temperature	100(2) K	
Wavelength	0.71073 Å	
Crystal system	Triclinic	
Space group	P-1	
Unit cell dimensions	a = 10.5656(4) Å	$\alpha = 107.5910(10)^\circ$.
	b = 11.0102(6) Å	$\beta = 92.5690(10)^\circ$.
	c = 15.1568(6) Å	$\gamma = 118.6580(10)^\circ$.
Volume	1436.38(11) Å ³	
Z	2	
Density (calculated)	1.373 Mg/m ³	
Absorption coefficient	0.094 mm ⁻¹	
F(000)	628	
Crystal size	0.40 x 0.38 x 0.30 mm ³	
Theta range for data collection	1.45 to 32.48°	
Index ranges	-15<=h<=15, -16<=k<=16, -22<=l<=22	
Reflections collected	19105	
Independent reflections	9897 [R(int) = 0.0196]	
Completeness to theta = 32.48°	95.4 %	
Absorption correction	Sadabs	
Max. and min. transmission	0.9722 and 0.9632	
Refinement method	Full-matrix least-squares on F ²	
Data / restraints / parameters	9897 / 0 / 537	
Goodness-of-fit on F ²	1.215	
Final R indices [I>2sigma(I)]	R1 = 0.0594, wR2 = 0.1463	
R indices (all data)	R1 = 0.0767, wR2 = 0.1558	
Largest diff. peak and hole	0.500 and -0.222 e.Å ⁻³	

Table A1. Atomic coordinates ($\times 10^4$) and equivalent isotropic displacement parameters ($\text{\AA}^2 \times 10^3$) for bb1026t. $U(\text{eq})$ is defined as one third of the trace of the orthogonalized U^{ij} tensor.

	x	y	z	$U(\text{eq})$
N(1)	3389(1)	-1713(1)	1005(1)	24(1)
C(1)	7109(1)	6690(1)	4507(1)	27(1)
O(1)	6350(1)	9489(1)	4504(1)	49(1)
N(2)	2616(1)	-2515(1)	2319(1)	25(1)
C(2)	6439(1)	7347(1)	4194(1)	25(1)
O(2)	8251(1)	9676(1)	5257(1)	45(1)
C(3)	5207(1)	6544(1)	3452(1)	24(1)
N(3)	7059(1)	8950(1)	4686(1)	30(1)
O(3)	8279(1)	4382(1)	3947(1)	49(1)
C(4)	4633(1)	5027(1)	3004(1)	23(1)
O(4)	7003(1)	4171(1)	5083(1)	33(1)
C(5)	5305(1)	4315(1)	3270(1)	22(1)
O(5)	3096(1)	4339(1)	1523(1)	42(1)
C(6)	6541(1)	5178(1)	4039(1)	24(1)
O(6)	2137(1)	3254(1)	2554(1)	45(1)
C(7)	7373(1)	4523(1)	4333(1)	26(1)
C(8)	7764(2)	3550(2)	5433(1)	42(1)
C(9)	4778(1)	2731(1)	2705(1)	23(1)
C(10)	4660(1)	2290(1)	1723(1)	26(1)
C(11)	4206(1)	832(1)	1176(1)	26(1)
C(12)	3828(1)	-227(1)	1596(1)	22(1)
C(13)	3901(1)	183(1)	2573(1)	23(1)
C(14)	4403(1)	1668(1)	3119(1)	23(1)
C(15)	3390(1)	-979(1)	3026(1)	26(1)
C(16)	3451(1)	-2555(1)	1576(1)	28(1)
C(17)	1869(1)	-2535(1)	425(1)	26(1)
C(18)	715(1)	-3074(1)	995(1)	24(1)
C(19)	1111(1)	-3023(1)	1903(1)	25(1)
C(20)	25(1)	-3491(2)	2416(1)	32(1)
C(21)	-1433(1)	-4006(2)	2031(1)	34(1)
C(22)	-1854(1)	-4074(1)	1125(1)	30(1)
C(23)	-762(1)	-3603(1)	620(1)	27(1)
C(24)	-3439(2)	-4651(2)	695(1)	39(1)
C(25)	3216(1)	4164(1)	2256(1)	24(1)
C(26)	635(1)	2294(2)	1937(1)	36(1)
C(27)	260(1)	690(2)	1612(1)	36(1)
C(28)	317(2)	244(2)	2468(1)	36(1)
C(29)	-759(1)	451(2)	3042(1)	35(1)
C(30)	-344(2)	2072(2)	3381(1)	37(1)
C(31)	-409(2)	2519(2)	2527(1)	35(1)
C(32)	-1988(2)	1530(2)	1901(1)	38(1)
C(33)	-2406(1)	-97(2)	1554(1)	36(1)
C(34)	-1316(2)	-283(2)	979(1)	40(1)
C(35)	-2334(2)	-542(2)	2411(1)	43(1)

Table A2. Bond lengths [Å] and angles [°] for **21e**.

N(1)-C(12)	1.4298(14)	C(22)-C(24)	1.5042(17)
N(1)-C(16)	1.4666(15)	C(23)-H(23)	0.938(15)
N(1)-C(17)	1.4732(15)	C(24)-H(24A)	0.91(2)
C(1)-C(2)	1.3837(16)	C(24)-H(24B)	0.975(19)
C(1)-C(6)	1.3874(16)	C(24)-H(24C)	1.02(2)
C(1)-H(1)	0.944(16)	C(26)-C(31)	1.514(2)
O(1)-N(3)	1.2227(14)	C(26)-C(27)	1.518(2)
N(2)-C(19)	1.4436(14)	C(26)-H(26)	1.007(18)
N(2)-C(16)	1.4635(16)	C(27)-C(28)	1.528(2)
N(2)-C(15)	1.4753(15)	C(27)-C(34)	1.5373(19)
C(2)-C(3)	1.3806(16)	C(27)-H(27)	1.007(18)
C(2)-N(3)	1.4671(15)	C(28)-C(29)	1.522(2)
O(2)-N(3)	1.2216(14)	C(28)-H(28A)	0.992(18)
C(3)-C(4)	1.3869(16)	C(28)-H(28B)	0.995(17)
C(3)-H(3)	0.986(17)	C(29)-C(30)	1.521(2)
O(3)-C(7)	1.1924(15)	C(29)-C(35)	1.5359(19)
C(4)-C(5)	1.4079(15)	C(29)-H(29)	0.929(17)
C(4)-C(25)	1.5031(15)	C(30)-C(31)	1.5271(19)
O(4)-C(7)	1.3250(15)	C(30)-H(30A)	0.968(17)
O(4)-C(8)	1.4509(16)	C(30)-H(30B)	1.011(17)
C(5)-C(6)	1.4038(15)	C(31)-C(32)	1.5358(18)
C(5)-C(9)	1.4865(15)	C(31)-H(31)	0.990(18)
O(5)-C(25)	1.1953(14)	C(32)-C(33)	1.527(2)
C(6)-C(7)	1.5024(15)	C(32)-H(32A)	0.97(2)
O(6)-C(25)	1.3163(14)	C(32)-H(32B)	1.055(18)
O(6)-C(26)	1.4734(15)	C(33)-C(34)	1.529(2)
C(8)-H(8A)	0.91(2)	C(33)-C(35)	1.532(2)
C(8)-H(8B)	0.990(18)	C(33)-H(33)	0.941(17)
C(8)-H(8C)	0.937(19)	C(34)-H(34A)	1.011(19)
C(9)-C(14)	1.3931(16)	C(34)-H(34B)	0.937(19)
C(9)-C(10)	1.3988(16)	C(35)-H(35A)	0.999(19)
C(10)-C(11)	1.3837(17)	C(35)-H(35B)	1.06(2)
C(10)-H(10)	0.978(16)	C(12)-N(1)-C(16)	111.11(9)
C(11)-C(12)	1.3957(16)	C(12)-N(1)-C(17)	112.01(9)
C(11)-H(11)	1.003(16)	C(16)-N(1)-C(17)	107.73(9)
C(12)-C(13)	1.3991(16)	C(2)-C(1)-C(6)	118.61(11)
C(13)-C(14)	1.3959(16)	C(2)-C(1)-H(1)	118.8(9)
C(13)-C(15)	1.5171(15)	C(6)-C(1)-H(1)	122.5(9)
C(14)-H(14)	0.977(15)	C(19)-N(2)-C(16)	109.94(9)
C(15)-H(15A)	1.004(14)	C(19)-N(2)-C(15)	112.37(9)
C(15)-H(15)	0.981(16)	C(16)-N(2)-C(15)	108.09(9)
C(16)-H(16A)	0.987(16)	C(3)-C(2)-C(1)	122.34(11)
C(16)-H(16B)	1.002(15)	C(3)-C(2)-N(3)	119.46(10)
C(17)-C(18)	1.5141(16)	C(1)-C(2)-N(3)	118.20(10)
C(17)-H(17A)	0.993(15)	C(2)-C(3)-C(4)	118.43(10)
C(17)-H(17B)	0.967(15)	C(2)-C(3)-H(3)	121.3(10)
C(18)-C(23)	1.3946(16)	C(4)-C(3)-H(3)	120.2(10)
C(18)-C(19)	1.3975(16)	O(2)-N(3)-O(1)	123.44(11)
C(19)-C(20)	1.3930(17)	O(2)-N(3)-C(2)	118.44(10)
C(20)-C(21)	1.3842(18)	O(1)-N(3)-C(2)	118.11(11)
C(20)-H(20)	0.960(17)	C(3)-C(4)-C(5)	121.48(10)
C(21)-C(22)	1.3923(18)	C(3)-C(4)-C(25)	117.02(10)
C(21)-H(21)	0.976(17)	C(5)-C(4)-C(25)	121.43(10)
C(22)-C(23)	1.3905(17)	C(7)-O(4)-C(8)	115.88(11)
		C(6)-C(5)-C(4)	117.76(10)
		C(6)-C(5)-C(9)	121.70(10)

C(4)-C(5)-C(9)	120.39(10)	C(19)-C(20)-H(20)	121.6(10)
C(1)-C(6)-C(5)	121.31(10)	C(20)-C(21)-C(22)	121.15(12)
C(1)-C(6)-C(7)	117.47(10)	C(20)-C(21)-H(21)	119.1(10)
C(5)-C(6)-C(7)	121.03(10)	C(22)-C(21)-H(21)	119.8(10)
C(25)-O(6)-C(26)	119.33(10)	C(23)-C(22)-C(21)	117.85(11)
O(3)-C(7)-O(4)	124.95(11)	C(23)-C(22)-C(24)	120.57(12)
O(3)-C(7)-C(6)	123.43(11)	C(21)-C(22)-C(24)	121.57(12)
O(4)-C(7)-C(6)	111.59(10)	C(22)-C(23)-C(18)	122.02(11)
O(4)-C(8)-H(8A)	103.5(13)	C(22)-C(23)-H(23)	118.7(9)
O(4)-C(8)-H(8B)	109.7(11)	C(18)-C(23)-H(23)	119.3(9)
H(8A)-C(8)-H(8B)	110.4(16)	C(22)-C(24)-H(24A)	109.3(13)
O(4)-C(8)-H(8C)	108.4(11)	C(22)-C(24)-H(24B)	110.3(11)
H(8A)-C(8)-H(8C)	111.1(17)	H(24A)-C(24)-H(24B)	110.6(17)
H(8B)-C(8)-H(8C)	113.2(16)	C(22)-C(24)-H(24C)	111.9(11)
C(14)-C(9)-C(10)	118.70(10)	H(24A)-C(24)-H(24C)	109.4(18)
C(14)-C(9)-C(5)	122.37(10)	H(24B)-C(24)-H(24C)	105.3(15)
C(10)-C(9)-C(5)	118.93(10)	O(5)-C(25)-O(6)	125.93(11)
C(11)-C(10)-C(9)	120.61(10)	O(5)-C(25)-C(4)	124.28(10)
C(11)-C(10)-H(10)	120.4(10)	O(6)-C(25)-C(4)	109.72(9)
C(9)-C(10)-H(10)	119.0(10)	O(6)-C(26)-C(31)	107.05(11)
C(10)-C(11)-C(12)	120.29(11)	O(6)-C(26)-C(27)	108.29(11)
C(10)-C(11)-H(11)	120.1(9)	C(31)-C(26)-C(27)	110.93(11)
C(12)-C(11)-H(11)	119.6(9)	O(6)-C(26)-H(26)	105.9(10)
C(11)-C(12)-C(13)	119.98(10)	C(31)-C(26)-H(26)	113.4(10)
C(11)-C(12)-N(1)	118.34(10)	C(27)-C(26)-H(26)	111.0(10)
C(13)-C(12)-N(1)	121.68(10)	C(26)-C(27)-C(28)	110.35(11)
C(14)-C(13)-C(12)	118.96(10)	C(26)-C(27)-C(34)	107.09(12)
C(14)-C(13)-C(15)	120.57(10)	C(28)-C(27)-C(34)	109.98(12)
C(12)-C(13)-C(15)	120.44(10)	C(26)-C(27)-H(27)	110.6(10)
C(9)-C(14)-C(13)	121.42(11)	C(28)-C(27)-H(27)	109.0(10)
C(9)-C(14)-H(14)	121.3(9)	C(34)-C(27)-H(27)	109.8(10)
C(13)-C(14)-H(14)	117.3(9)	C(29)-C(28)-C(27)	109.49(11)
N(2)-C(15)-C(13)	112.72(10)	C(29)-C(28)-H(28A)	112.5(10)
N(2)-C(15)-H(15A)	107.0(8)	C(27)-C(28)-H(28A)	109.7(10)
C(13)-C(15)-H(15A)	111.4(8)	C(29)-C(28)-H(28B)	110.6(9)
N(2)-C(15)-H(15)	108.4(9)	C(27)-C(28)-H(28B)	110.7(9)
C(13)-C(15)-H(15)	110.4(9)	H(28A)-C(28)-H(28B)	103.7(14)
H(15A)-C(15)-H(15)	106.6(12)	C(30)-C(29)-C(28)	109.80(11)
N(2)-C(16)-N(1)	112.34(9)	C(30)-C(29)-C(35)	109.40(12)
N(2)-C(16)-H(16A)	110.5(9)	C(28)-C(29)-C(35)	109.15(13)
N(1)-C(16)-H(16A)	107.5(9)	C(30)-C(29)-H(29)	111.1(10)
N(2)-C(16)-H(16B)	108.7(9)	C(28)-C(29)-H(29)	108.5(10)
N(1)-C(16)-H(16B)	109.1(9)	C(35)-C(29)-H(29)	108.8(10)
H(16A)-C(16)-H(16B)	108.6(12)	C(29)-C(30)-C(31)	109.81(11)
N(1)-C(17)-C(18)	112.17(9)	C(29)-C(30)-H(30A)	112.9(10)
N(1)-C(17)-H(17A)	108.9(8)	C(31)-C(30)-H(30A)	108.7(10)
C(18)-C(17)-H(17A)	109.1(8)	C(29)-C(30)-H(30B)	110.6(9)
N(1)-C(17)-H(17B)	107.9(8)	C(31)-C(30)-H(30B)	108.8(10)
C(18)-C(17)-H(17B)	109.1(8)	H(30A)-C(30)-H(30B)	105.9(14)
H(17A)-C(17)-H(17B)	109.7(12)	C(26)-C(31)-C(30)	109.93(11)
C(23)-C(18)-C(19)	119.12(10)	C(26)-C(31)-C(32)	108.29(11)
C(23)-C(18)-C(17)	119.88(10)	C(30)-C(31)-C(32)	109.41(12)
C(19)-C(18)-C(17)	120.99(10)	C(26)-C(31)-H(31)	108.6(10)
C(20)-C(19)-C(18)	119.32(11)	C(30)-C(31)-H(31)	110.6(10)
C(20)-C(19)-N(2)	119.15(10)	C(32)-C(31)-H(31)	110.0(10)
C(18)-C(19)-N(2)	121.52(10)	C(33)-C(32)-C(31)	109.38(11)
C(21)-C(20)-C(19)	120.53(11)	C(33)-C(32)-H(32A)	112.5(11)
C(21)-C(20)-H(20)	117.8(10)	C(31)-C(32)-H(32A)	108.7(11)

C(33)-C(32)-H(32B) 111.0(9)
C(31)-C(32)-H(32B) 108.3(10)
H(32A)-C(32)-H(32B) 106.8(15)
C(32)-C(33)-C(34) 109.20(12)
C(32)-C(33)-C(35) 109.38(12)
C(34)-C(33)-C(35) 109.41(13)
C(32)-C(33)-H(33) 108.7(10)
C(34)-C(33)-H(33) 108.9(10)
C(35)-C(33)-H(33) 111.3(10)
C(33)-C(34)-C(27) 109.65(11)
C(33)-C(34)-H(34A) 108.9(10)
C(27)-C(34)-H(34A) 111.4(10)
C(33)-C(34)-H(34B) 112.2(11)

C(27)-C(34)-H(34B) 109.9(11)
H(34A)-C(34)-H(34B) 104.8(15)
C(33)-C(35)-C(29) 109.75(11)
C(33)-C(35)-H(35A) 109.2(11)
C(29)-C(35)-H(35A) 108.2(11)
C(33)-C(35)-H(35B) 112.3(11)
C(29)-C(35)-H(35B) 110.0(10)
H(35A)-C(35)-H(35B) 107.2(14)

A.2 CRYSTAL STRUCTURE DATA FOR COMPOUND 22D

Identification code	bb1207s	
Empirical formula	C ₃₅ H ₃₇ N ₃ O ₄	
Formula weight	563.68	
Temperature	295(2) K	
Wavelength	0.71073 Å	
Crystal system	Triclinic	
Space group	P-1	
Unit cell dimensions	a = 10.5029(8) Å	a = 111.473(2)°
	b = 10.8884(8) Å	b = 91.313(2)°
	c = 13.5626(10) Å	g = 91.299(2)°
Volume	1442.18(19) Å ³	
Z	2	
Density (calculated)	1.298 Mg/m ³	
Absorption coefficient	0.085 mm ⁻¹	
F(000)	600	
Crystal size	0.26 x 0.14 x 0.14 mm ³	
Theta range for data collection	1.61 to 27.50°	
Index ranges	-13<=h<=13, -14<=k<=14, -17<=l<=17	
Reflections collected	14215	
Independent reflections	6592 [R(int) = 0.0299]	
Completeness to theta = 27.50°	99.5 %	
Absorption correction	None	
Max. and min. transmission	0.9882 and 0.9782	
Refinement method	Full-matrix least-squares on F ²	
Data / restraints / parameters	6592 / 0 / 387	
Goodness-of-fit on F ²	0.966	
Final R indices [I>2sigma(I)]	R1 = 0.0563, wR2 = 0.1380	
R indices (all data)	R1 = 0.1165, wR2 = 0.1595	
Largest diff. peak and hole	0.222 and -0.184 e.Å ⁻³	

Table A3. Atomic coordinates ($\times 10^4$) and equivalent isotropic displacement parameters ($\text{Å}^2 \times 10^3$) for bb1207s. U(eq) is defined as one third of the trace of the orthogonalized U^{ij} tensor.

	x	y	z	U(eq)
O(1)	7404(1)	7932(1)	391(1)	55(1)
N(1)	5768(2)	6813(2)	5338(1)	53(1)
C(1)	6692(2)	7615(2)	6124(2)	49(1)
N(2)	7518(2)	5869(2)	4192(1)	55(1)
O(2)	5275(1)	8201(2)	452(1)	67(1)
C(2)	6275(2)	8668(2)	6979(2)	59(1)
C(3)	7123(2)	9446(2)	7762(2)	66(1)
O(3)	8147(2)	12743(2)	5014(1)	109(1)
N(3)	6976(3)	13331(3)	1649(3)	93(1)
O(4)	8160(2)	10647(2)	4674(1)	100(1)

C(4)	8408(2)	9187(2)	7733(2)	63(1)
C(5)	8816(2)	8140(2)	6869(2)	61(1)
C(6)	7990(2)	7357(2)	6045(2)	51(1)
C(7)	8467(2)	6281(2)	5076(2)	58(1)
C(8)	7350(2)	6864(2)	3738(2)	45(1)
C(9)	6280(2)	7633(2)	3922(2)	46(1)
C(10)	5284(2)	7504(2)	4666(2)	55(1)
C(11)	6332(2)	5601(2)	4635(2)	61(1)
C(12)	9314(3)	9978(3)	8632(2)	96(1)
C(13)	8294(2)	7059(2)	3113(2)	51(1)
C(14)	8216(2)	8037(2)	2701(2)	51(1)
C(15)	7172(2)	8853(2)	2897(1)	44(1)
C(16)	6205(2)	8600(2)	3471(2)	49(1)
C(17)	7148(2)	10034(2)	2578(2)	44(1)
C(18)	6722(2)	9916(2)	1562(2)	47(1)
C(19)	6641(2)	10989(2)	1258(2)	57(1)
C(20)	7008(2)	12245(2)	1953(2)	59(1)
C(21)	7439(2)	12382(2)	2960(2)	56(1)
C(22)	7500(2)	11314(2)	3285(2)	47(1)
C(23)	6352(2)	8583(2)	749(2)	51(1)
C(24)	7389(2)	6591(2)	-424(2)	48(1)
C(25)	6823(2)	6560(2)	-1474(2)	60(1)
C(26)	6992(3)	5180(2)	-2309(2)	70(1)
C(27)	6290(2)	4177(2)	-1963(2)	74(1)
C(28)	6848(2)	4216(2)	-907(2)	66(1)
C(29)	6705(2)	5603(2)	-67(2)	58(1)
C(30)	8409(3)	4874(3)	-2411(2)	79(1)
C(31)	8949(2)	4904(2)	-1358(2)	72(1)
C(32)	8241(2)	3899(2)	-1020(2)	75(1)
C(33)	8792(2)	6291(2)	-528(2)	64(1)
C(34)	7963(2)	11645(2)	4401(2)	55(1)
C(35)	8525(3)	10846(3)	5754(2)	104(1)

Table A4. Bond lengths [\AA] and angles [$^\circ$] for **22d**.

O(1)-C(23)	1.329(2)	C(24)-C(29)	1.506(3)
O(1)-C(24)	1.473(2)	C(24)-C(33)	1.515(3)
N(1)-C(1)	1.440(3)	C(24)-C(25)	1.519(3)
N(1)-C(11)	1.464(3)	C(25)-C(26)	1.532(3)
N(1)-C(10)	1.468(3)	C(25)-H(25A)	0.9700
C(1)-C(2)	1.386(3)	C(25)-H(25B)	0.9700
C(1)-C(6)	1.397(3)	C(26)-C(27)	1.520(3)
N(2)-C(8)	1.441(2)	C(26)-C(30)	1.530(3)
N(2)-C(11)	1.463(3)	C(26)-H(26A)	0.9800
N(2)-C(7)	1.471(3)	C(27)-C(28)	1.521(3)
O(2)-C(23)	1.204(2)	C(27)-H(27A)	0.9700
C(2)-C(3)	1.379(3)	C(27)-H(27B)	0.9700
C(2)-H(2A)	0.9300	C(28)-C(32)	1.509(3)
C(3)-C(4)	1.384(3)	C(28)-C(29)	1.536(3)
C(3)-H(3A)	0.9300	C(28)-H(28A)	0.9800
O(3)-C(34)	1.189(2)	C(29)-H(29A)	0.9700
N(3)-C(20)	1.388(3)	C(29)-H(29B)	0.9700
N(3)-H(3NB)	0.93(3)	C(30)-C(31)	1.514(3)
N(3)-H(3NA)	0.80(3)	C(30)-H(30A)	0.9700
O(4)-C(34)	1.289(3)	C(30)-H(30B)	0.9700
O(4)-C(35)	1.441(3)	C(31)-C(32)	1.518(3)
C(4)-C(5)	1.386(3)	C(31)-C(33)	1.534(3)
C(4)-C(12)	1.509(3)	C(31)-H(31A)	0.9800
C(5)-C(6)	1.398(3)	C(32)-H(32A)	0.9700
C(5)-H(5A)	0.9300	C(32)-H(32B)	0.9700
C(6)-C(7)	1.510(3)	C(33)-H(33A)	0.9700
C(7)-H(7A)	0.9700	C(33)-H(33B)	0.9700
C(7)-H(7B)	0.9700	C(35)-H(35A)	0.9600
C(8)-C(13)	1.381(3)	C(35)-H(35B)	0.9600
C(8)-C(9)	1.389(3)	C(35)-H(35C)	0.9600
C(9)-C(16)	1.400(3)		
C(9)-C(10)	1.509(3)	C(23)-O(1)-C(24)	123.23(15)
C(10)-H(10A)	0.9700	C(1)-N(1)-C(11)	110.84(17)
C(10)-H(10B)	0.9700	C(1)-N(1)-C(10)	111.80(16)
C(11)-H(11A)	0.9700	C(11)-N(1)-C(10)	106.93(17)
C(11)-H(11B)	0.9700	C(2)-C(1)-C(6)	119.5(2)
C(12)-H(12A)	0.9600	C(2)-C(1)-N(1)	118.84(19)
C(12)-H(12B)	0.9600	C(6)-C(1)-N(1)	121.63(19)
C(12)-H(12C)	0.9600	C(8)-N(2)-C(11)	111.01(16)
C(13)-C(14)	1.376(3)	C(8)-N(2)-C(7)	112.31(16)
C(13)-H(13A)	0.9300	C(11)-N(2)-C(7)	105.75(17)
C(14)-C(15)	1.395(3)	C(3)-C(2)-C(1)	120.9(2)
C(14)-H(14A)	0.9300	C(3)-C(2)-H(2A)	119.6
C(15)-C(16)	1.377(3)	C(1)-C(2)-H(2A)	119.6
C(15)-C(17)	1.500(3)	C(2)-C(3)-C(4)	121.2(2)
C(16)-H(16A)	0.9300	C(2)-C(3)-H(3A)	119.4
C(17)-C(18)	1.398(3)	C(4)-C(3)-H(3A)	119.4
C(17)-C(22)	1.407(3)	C(20)-N(3)-H(3NB)	110.4(19)
C(18)-C(19)	1.378(3)	C(20)-N(3)-H(3NA)	114(2)
C(18)-C(23)	1.502(3)	H(3NB)-N(3)-H(3NA)	135(3)
C(19)-C(20)	1.387(3)	C(34)-O(4)-C(35)	120.27(19)
C(19)-H(19A)	0.9300	C(3)-C(4)-C(5)	117.4(2)
C(20)-C(21)	1.382(3)	C(3)-C(4)-C(12)	121.0(2)
C(21)-C(22)	1.389(3)	C(5)-C(4)-C(12)	121.6(2)
C(21)-H(21A)	0.9300	C(4)-C(5)-C(6)	122.9(2)
C(22)-C(34)	1.489(3)	C(4)-C(5)-H(5A)	118.6

C(6)-C(5)-H(5A)	118.6	C(20)-C(21)-C(22)	122.1(2)
C(1)-C(6)-C(5)	118.0(2)	C(20)-C(21)-H(21A)	119.0
C(1)-C(6)-C(7)	120.01(19)	C(22)-C(21)-H(21A)	119.0
C(5)-C(6)-C(7)	121.96(19)	C(21)-C(22)-C(17)	120.33(19)
N(2)-C(7)-C(6)	112.02(17)	C(21)-C(22)-C(34)	114.92(18)
N(2)-C(7)-H(7A)	109.2	C(17)-C(22)-C(34)	124.75(19)
C(6)-C(7)-H(7A)	109.2	O(2)-C(23)-O(1)	126.31(19)
N(2)-C(7)-H(7B)	109.2	O(2)-C(23)-C(18)	124.82(19)
C(6)-C(7)-H(7B)	109.2	O(1)-C(23)-C(18)	108.83(17)
H(7A)-C(7)-H(7B)	107.9	O(1)-C(24)-C(29)	111.92(16)
C(13)-C(8)-C(9)	119.61(18)	O(1)-C(24)-C(33)	102.64(15)
C(13)-C(8)-N(2)	118.48(18)	C(29)-C(24)-C(33)	109.53(18)
C(9)-C(8)-N(2)	121.90(18)	O(1)-C(24)-C(25)	111.51(16)
C(8)-C(9)-C(16)	118.32(18)	C(29)-C(24)-C(25)	110.79(17)
C(8)-C(9)-C(10)	120.42(18)	C(33)-C(24)-C(25)	110.16(18)
C(16)-C(9)-C(10)	121.06(18)	C(24)-C(25)-C(26)	108.28(17)
N(1)-C(10)-C(9)	111.50(16)	C(24)-C(25)-H(25A)	110.0
N(1)-C(10)-H(10A)	109.3	C(26)-C(25)-H(25A)	110.0
C(9)-C(10)-H(10A)	109.3	C(24)-C(25)-H(25B)	110.0
N(1)-C(10)-H(10B)	109.3	C(26)-C(25)-H(25B)	110.0
C(9)-C(10)-H(10B)	109.3	H(25A)-C(25)-H(25B)	108.4
H(10A)-C(10)-H(10B)	108.0	C(27)-C(26)-C(30)	109.7(2)
N(2)-C(11)-N(1)	112.12(16)	C(27)-C(26)-C(25)	108.6(2)
N(2)-C(11)-H(11A)	109.2	C(30)-C(26)-C(25)	109.91(19)
N(1)-C(11)-H(11A)	109.2	C(27)-C(26)-H(26A)	109.5
N(2)-C(11)-H(11B)	109.2	C(30)-C(26)-H(26A)	109.5
N(1)-C(11)-H(11B)	109.2	C(25)-C(26)-H(26A)	109.5
H(11A)-C(11)-H(11B)	107.9	C(26)-C(27)-C(28)	110.01(18)
C(4)-C(12)-H(12A)	109.5	C(26)-C(27)-H(27A)	109.7
C(4)-C(12)-H(12B)	109.5	C(28)-C(27)-H(27A)	109.7
H(12A)-C(12)-H(12B)	109.5	C(26)-C(27)-H(27B)	109.7
C(4)-C(12)-H(12C)	109.5	C(28)-C(27)-H(27B)	109.7
H(12A)-C(12)-H(12C)	109.5	H(27A)-C(27)-H(27B)	108.2
H(12B)-C(12)-H(12C)	109.5	C(32)-C(28)-C(27)	109.4(2)
C(14)-C(13)-C(8)	121.09(19)	C(32)-C(28)-C(29)	109.59(19)
C(14)-C(13)-H(13A)	119.5	C(27)-C(28)-C(29)	109.20(19)
C(8)-C(13)-H(13A)	119.5	C(32)-C(28)-H(28A)	109.5
C(13)-C(14)-C(15)	120.71(19)	C(27)-C(28)-H(28A)	109.5
C(13)-C(14)-H(14A)	119.6	C(29)-C(28)-H(28A)	109.5
C(15)-C(14)-H(14A)	119.6	C(24)-C(29)-C(28)	108.73(18)
C(16)-C(15)-C(14)	117.55(19)	C(24)-C(29)-H(29A)	109.9
C(16)-C(15)-C(17)	120.76(18)	C(28)-C(29)-H(29A)	109.9
C(14)-C(15)-C(17)	121.48(18)	C(24)-C(29)-H(29B)	109.9
C(15)-C(16)-C(9)	122.55(19)	C(28)-C(29)-H(29B)	109.9
C(15)-C(16)-H(16A)	118.7	H(29A)-C(29)-H(29B)	108.3
C(9)-C(16)-H(16A)	118.7	C(31)-C(30)-C(26)	109.32(19)
C(18)-C(17)-C(22)	116.68(18)	C(31)-C(30)-H(30A)	109.8
C(18)-C(17)-C(15)	120.91(17)	C(26)-C(30)-H(30A)	109.8
C(22)-C(17)-C(15)	122.37(17)	C(31)-C(30)-H(30B)	109.8
C(19)-C(18)-C(17)	122.28(18)	C(26)-C(30)-H(30B)	109.8
C(19)-C(18)-C(23)	117.47(18)	H(30A)-C(30)-H(30B)	108.3
C(17)-C(18)-C(23)	120.24(18)	C(30)-C(31)-C(32)	110.3(2)
C(18)-C(19)-C(20)	120.8(2)	C(30)-C(31)-C(33)	108.4(2)
C(18)-C(19)-H(19A)	119.6	C(32)-C(31)-C(33)	109.5(2)
C(20)-C(19)-H(19A)	119.6	C(30)-C(31)-H(31A)	109.6
C(21)-C(20)-C(19)	117.8(2)	C(32)-C(31)-H(31A)	109.6
C(21)-C(20)-N(3)	120.6(2)	C(33)-C(31)-H(31A)	109.6
C(19)-C(20)-N(3)	121.6(2)	C(28)-C(32)-C(31)	109.7(2)

C(28)-C(32)-H(32A)	109.7	H(33A)-C(33)-H(33B)	108.2
C(31)-C(32)-H(32A)	109.7	O(3)-C(34)-O(4)	121.0(2)
C(28)-C(32)-H(32B)	109.7	O(3)-C(34)-C(22)	123.6(2)
C(31)-C(32)-H(32B)	109.7	O(4)-C(34)-C(22)	115.35(18)
H(32A)-C(32)-H(32B)	108.2	O(4)-C(35)-H(35A)	109.5
C(24)-C(33)-C(31)	109.39(18)	O(4)-C(35)-H(35B)	109.5
C(24)-C(33)-H(33A)	109.8	H(35A)-C(35)-H(35B)	109.5
C(31)-C(33)-H(33A)	109.8	O(4)-C(35)-H(35C)	109.5
C(24)-C(33)-H(33B)	109.8	H(35A)-C(35)-H(35C)	109.5
C(31)-C(33)-H(33B)	109.8	H(35B)-C(35)-H(35C)	109.5

BIBLIOGRAPHY

1. (a) Merrifield, R. B. *J. Am. Chem. Soc.* **1963**, *85*(14), 2149-2154 (b) Merrifield, R. B. *J. Am. Chem. Soc.* **1964**, *86*(2), 304-305 (c) Merrifield, R.B., Solid phase synthesis (Nobel lecture). *Angew. Chem.* **1985**, *97*, 801-812. (d) Lam, K.S.; Salmon, S.E.; Hersh, E.M.; Hruby, V.J.; Kazmierski, W.M.; Knapp, R.J. *Nature*, *354*, **1991**, 82-84. (e) Han, H.; Wolfe, M.M.; Brenner, S.; Janda, K.D. *Proc. Natl. Acad. Sci. USA.* **1995**, *92*, 6419-6423. (f) Ellman, J.A. *Acc. Chem. Res.* **1996**, *29*, 132-143.
2. Dolle, R. E. *J. Comb. Chem.* **2005**, *7*(6), 739-798.
3. (a) Chen, S.; Janda, K. D. *Tet. Lett.* **1998**, *39*, 3943. (b) Ley, S. V.; Massi, A. *Perkin.* **2000**, *1*, 3645-3654. (c) Lopez-Pelegrin, J. A.; Wentworth, P.; Sieber, F.; Metz, W. A.; Janda, K. *D. J. Org. Chem.* **2000**, *65*(25), 8527-8531.
4. Vaino, A. R.; Janda, K. D. *J. Comb. Chem.* **2000**, *2*, 579-596.
5. Sarin, V. K.; Kent, S. B. H.; Merrifield, R. B. *J. Am. Chem. Soc.* **1980**, *102*, 5463-5470.
6. Hudson, D. *J. Comb. Chem.* **1999**, *1*(6), 403-457.
7. Ford, W. T.; Blum, D. B. *J. Poly. Sci. A.* **1990**, *28*, 931-934 and references therein.
8. Wiley, R. H. *Pure Appl. Chem.* **1975**, *43*, 57.
9. (a) Ueberreiter, K.; Kanig, G. *J. Chem. Phys.* **1950**, *18*, 399. (b) Fox, T. G. *Bull. Am. Phys. Soc.* **1956**, *1*, 123. (c) Ferry, J. D. *Viscoelastic Properties of Polymers*; John Wiley & Sons: New York, 1961. (d) Couchman, P. R.; Karasz, F. E. *Macromolecules* **1978**, *11*, 117. (e) Pochan, J. M.; Beatty, C. L.; Pochan, D. F. *Polymer* **1979**, *20*, 879. (f) Brinke, G. T.; Karasz, F. E.; Ellis, T. S. *Macromolecules* **1983**, *16*, 244. (g) Gutierrez, M. H.; Ford, W. T. *J. Polym. Sci.: Part A: Polym. Chem.* **1986**, *24*, 655.
10. Toy, P. H.; Janda, K. D. *Tetrahedron Lett.* **1999**, *40*, 6329.

-
11. Bayer, E. *Angew. Chem., Int. Ed. Engl.* **1991**, *30*, 113.
 12. Vaino, A. R.; Goodin, D. B.; Janda, K. D. *J. Comb. Chem.* **2000**, *2*, 330.
 13. Itsuno, S.; Sakurai, Y.; Maruyama, T.; Nakahama, S.; Frechet, J. M. J. *J. Org. Chem.* **1990**, *55*, 304.
 14. (a) Regen, S. L.; Bolikal, D. *J. Am. Chem. Soc.* **1981**, *103*, 5248. (b) Tomoi, M.; Ford, W. T. *J. Am. Chem. Soc.* **1981**, *103*, 3821. (c) Shea, K. J.; Stoddard, G. J.; Sasaki, D. Y. *Macromolecules* **1989**, *22*, 4303. (d) Wilson, M. E.; Wilson, J. A.; Kurth, M. J. *Macromolecules* **1997**, *30*, 3340.
 15. Hori M.; Gravert D.J.; Wentworth P.; Janda K.D. *Bioorg. Med. Chem. Lett.* **1998**, *8*, 2363-2368.
 16. Richter, L. S.; Gadek, T. R. *Tetrahedron Lett.* **1994**, *35*, 4705–4706.
 17. (a) Groth, T.; Grötli, M.; Meldal, M. *J. Comb. Chem.* **2001**, *3*, 461-468. (b) Jürgen, K.; Zanaletti, R.; Rose, A.; Frey, J. G.; Brocklesby, W. S.; Ladlow, M.; Bradley, M. *J. Comb. Chem.* **2003**, *5*, 28-32.
 18. Roucis, J. B.; Ekerdt, J. G. *J. App. Poly. Sci.* **1982**, *27*, 3841-3849.
 19. Gambs, C.; Dickerson, T.J.; Mahajan, S.; Pasternack, L.B.; and Janda, K.D. *J. Org. Chem.* **2003**, *68*, *9*, 3673 – 3678.
 20. Tomoi, M.; Ford, W. T. *J. Am. Chem. Soc.* **1980**, *102*, 7141.
 21. (a) Stranix, B. R.; Liu, H. Q.; Darling, G. D. *J. Org. Chem.* **1997**, *62*, 6183. (b) Yan, B. *Acc. Chem. Res.* **1998**, *31*, 621. (c) Li, W.; Xiao, X.; Czarnik, A. W. *J. Comb. Chem.* **1999**, *1*, 127. (d) Rana, S.; White, P.; Bradley, M. *J. Comb. Chem.* **2001**, *3*, 9–15.
 22. Morphy, J. R.; Rankovic, Z.; York, M. *Tetrahedron.* **2003**, *59*, *12*, 2137-2145.
 23. T. Horváth, D. P. Curran, J. A. Gladysz, in *Handbook of Fluorous Chemistry*, J. A. Gladysz, D. P. Curran, I. T. Horváth, Eds. (Wiley/VCH, Weinheim, Germany, 2004), pp. 1-4.
 24. Pivonka, D.E.; Palmer, D.L. *J. Comb. Chem.* **1999**, *1*, 294-296.
 25. Goldwasser, J. M.; Leznoff, C. C. *Can. J. Chem.* **1978**, *56*, 1562-1568.
 26. Merrifield, R. B.; Mitchell, A. R.; Clarke, J. E. *J. Org. Chem.* **1974**, *39*, 660-668.
 27. Chen, W. Y.; Foutch, G. L. *Chem. Eng. Sci.* **1989**, *44*, 2760-2762.
 28. Raymond, P. J.; Scott, P. E. *AIChE Annual Meeting*, **1987**, New York.
 29. Tam, J. P. *Proceedings of Ninth American Peptide Symposium*, **1985**, 423-425.

-
30. Esko, K.; Karlson, S. *Acta Chem. Scand.* **1970**, *24*, 1415-1422.
31. Wang, S.; Foutch, G. L. *Chem. Eng. Sci.* **1990**, *46*, 2373-2376.
32. Leffler, J. E.; Grunwald, E. *Rates and Equilibria of Organic Reactions*, Wiley: New York, **1963**.
33. (a) Hall, D.; Minton, A. P. *Biochim. Biophys. Acta* **2003**, *1649*, 127-139. (b) Minton, A. P. *J. Biol. Chem.* **2001**, *276*, 10577-10580.
34. Einstein, A. *Investigations on the Theory of the Brownian Movement*, Methuen & Co. Ltd., London, **1926**.
35. (a) Chandrasekhar, S. *Rev. Mod. Phys.* **1943**, *15*, 1-89. (b) Turing, A. M. *Phil. Trans. R. Soc.* **1952**, *B327*, 37-72. (c) Gierer, A.; Meinhardt, H. *Kybernetik*, **1972**, *12*, 30-39 (d) Berg, H.; Purcell, E. M. *Biophys. Jour.* **1977**, *20*, 193-219. (e) Berg, H. "Random Walks in Biology", Princeton University Press, **1983**. (f) Kopelman, R. *Science*. **1988**, *241*, 1620-1626. (g) Devreotes, P. N. *Science*, **1989**, *245*, 1054-1058.
36. von Smoluchowski, M. *Z. Phys. Chem.* **1917**, *92*, 129.
37. Arita, T.; Kajimoto, O.; Terazima, M.; Kimura, Y. *J. Chem. Phys.* **2004**, *120*, 7071-7074.
38. Collins, F. C.; Kimball, J. J. *Colloid Sci.* **1949**, *4*, 425.
39. (a) Debye, P. *Trans. Electrochem. Soc.* **1942**, *82*, 265. (b) Noyes, R. M. *Prog. React. Kinet.* **1961**, *1*, 131.
40. Katz, S. M.; Kubu, E. T.; Wakelin, J. H. *Textile Res. J.* **1950**, *20*, 754-759.
41. (a) Crank, J. "The Mathematics of Diffusion", 2nd ed. Oxford University Press, London, **1975**. (b) Carslaw, H. S.; Jaeger, J. C. "Conduction of Heat in Solids", 2nd Edition, Oxford Press, London, **1959**.
42. Reese, C. E.; Eyring, H. *Textile Res. J.* **1950**, *20*, 743-753.
43. Danckwerts, P. V. *Trans. Faraday Soc.* **1951**, *47*, 1014.
44. To reduce instabilities, we used the numerical methods of: (a) Douglas, J., Jr. *J. Soc. Ind. Appl. Math.* **1955**, *3*, 42-65. (b) Douglas, J., Jr.; Jones, B. F. *J. Soc. Ind. Appl. Math.* **1963**, *11*, 195-203.
45. Tyrrel, H. J.; Harris, K. R. *Diffusion in Liquids*, Butterworths: London, **1984**.

-
46. Fujita, H. in *Diffusion in Polymers*, Crank, J.; Park, G. H. Eds., Academic Press: New York, **1968**.
47. Halperin, W. P.; D'Orazio, F.; Bhattacharja, S.; Tarczon, J. C. in *Molecular Dynamics in Restricted Geometries*, Wiley: New York, **1989**.
48. Mitra, P. P.; Sen, P. N.; Schwartz, L. M.; Le Doussal, P. *Phys. Rev. Lett.* **1992**, *68*, 3555.
49. Le Bihan D. *Radiology.* **1990**, *177(2)*, 328.
50. Mackie, J.S.; Meares, P. *Proc. Roy. Soc. London, Series A*, **1955**, *267*, 498-506.
51. Pickup, S.; Blum, F. D.; Ford, W. T.; Periyasamy, M. *J. Am. Chem. Soc.* **1986**, *108(14)*, 3987-3990.
52. Matsukawa, S.; Ando, Isao. *Macromolecules* **1999**, *32*, 1865-1871.
53. Wilke, C. R.; Chang, P. *AIChE J.* **1955**, *1*, 264-270.
54. Lebedev, Y. S. *Kinetika I Kataliz*, **1965**, *6*, 522-531. (*Chem. Abs.* 56:8921g).
55. Yang, Jaemoon, Ph. D. Dissertation, University of Pittsburgh, **2000**.
56. London, F. *Z. Physik. Chem.* **1930**, *B, 11*, 222.
57. Parsegian, V. A. *Van der Waals Forces: A Handbook for Biologists, Chemists, Engineers, and Physicists*, Cambridge University Press, **2005**.
58. (a) Casimir H. B. G. *Proc. Kon. Nederland. Akad. Wetensch.* **1948**, *B51*, 793. (b) Lamoreaux S. K. *Phys. Rev. Lett.* **1997**, *78*, 5-8.
59. (a) Burley, S.K.; Petsko, G. A. *J. Am. Chem. Soc.* **1986**, *108*, 7995-8001. (b) Kobayashi, K.; Asakawa, Y.; Kikuchi, Y.; Toi, H.; Aoyama, Y. *J. Am. Chem. Soc.* **1993**, *115*, 2648-2654. (c) Hunter, C. A. *Phil. Tran. R. Soc. Lond. A* **1993**, *345*, 77-85. (d) Chen, C-T.; Siegel, J. S. *J. Am. Chem. Soc.* **1994**, *116*, 5959-. (e) Nishio, M.; Umezawa, Y.; Hirota, M.; Takeuchi, Y. *Tetrahedron* **1995**, *51* 8665-8701. (f) Waters, M. L. *Curr. Opinion Chem. Bio.*, **2002**, *6*, 736-741. (g) Meyer, E. A.; Castellano, R. K.; Diederich, F. *Angew. Chem. Int. Ed.*, **2003**, *42*, 1210-1250. (h) Nishio, M. *Cryst. Eng. Comm*, **2004**, *6*, 130-158. (i) Lavieri, S.; Zoltewicz, J. A. *J. Org. Chem.* **2001**, *66*, 7227-7230. (j) Jennings, W. B.; Farrell, B. M.; Malone, J. F. *Acc. Chem. Res.* **2001**, *34*, 885-894. (k) Anderson, D. E.; Hurley, J. H.; Nicholson, H.; Baase, W. A.; Matthews, B. W. *Protein Sci.* **1993**, *2*, 1285-1290. (l) Gould, R. O.; Gray, A. M.; Taylor, P.; Walkinshaw, M. D. *J. Am. Chem. Soc.* **1985**, *107*, 5921-5927 (m) Ehama, R.;

Tsushima, M.; Yuzuri, T.; Suezawa, H.; Sakakibara, K.; Hirota, M. *Bull Chem. Soc. Jpn.* **1993**, *66*, 814-818.

60. (a) Reid, D. S. C.; Lindley, P. F., Thornton, J. M. *FEBS* **1985**, *190*, 209-213. (b) Burley, S. K.; Petsko, G. A. *FEBS* **1986**, *203*, 139-143. (c) Oku, K.; Watanabe, H.; Kubota, M.; Fukuda, S.; Kurimoto, M.; Tsujisaka, Y.; Komori, M.; Inoue, Y.; Sakurai, M. *J. Am. Chem. Soc.* **2003**, *125*, 12739-12748. (d) Sulpizi, M.; Carloni, P. *J. Phys. Chem. B* **2000**, *104*, 10087-10091. (e) Scrutton, N. S.; Raine, A. R. C. *Biochem. J.* **1996**, *319*, 1-8.

61. Xiao, G.; Liu, S.; Ji, X.; Johnson, W. W.; Chen, J.; Parsons, J. F.; Stevens, W. J.; Gilliland, G. L.; Armstrong, R. N. *Biochemistry* **1996**, *35*, 4753-4765. Jiang, L.; Lai, L. **2002**, *277*, 37732-37740. Scheiner, S.; Kar, T.; Gu, Y. *J. Biol. Chem.* **2001**, *276*, 9832-9837.

62. (a) Dougherty, D. A.; Stauffer, D. A. *Science* **1990** *250*, 1558-1560. (b) M. M.; Mowbray, S. L. *J. Mol. Biol.* **1994**, *235*, 709-717. (c) Kim, K. S.; Lee, J. Y.; Lee, S. J.; Ha, T-K.; Kim, D. H. *J. Am. Chem. Soc.* **1994**, *116*, 7399-7400. (d) Ngola, S. M.; Dougherty, D. A. *J. Org. Chem.* **1998**, *63*, 4566-4567. (e) Bartoli, S.; Roelens, S. *J. Am. Chem. Soc.* **2002**, *124*, 8307-8315. (f) Cubero, E.; Orozco, M.; Luque, F. J. *J. Phys. Chem. A* **1999**, *103*, 315-321. (g) Felder, C.; Jiang, H-L.; Zhu, W-L.; Chen, K-X.; Silman, I.; Botti, S. A.; Sussman, J. L. *J. Phys. Chem. A* **2001**, *105*, 1326-1333.

63. (a) Wimley, W. C.; Gawrisch, K.; Creamer, T. P.; White, S. H. *Proc. Natl. Acad. Sci. USA* **1996**, *93*, 2985-2990. (b) Luo, R.; David, L.; Hung, H.; Devaney, J.; Gilson, M. K. *J. Phys. Chem. B* **1999**, *103*, 727-736. (c) Kumar, S.; Nussinov, R. *J. Mol. Biol.* **1999**, *293*, 1241-1255. (d) Kiehna, S. E.; Waters, M. L. *Protein Science* **2003**, *12*, 2657-2667. (e) Kaas, Q.; Aumelas, A.; Kubo, S.; Chino, N.; Kobayashi, Y.; Chiche, L. *Biochemistry* **2002**, *41*, 11099-11108. (f) Aliste, M. P.; MacCallum, J. L.; Tieleman, D. P. *Biochemistry* **2003**, *42*, 8976-8987. (g) Ibarra-Molero, B.; Zitzewitz, J. A.; Matthews, C. R. *J. Mol. Biol.* **2004**, *336*, 989-996.

64. (a) Cody, V.; Murray-Rust, P. *J. Mol. Struct.* **1984**, *112*, 189-199. (b) Kollman, P.; Dearing, A.; Kochanski, E. *J. Phys. Chem.* **1982**, *86*, 1606-1610. (c) Loc Nguyen, Horton, P. N.; Hursthouse, M. B.; Legon, A. C.; Bruce, D. W. *J. Amer. Chem. Soc.* **2004**, *126*, 16-17. (d) Webb, J. A.; Klijn, J. E.; Hill, P. A.; Bennett, J. L.; Goroff, N. S. *J. Org. Chem.* **2004**, *69*, 660-664. (e) Auffinger, P.; Hays, F. A.; Westhof, E.; Ho, P. S. *Proc. Natl. Acad. Sci. USA*, **2004** *101*,

16789-16794. (f) Hof, F.; Scofield, D. M.; Schweizer, W. B.; Diederich, F. *Angew. Chem. Int. Ed.* **2004**, *43*, 5056-5059.

65. (a) Kauzmann, W. *Adv. Protein. Chem.* **1959**, *14*, 1-63. (b) Anfinsen, C. B.; *Science*, **1973**, *181*, 223-230. (c) Gardner, R. R.; Christianson, L. A.; Gellman, S. H. *J. Am. Chem. Soc.* **1997**, *119*, 5041-5042.

66. For most recent computational studies see: (a) Morita, S.-i.; Fujii, A.; Mikami, N.; Tsuzuki, S. *J. Phys. Chem. A.* **2006**, *110*(36), 10583-10590. (b) Tsuzuki, S.; Honda, K.; Uchamaru, T.; Mikami, M.; Fujii, A. *J. Phys. Chem. A.* **2006**, *110*(33), 10163-10168. (c) Shibasaki, K.; Fujii, A.; Mikami, N.; Tsuzuki, S. *J. Phys. Chem. A.* **2006**, *110*(13), 4397-4404.

67. Itaka, Y. Kodama, K. Nishihata and M. Nishio *JCS Chem. Comm.* **1974**, 389.

68. Cramer, C. J. *Essentials of Computational Chemistry: Theories and Models*, 2nd ed.; Wiley: New York, **2002**.

69. Kaminski, G.; Jorgensen, W. L. *J. Phys. Chem.* **1996**, *100*(46), 18010-18013.

70. (a) Garcia, J. I.; Mayoral, J. A.; Salvatella, L. *Acc. Chem. Res.* **2000**, *33*, 658. (b) Ujaque, G.; Lee, P. S.; Houk, K. N.; Hentemann, M. F.; Danishefsky, S. J. *Chem. Eur. J.* **2002**, *8*, 3423. (c) Bakalova, S. M.; Santos, A. G. *J. Org. Chem.* **2004**, *69*(24), 8475-8481.

71. Chen, J.; Im, W.; Brooks, C. L. *J. Am. Chem. Soc.* **2006**, *128*, 3728-3736.

72. Franks, F. (Ed) *Water, A Comprehensive Treatise*, Plenum Press: New York, **1982**.

73. Lum, K.; Chandler, D.; Weeks, J. D. *J. Phys. Chem. B* **1999**, *103*, 4570-4580. (b) Huang, D. M.; Chandler, D. *Proc. Natl. Acad. Sci.* **2000**, *97*, 8324-8327.

74. Reichart, C. *Solvents and Solvent Effects in Organic Chemistry*, 2nd ed. Verlag Chemie: Weinheim, **1990**.

75. Duan, Y. and Kollman, P.A. *Science* **1998**, *282*, 740-744.

76. Still, W. C.; Tempczyk, A.; Hawley, R. C.; Hendrickson, T. J. *J. Am. Chem. Soc.* **1990**, *112*, 6127-6133.

77. Lee, B.; Richards, F. M. *J. Mol. Biol.* **1971**, *55*, 379-400.

78. Rose, G. D.; Geselowitz, A. R.; Lesse, G. J.; Lee, R. H.; Zehfus, M. H. *Science* **1985**, *229*, 834-837.

79. (a) Chan, H. S.; Dill, K. A. *Annu. Rev. Biophys. Biomol. Struct.* **1997**, *26*, 425-59. (b) Brem, R.; Chan, H. S.; Dill, K. A. *J. Phys. Chem. B*, **2000**, *104* (31), 7471 -7482.

-
80. Sharp, K. A. , Nicholls, A. , Fine, R. & Honig, B. *Science* **1991**, *252*, 106–109.
81. Houk, K. N.; Leach, A. G.; Kim, S. P.; Zhang, X. *Ang. Chem. Int. Ed.* **2003**, *42*, 4872-4897.
82. (a) Frank, H. S.; Evans, M. W. *J. Chem. Phys.* **1945**, *13*, 507. (b) Southall, N. T.; Dill, K. A.; Haymet, A. D. J. *J. Phys. Chem. B.* **2002**, *106*(3), 521-533.
83. Stauffer, D. A.; Barrans, J., R.E.; Dougherty, D. A. *J. Org. Chem.* **1990**, *55*, 2762-2767.
84. Stillinger, F. H. *Science.* **1980**, *209*, 451.
85. Huang, X.; Margulis, C. J.; Berne, B. J. *J. Phys. Chem. B.* **2003**; *107*(42); 11742-11748.
86. Bartlett, P.A.; Yusuff, N.; Rico, A.C.; Lindvall, M.K. *J. Am. Chem. Soc.* **2002**, *124*, 3853-3857.
87. (a) Paliwal, S.; Geib, S.; Wilcox, C. S. *J. Am. Chem. Soc.* **1994**, *116*, 4497. (b) Kim, E.-i.; Paliwal, S.; Wilcox, C. S. *J. Am. Chem. Soc.* **1998**, *120*(43), 11192-11193.
88. Kim, E-I. Ph. D. Dissertation, University of Pittsburgh, **1996**.
89. Paliwal, S. Ph. D. Dissertation, University of Pittsburgh, **1996**.
90. Nakamura, K.; Houk, K. N. *Org. Lett.* **1999**, *1*(13), 2049-2051.
91. Ribas, J.; Cubero, E.; Luque, F. J.; Orozco, M. *J. Org. Chem.* **2002**, *67*(20), 7057-7065.
92. Cockroft, S. L.; Hunter, C. A. *Chem. Comm.* **2006**, 3806 – 3808.
93. (a) Wallenfels, K.; Friedrich, K.; Witzler, F. *Tetrahedron* **1967**, *23*(3), 1353-1358. (b) Padwa, A.; Krumpke, Keith E.; Kassir, Jamal M. *J. Org. Chem.* **1992**, *57*(18), 4940-8. (c) Chen, M. H.; Davidson, J. G.; Freisler, J. T.; Iakovleva, E.; Magano, J. *Organic Preparations and Procedures International* **2000**, *32*(4), 381-384.
94. Gelmont, Mark; Oren, Jakob. *Organic Process Research & Development* **2002**, *6*(5), 591-596.
95. (a) Barder, T. E.; Walker, S. D.; Martinelli, J. R.; Buchwald, S. L. *J. Am. Chem. Soc.* **2005**, *127*, 4685-4696. (b) Walker, S. D.; Barder, T. E.; Martinelli, J. R.; Buchwald, S. L. *Angew. Chem., Int. Ed.* **2004**, *43*, 1871-1876. (c) Altenhoff, G.; Goddard, R.; Lehmann, C. W.;

-
- Glorius, F. *Angew. Chem., Int. Ed.* **2003**, *42*, 3690-3693. (d) Schnyder, A.; Indolese, A. F.; Studer M.; Blaser H. *Angew. Chem., Int. Ed.* **2002**, *41*, 3668-3671.
96. Srikrishna, A.; Sharma, G. V. R. *Tetrahedron Lett.* **1989**, *30*, 3579 – 3580.
97. Webb, T. H.; Wilcox, C. S. *J. Org. Chem.* **1990**, *55*(1), 363-365.
98. Ishiyama, T.; Murata, M.; Miyaura, N. *J. Org. Chem.* **1995**, *60*, 7508–7510.
99. Stream Chemicals, catalog no: 46-0270.
100. Nicolaou, K. C.; Estrada, A. A.; Zak, M.; Lee, S, H.; Safina, B. S. *Angew. Chem., Int. Ed.* **2005**, *44*, 1378-1382.
101. Reich, H. J. *J. Chem. Ed. Software* **1996**, *3D*, 2.
102. Hanford, W. E.; Adams, R. *J. Am. Chem. Soc.* **1935**, *57*(9), 1592-1595.
103. (a) Persson, B; Drakenberg, T; Lindman, B. *J. Phys. Chem.* **1976**, *80*(19), 2124-2125. (b) Persson, B; Drakenberg, T; Lindman, B. *J. Phys. Chem.* **1979**, *83*(23), 3011-3015.
104. Doebler, R; Bakaran, N; Goldston, H; Holloway, P. W. *Biophys J.* **1999**, *76*(2), 928–936.
105. Hofmeister, F. *Arch. Exp. Path. Pharmacol.* **1888**, *24*, 247-260.
106. Collins, K.D.; Washbaugh, M. W. *Q. Rev. Biophys.* **1985**, *18*, 323-422.
107. Baldwin, R. L. *Biophys. J.* **1996**, *71*, 2056-2063.
108. Park, B. K.; Kitteringham, N. R. *Drug Metabol. Rev.* **1994**, *26*, 605.
109. (a) Ojima, I.; Kwon, H. B. *J. Am. Chem. Soc.* **1988**, *110*, 5617. (b) Quan, R. W.; Li, Z.; Jacobsen, E. N. *J. Am. Chem. Soc.* **1996**, *118*, 8156.
110. Battaglia and coworkers have experimentally calculated the electric quadrupole moment of benzene to be $-(29.0 \pm 1.7) 10^{-40} \text{ Cm}^2$ while that of hexafluorobenzene to be $(31.7 \pm 1.7) 10^{-40} \text{ Cm}^2$. See Battaglia, M. R.; Buckingham, A. D.; Williams, J. H. *Chem. Phys. Letters* **1981**, *78*(3), 421.
- 111 Tsuzuki, S.; Honda, K.; Uchimaru, T.; Mikami, M.; Tanabe, K. *J. Phys. Chem. A* **2002**, *106*, 4423 – 4428.
112. Gallivan, J. P.; Dougherty, D. A. *Org. Lett.* **1999**, *1*(1), 103-106.
113. Danten, Y.; Tassaing, T.; Besnard, M. *J. Phys. Chem. A.* **1999**, *103*(18), 3530-3534.
114. Besnard, M.; Danten, Y.; Tassaing, T. *J. Chem. Phys.* **2000**, *113*(9), 3741 – 3748.

115. Mountford, A. J.; Lancaster, S. J.; Coles, S. J.; Horton, P. N.; Hughes, D. L.; Hursthouse, M. B.; Light, M. E. *Inorg. Chem.* **2005**, *44*(16), 5921-5933.